

ornl

OAK RIDGE
NATIONAL
LABORATORY

MARTIN MARIETTA

MARTIN MARIETTA ENERGY SYSTEMS LIBRARIES

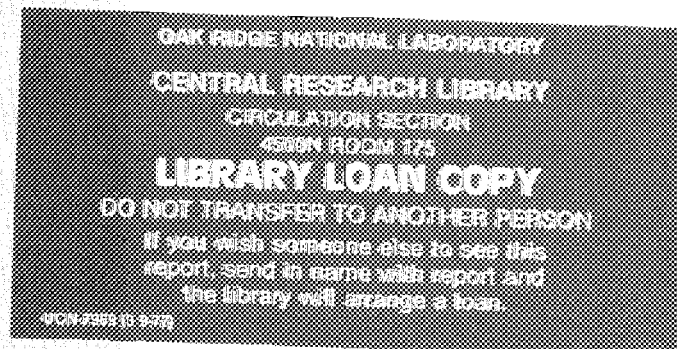


3 4456 0353261 1

ORNL/TM-11956

Reactor Physics Input to the Safety Analysis Report for the High Flux Isotope Reactor

R. T. Primm, III



MANAGED BY
MARTIN MARIETTA ENERGY SYSTEMS, INC.
FOR THE UNITED STATES
DEPARTMENT OF ENERGY

This report has been reproduced directly from the best available copy.

Available to DOE and DOE contractors from the Office of Scientific and Technical Information, P.O. Box 62, Oak Ridge, TN 37831; prices available from (615) 574-8401, FTS 626-8401.

Available to the public from the National Technical Information Service, U.S. Department of Commerce, 5285 Port Royal Rd., Springfield, VA 22161.

This report was prepared as an account of work sponsored by an agency of the United States Government. Neither the United States Government nor any agency thereof, nor any of their employees, makes any warranty, express or implied, or assumes any legal liability or responsibility for the accuracy, completeness, or usefulness of any information, apparatus, product, or process disclosed, or represents that its use would not infringe privately owned rights. Reference herein to any specific commercial product, process, or service by trade name, trademark, manufacturer, or otherwise, does not necessarily constitute or imply its endorsement, recommendation, or favoring by the United States Government or any agency thereof. The views and opinions of authors expressed herein do not necessarily state or reflect those of the United States Government or any agency thereof.

Engineering Physics and Mathematics Division

**Reactor Physics Input to the
Safety Analysis Report
for the High Flux Isotope Reactor**

R. T. Primm, III

DATE PUBLISHED — March 1992

NOTICE This document contains information of a preliminary nature.
It is subject to revision or correction and therefore does not represent a
final report.

Prepared by the
OAK RIDGE NATIONAL LABORATORY
Oak Ridge, Tennessee 37831
managed by
MARTIN MARIETTA ENERGY SYSTEMS, INC.
for the
U.S. DEPARTMENT OF ENERGY
under contract DE-AC05-84OR21400

MARTIN MARIETTA ENERGY SYSTEMS LIBRARIES



3 4456 0353261 1

TABLE OF CONTENTS

ACKNOWLEDGEMENTS	xi
ABSTRACT	xii
1. INTRODUCTION	1
2. CROSS SECTION PROCESSING	3
2.1. Nuclear Data Library	3
2.2. Computer Programs Used to Process Nuclear Data	3
2.3. Coupled Neutron-Gamma Library	7
3. ANALYSES OF CRITICAL EXPERIMENTS	9
3.1. Method of Analysis	9
3.1.1. Fuel Region	9
3.1.2. Control Blades	10
3.2. Results of Calculations	10
4. TWO DIMENSIONAL FLUX - EIGENVALUE CALCULATION	29
4.1. Method of Analysis	29
4.2. VENTURE Input	29
4.2.1. Target Region	29
4.2.2. Fuel Region	29
4.2.3. Control Blades	30
4.3. Fission Product Treatment	30
4.4. Actinide Production	32
4.5. Control Blade Position	32
4.6. Results of Calculations	37
4.6.1. Power Distribution Profiles	40
4.6.2. Specification of End-of-Life Conditions	60
5. CONCLUSIONS	83
6. REFERENCES	85
APPENDIX A	87
APPENDIX B	109

LIST OF TABLES

Table 2.1. HFIR Target Rod Initial Composition	4
Table 2.2. Group Structure for 7-Group Cross Section Library	7
Table 3.1. Calculated k-effectives for HFIR Critical Experiments	10
Table 3.2. Effect of Mesh Point Spacing on Calculated k-effectives	11
Table 3.3. HFIR Critical Experiment 4.1, Inner Annulus	12
Table 3.4. HFIR Critical Experiment 4.1, Outer Annulus	13
Table 3.5. HFIR Critical Experiment 4.2, Inner Annulus	14
Table 3.6. HFIR Critical Experiment 4.2, Outer Annulus	15
Table 3.7. HFIR Critical Experiment 4.3, Inner Annulus	16
Table 3.8. HFIR Critical Experiment 4.3, Outer Annulus	17
Table 3.9. HFIR Critical Experiment 4.4, Inner Annulus	18
Table 3.10. HFIR Critical Experiment 4.4, Outer Annulus	19
Table 3.11. HFIR Critical Experiment 4.5, Inner Annulus	20
Table 3.12. HFIR Critical Experiment 4.5, Outer Annulus	21
Table 3.13. HFIR Critical Experiment 4.6, Inner Annulus	22
Table 3.14. HFIR Critical Experiment 4.6, Outer Annulus	23
Table 3.15. Peak Power Locations for Critical Experiments	24
Table 3.16. HFIR Critical Experiment 4.6, Inner Annulus Finer Computational Mesh	25
Table 3.17. HFIR Critical Experiment 4.6, Outer Annulus Finer Computational Mesh	26
Table 3.18. Comparison of Experimental and Calculated Axially Averaged Relative Power Densities	27

LIST OF TABLES (cont'd.)

Table 3.19. Local Power Density Ratios for HFIR Critical Experiments	27
Table 4.1. Constituents of the Moderately Absorbing Lumped Fission Product	32
Table 4.2. Constitutents of Weakly Absorbing Lumped Fission Product	33
Table 4.3. Calculated k-effectives for HFIR Fuel Cycles	37
Table 4.4. Summary of Neutronics Parameters	41
Table 4.5. Inner Annulus Relative Power Distribution, Time=0.0 Days	61
Table 4.6. Outer Annulus Relative Power Distribution, Time=0.0 Days	62
Table 4.7. Inner Annulus Relative Power Distribution, Time=0.588 Days	63
Table 4.8. Outer Annulus Relative Power Distribution, Time=0.588 Days	64
Table 4.9. Inner Annulus Relative Power Distribution, Time=1.176 Days	65
Table 4.10. Outer Annulus Relative Power Distribution, Time=1.176 Days	66
Table 4.11. Inner Annulus Relative Power Distribution, Time=14.117 Days	67
Table 4.12. Outer Annulus Relative Power Distribution, Time=14.117 Days	68
Table 4.13. Inner Annulus Relative Power Distribution, Time=18.823 Days	69
Table 4.14. Outer Annulus Relative Power Distribution, Time=18.823 Days	70
Table 4.15. Inner Annulus Relative Power Distribution, Time=21.176 Days	71
Table 4.16. Outer Annulus Relative Power Distribution, Time=21.176 Days	72
Table 4.17. Inner Annulus Relative Power Distribution, Time=23.529 Days	73
Table 4.18. Outer Annulus Relative Power Distribution, Time=23.529 Days	74

LIST OF TABLES (cont'd)

Table 4.19. Inner Annulus Relative Power Distribution, Time=27.058 Days	75
Table 4.20. Outer Annulus Relative Power Distribution, Time=27.058 Days	76
Table 4.21. Comparison of Calculated and Measured HFIR Fuel Depletion	79
Table 4.22. Whole Core Quantities of Fuel and Burnable Poison	80
Table 4.23. End-of-Life Constituents of Both HFIR Fuel Elements	81
Table 4.24. End-of-Life Constituents of HFIR Target Rods	82

LIST OF FIGURES

Fig. 4.1. Fission Product Chains Explicitly Represented in the Burner Input.	31
Fig. 4.2. Actinide Production Chains (Part I).	34
Fig. 4.3. Actinide Production Chains (Part II).	35
Fig. 4.4. HFIR Control Blade Position	36
Fig. 4.5. Comparison of VENTURE Mode to Actual HFIR Control Blade Position.	38
Fig. 4.6. Calculated k-effectives during HFIR fuel cycle.	39
Fig. 4.7. Radial flux profile at axial location of 43.4 mm, beginning-of-life.	42
Fig. 4.8. Radial flux profile at axial location of 43.4 mm, end-of-life.	43
Fig. 4.9. Radial fast/thermal flux ratio profile at axial location of 43.4 mm.	44
Fig. 4.10. Radial epithermal/thermal flux ratio profile at axial location of 43.4 mm.	45
Fig. 4.11. Axial flux profile at island hydraulic tube, beginning-of-life.	46
Fig. 4.12. Axial flux profile at island hydraulic tube, end-of-life.	47
Fig. 4.13. Axial flux profile at curium target rods, beginning-of-life.	48
Fig. 4.14. Axial flux profile at curium target rods, end-of-life.	49
Fig. 4.15. Axial flux profile at removable Be facilities, beginning-of-life.	50
Fig. 4.16. Axial flux profile at removable Be facilities, end-of-life.	51
Fig. 4.17. Axial flux profile at control rod access plug facilities, beginning-of-life.	52
Fig. 4.18. Axial flux profile at control rod access plug facilities, end-of-life.	53
Fig. 4.19. Axial flux profile at inner small VXF facilities, beginning-of-life.	54

LIST OF FIGURES (cont'd.)

Fig. 4.20. Axial flux profile at inner small VXF facilities, end-of-life.	55
Fig. 4.21. Axial flux profile at outer small VXF facilities, beginning-of-life.	56
Fig. 4.22. Axial flux profiles at outer small VXF facilities, end-of-life.	57
Fig. 4.23. Axial flux profile at large VXF facilities, beginning-of-life.	58
Fig. 4.24. Axial flux profile at large VXF facilities, end-of-life.	59
Fig. 4.25. Fuel depletion in HFIR at end-of-cycle.	77

ACKNOWLEDGEMENTS

R. Q. Wright provided valuable assistance in extracting, from the ENDF/B data files, the fission product yield data for several fissile nuclides. W. E. Engle and J. V. Pace provided program management within Engineering Physics and Mathematics Division. R. B. Rothrock set program goals and served as technical and administrative liaison to Research Reactors Division. R. D. Lawson supervised publication of this report.

ABSTRACT

HFIR specific, few group neutron and coupled neutron-gamma libraries have been prepared. These are based on data from ENDF/B-V and beginning-of-life (BOL) conditions. The neutron library includes actinide data for curium target rods. Six critical experiments, collectively designated HFIR critical experiment 4, were analyzed. Calculated k-effective was 2% high at BOL-typical conditions but was 1.0 at end-of-life-typical conditions.

The local power density distributions were calculated for each of the critical experiments. The axially averaged values at a given radius were frequently within experimental error. However at individual points, the calculated local power densities were significantly different from the experimentally derived values (several times greater than experimental uncertainty). A reassessment of the foil activation data with transport theory techniques seems desirable.

Using the results of the critical experiments study, a model of the current HFIR configuration was prepared. As with the critical experiments, BOL k-effective was high (3%). However, end-of-life k-effective was also high (2%). The end-of-life concentrations of fission products were compared to those generated using the ORIGEN code. Agreement was generally good through differences in the inventories of some important nuclides, Xe and I, need to be understood. End-of-cycle curium target isotopics based on measured, discharged target rods were compared to calculated values and agreement was good.

Axial flux plots at various irradiation positions were generated. Time-dependent power distributions based on two-dimensional calculations were provided.

1. INTRODUCTION

During late 1989 and early 1990, personnel from the Research Reactors Division identified a need for reactor physics calculations for the High Flux Isotope Reactor (HFIR). Some original calculations had been proven to be unsatisfactory; for instance, the 2300 megawatt-day core lifetime had been predicted to be only 1100 megawatt-days. There had been changes in the HFIR operation which were not previously taken into account including use of curium targets and reduction in "full" power from 100 MW to 85 MW. Finally, there have been significant improvements in nuclear data and methods since the original HFIR nuclear design study (Ref. 1).

This memorandum provides documentation of the cross section processing methodology utilized to generate a few group cross section library, the calculated reactor physics parameters, and the end-of-life nuclide concentrations in the reactor core. In the discussion presented here, it is assumed that the reader has knowledge of the information contained in Ref. 1.

2. CROSS SECTION PROCESSING

Before physics parameters can be calculated, nuclear data must be processed into a usable format. A description of the nuclear data source and the computer programs used to process the data follows. The processing models are described to a sufficient degree so as to allow for recreation of the few group library should that be necessary. Finally, a discussion is given of the few group library which is the end product of the cross section processing procedure.

2.1. Nuclear Data Library

The starting point for nuclear data preparation is the 39 group ANSL-V General Purpose Neutron library (Ref. 2). All of the data extracted from this library for use in the HFIR calculations were derived from data from the Evaluated Nuclear Data File/B - Version V (ENDF/B-V, Ref. 3). The procedure by which ENDF/B-V data were collapsed to the 39 group structure is described in Ref. 2.

The 39 group library is in what is termed "AMPX master format". This means that each nuclide in the library must be processed further to obtain correct cross section values for the unresolved and resolved resonance regions for that nuclide. A description of the AMPX master format is contained in Ref. 2.

2.2. Computer Programs Used to Process Nuclear Data

All programs described in this section are modules of the AMPX system (Ref. 4). However, better documentation of the programs and required input can be found in Ref. 5. The input for each program is provided in Appendix A.

The first program executed is the AJAX module. The sole purpose of this step is to extract only those nuclides from the library which are to be used in modeling the HFIR reactor. A new AMPX master library is created which will be used in subsequent steps. By creating a small subset of the original 39 group library some computational time is saved in succeeding steps.

The second program executed is the BONAMI module. The purpose of this step is to generate correct cross section values for the unresolved resonance energy range (see Ref. 5). The algorithm to accomplish this task is simple. Infinitely dilute values of the various reactions exist for each nuclide. The "Bondarenko factors" are determined by calculating each nuclide's cross section as a function of "background" cross section and generating the ratio of that value to the infinitely dilute value. By generating cross sections corresponding to several background cross section values and for several temperatures, a table can be constructed and interpolation used to determine intermediate values. The BONAMI code performs this interpolation step.

The BONAMI step and the two succeeding steps require some identification of a "unit cell". This unit cell geometry is input directly into the BONAMI and XSDRNPM (described subsequently) steps and indirectly into the NITAWL (described next) step.

For a conventional power reactor, a unit fuel cell is defined as a single fuel pin and its surrounding water channel. The analogy for HFIR would be to select a single involute plate and its associated water channel. However this assumption would be inappropriate due to the small size of the HFIR core.

In a power reactor, the external dimensions of the reactor core are very large compared to the diameter of a fuel pin (several hundred times larger). But for the HFIR, the thickness of the fuel region of the annular core is only about 140 mm. The escape probability for a neutron born in the HFIR is much, much greater than for one born in a power reactor core. Indeed, the purpose of the HFIR is to leak neutrons to the central region where they may be absorbed in target rods.

The neutron spectra in the core is dominated by the thermal neutrons returning from the beryllium reflector. It is noted in Ref. 1 that the homogenization of fuel, clad and coolant is acceptable since the thermal flux depression from coolant centerline to fuel centerline is only 6.8%. Consequently, for the HFIR, the "unit cell" is the entire reactor.

For the BONAMI step, a cylindrical, four zone problem was created. The inner zone was a homogenized HFIR target. Surrounding this region was a representative fuel region with only trace amounts of fission products. Adjacent to the fuel was a control region. The outermost region was beryllium.

The target region actinide composition is shown in Table 2.1. Table 2.1 is based on data for Transuranium Facility campaign 65 (January, 1986) supplied by C. W. Alexander, ORNL.

Table 2.1. HFIR Target Rod Initial Composition

Nuclide	Grams	Atom Density in "Fueled" Zone (atoms per barn*cm)
Pu238	0.00111	2.23946e-8
Pu239	0.00060	1.20546e-8
Pu240	0.21320	4.26554e-6
Pu241	0.00002	3.98485e-10
Pu242	0.00057	1.13099e-8
Am241	0.0459	9.14522e-7
Am243	0.1463	2.89092e-6
Cm244	4.5730	8.99933e-5
Cm245	0.0656	1.28569e-6
Cm246	3.1523	6.15306e-5
Cm247	0.0889	1.72823e-6
Cm248	0.5507	1.06626e-5
Cf252	0.000015	1.85818e-10

The pellets in the target rods are 0.632 cm in diameter and are assumed to be clad with 0.24 cm thick Al-6061. The rods are located on a triangular pitch of 1.689 cm. Appropriate atom densities for the constituents of water and Al-6061 were included with the smeared actinide atom densities in the BONAMI model.

One other input to the BONAMI model is the Dancoff (rod shadow) factor. Continuing the argument made previously, since the whole core is the unit cell, the Dancoff factor must be calculated for the whole core. In most instances, the Dancoff factor for a one lump object is 0.0. However the annular geometry for the HFIR means that there is some probability that a neutron entering the central target region will pass through and cause a fission on the "other side" of the annulus.

The CSAS1 module of the SCALE system (Ref. 5) was used to determine the Dancoff factor of an annulus having the same homogenized fuel region atom densities as the HFIR but with water in the central target region. The calculated Dancoff factor was 0.001774 and this value was input to the BONAMI program. Note that this exceptionally low value indicates that the annulus acts as if it were a single lump. Furthermore, inclusion of the target rods in the model would further shield the annulus and enhance the "single lump" assumption.

The third step in cross section processing is to execute the NITAWL module to properly process the resolved resonance energy region for those nuclides which have resolved resonances. With the exception of the uranium isotopes, all actinides are assumed to be present in "infinitely dilute" quantities. Likewise certain alloying agents in Al-6061 which have resolved resonance data are assumed to have infinitely dilute concentrations. The uranium isotopic ratios are assumed to be typical values from those reported in Ref. 1. The NITAWL model is based on the Nordheim integral treatment for a homogeneous annulus.

It is in the NITAWL step that the temperature of the nuclide is used to select appropriate scattering data for the thermal energy range and correctly doppler broaden the cross section resolved resonances. All of the target actinides and all of the fuel nuclides and fission products are assumed to have a temperature of 430 degrees Kelvin. The water coolant, structural materials and beryllium reflector are all assumed to have a temperature of 343 degrees Kelvin. Note that the master cross-section library contains nuclear data only at certain temperatures. The NITAWL code selects data at a temperature closest to that entered by the user. No interpolation is performed.

The final step in the cross section processing procedure is to execute the XSDRNPM program. XSDRNPM is a one-dimensional, discrete ordinates solution to the Boltzman transport equation. The model input to XSDRNPM is the same as that shown in Table A.6 of Ref. 1 except for two changes.

The central target zone was modified to be three zones with smeared atom densities corresponding to the current target configuration. The innermost zone corresponded to the hydraulic irradiation tube. The second zone represented the 15 curium target rods. The third zone represented the 16 irradiation positions (assumed to be Al tubes).

The second change was in regard to modeling the control blades. The computer model in Appendix A of Ref. 1 had only one control zone containing a Ta concentration described as "variable". In the current model, the control rod zone was split into two regions. This allowed for representation of both the europium "black" and the tantalum "grey" regions in the same model.

Consideration was given to having separate XSDRNPM models for the europium region and the tantalum region. However, it is not clear how one would create such models. Since the XSDRNPM code can only model a one-dimensional representation of a system, it is not possible to create an exact model of the control blades. The height of the Ta region is 12.5 cm whereas the height of the fueled region is 50.4 cm. Hence, a single leakage or buckling factor cannot represent both regions; yet, this is the only option in XSDRNPM. Furthermore, the effective height of the Eu region varies throughout the cycle as the control blade is withdrawn. For most of the cycle it is not adjacent to the fuel zone and thus cross-section collapse with a fixed source calculation (where the fixed source cannot be calculated with a one-dimensional model) would be required.

As a sensitivity check, cross-sections for Ta were calculated with two XSDRNPM models. The first model was that described previously - a Ta zone adjacent to a Eu zone, both having the radials thicknesses corresponding to the actual HFIR control blade. The second model replaced the Eu region with a voided zone, simulating having only the Ta portion of the blade adjacent to the core. The differences in thermal cross-section values between the two models were less than 1%. The epithermal cross-section value for the combined Eu and Ta model was 6% higher than for the solitary Ta model. Differences between fast group cross-sections were less than 3%. Considering the uncertainties in the ability to model the reactor accurately, the single XSDRNPM case scenario was chosen.

A k-effective calculation was performed with XSDRNPM using a buckling factor corresponding to the geometric height of the fueled region of the core (50.8 cm + extrapolation distance). The calculated value was 1.0691.

Forcing the calculated k-effective value to be 1.00 would have required a buckling height less than the physical height. However, the buckling factor for the thermal group is negative - flux peaking outside the core. For the epithermal and fast groups, it is likely to be close to the geometric buckling. Since the better procedure of having group dependent buckling is not available in XSDRNPM, the buckling height was set to the geometric height.

Another procedure would be to search on Eu or Ta concentration to determine a value which yields k-effective = 1.0. The problem with this method is that variation of the control poison from its nominal value might yield incorrect flux values at the edge of the fuel and consequent inaccurate cross-section collapse.

The 39 group cross section set was collapsed to a 7 group set with the energy boundaries shown in Table 2.2. The selection of these boundaries is based on parametric studies performed as a part of the design of the Advanced Neutron Source reactor (Ref. 6). This seven group library was generated in two formats - ISOTXS card image for VENTURE diffusion theory calculations and ANISN card image format for transport calculations.

In order to calculate temperature coefficients of reactivity, it is necessary to have cross-section data at elevated temperatures. Specifically, hydrogen and uranium datasets are needed at multiple temperatures. The same calculational sequence was used for the generation of elevated temperature datasets. Alternate temperature values were specified in the BONAMI and NITAWL datasets and the reformatting performed using the existing XSDRNPM dataset.

Table 2.2. Group Structure for 7-Group
Cross Section Library

Group Number	Upper Energy Boundary
1	20.0 MeV
2	100 keV
3	100 eV
4	0.625 eV
5	0.33 eV
6	0.162 eV
7	0.0300 eV
	0.00001 eV

2.3. Coupled Neutron-Gamma Library

In order to generate total heating rates for various experimental positions, the computational sequence described in Section 2.2 was repeated with the ANSL-V 39 neutron - 44 gamma-group library (Ref. 2). This library does not contain data for all the nuclides which are in the 39 group neutron library. In particular, almost no fission product data and no transplutonium data are present. However the major constituents of the reactor at beginning-of-life are present. The dataset used in the coupled neutron-gamma calculation is contained in Appendix A.

3. ANALYSES OF CRITICAL EXPERIMENTS

As a part of establishing the operating limits for the HFIR, a set of six critical experiments were performed shortly before the initial ascension to full power. The HFIR reactor physics report (Ref. 1) includes a description of the experiments with the following statement of objectives. "These experiments, referred to as the HFIRCE-4 experiments, were performed to (1) investigate small differences (between previous criticals) and the HFIR overall core assemblies, (2) obtain more detailed power-distribution data, (3) calibrate the control rods, and (4) investigate more thoroughly the question of reproducibility."

All experiments were critical. Variation in control rod height for the six experiments was achieved by the addition of soluble boron to the light water coolant. All but one of the experiments had a simulated water target in the central island of the reactor. The final experiment had a target believed at the time to accurately approximate the neutron absorption in the planned Pu-242 target rods.

The local power densities were determined through activation of uranium foils. The foils were counted in a gamma ionization chamber with a counting accuracy of $\pm 1\%$. "Performance of multiple irradiations indicated that the accuracy of the relative power distribution was about 5% (97% of the points agree within $\pm 5\%$)."¹ (Ref. 1) Power distribution data for a 1 cm (radial) by 2 cm (axial) grid are provided in Ref. 1 for each critical experiment. The power distributions are interpolations between or extrapolations from the locations with activated foils. Some foils were circular with a surface area of 0.5 cm^{**2} ; others were rectangular with a length of 6.35 cm and a width of 0.16 cm..

3.1. Method of Analysis

The BOLD-VENTURE system for nuclear reactor analysis was used to determine k-effectives, fluxes, and power distributions (Ref. 7). The VENTURE diffusion theory module of the system had, as input, an R - Z model created with 17 annular fuel zones, target, reflector and control blade regions. The input to the VENTURE system was based on data provided in Figs. A.8 through A.10 and Table A.6 of Ref. 1. This section will present those parts of the input dataset which differed from the description given in Ref. 1.

3.1.1. Fuel Region

Deviating from the description in Ref. 1, the fuel element sideplates were explicitly represented in the VENTURE model. Also, the atom densities for the constituents of the fuel zones were based on Al-6061 rather than pure Al. Both the Al filler and fuel plate clad were assumed to be Al-6061. The atom densities for the boron and uranium isotopes were calculated from Figs. A.9 and A.10 (schematic drawings of the inner and outer fuel plates respectively) and compared to values given in Table A.6 of Ref. 1. Agreement was excellent (usually within 1%). The total quantity of U-235 as tallied from the input was found to be 9.46 kg. The value quoted in Ref. 1 is 9.40 kg.

The radial mesh in the VENTURE model was the same as that noted in Table A.6 of Ref. 1. The axial mesh varied according to the critical experiment being modeled; the control blade position varied according to coolant boron loading for a given critical experiment.

3.1.2. Control Blades

In Ref. 1, the outer element sideplate and inner control blade and water gap between these structures were all homogenized into one region. In the VENTURE model these structures were represented separately. However, for the control blade, the Al clad was homogenized with the control poison material.

The "black" control material reported in Table A.6 of Ref. 1 is boron. The actual control blades used in the HFIRCE-4 experiments had europium in this region. The VENTURE model contains atom densities corresponding to the europium oxide - tantalum - Al design (still the current HFIR configuration). The dimensions and content of the control blade were supplied by R. W. Hobbs, Research Reactors Division.

Initial calculations of experiments with the control rod fully inserted yielded unusually low values of calculated k-effective. The nuclear data for the control region was examined and the diffusion coefficient for the europium region was modified via a procedure described in Appendix B. All calculated k-effective values reported here are for models incorporating the modified europium diffusion coefficient.

3.2. Results of Calculations

The calculated values of k-effective are shown in Table 3.1. The best agreement between calculation and experiment is seen in the "cleanest" core configuration (blades out). At this point, agreement is -0.3%. The worst case is with control blades fully inserted and a water target - agreement being 2.2%.

Table 3.1. Calculated k-effectives for HFIR Critical Experiments

Expt. No.	Control Blade Position (cm)	Boron Conc. in Coolant (g per L)	Target Material	k-effective
4.1	44.45	0.0	water	1.0219
4.2	49.28	0.527	water	.9872
4.3	54.09	0.910	water	.9872
4.4	61.72	1.25	water	.9890
4.5	67.31 (out)	1.35	water	.9967
4.6	42.16	0.0	sim. Pu	1.0206

The source of the discrepancy at beginning-of-life typical conditions (2%) is unknown. By comparison of cases 4.1 and 4.6, it would appear that the source of the discrepancy is independent of target material. The calculational bias changes sign as the control blade is withdrawn and then approaches 1.0. Based on the assumption that the 67.31 cm rod position represents end-of-life, there should be no bias applied to actual reactor calculations when attempting to determine cycle length for a given reactor configuration. It is noted that in the seven-group cross-section production model, there was no boron in the coolant.

The effect on k-effective of varying the number of mesh points in the fuel is shown in Table 3.2. For all cases examined, there is a slight increase in calculated k-effective (0.002 to 0.004) as the number of mesh points in the fuel is increased. However, the previously identified discrepancies remain largely unchanged.

Table 3.2. Effect of Mesh Point Spacing on Calculated k-effectives

Expt. No.	Mesh Points in Fuel		k-effective
	R	Z	
4.1	19	30	1.022
4.1	68	78	1.026
4.2	19	34	0.987
4.2	68	63	0.989
4.5	19	30	0.997
4.5	68	78	1.000
4.6	19	30	1.021
4.6	68	86	1.024

HFIR procedures stipulate that any change in the configuration of experiments must be certified to cause no more than a 5% increase in local power density at the limiting position in the reactor. Frequently this certification is made by comparison to previously performed experiments. For new materials or designs, certification must rely on computations.

Comparisons of calculated and experimentally derived local power densities for each of the six critical experiments are given in Tables 3.3 through 3.14. Note that the description of the experiments, the measurement procedure, some of the experimental data, and all of the experimentally derived local power densities are contained in Ref. 1.

For convenience, the locations and values of the maximum point power densities are contained in Table 3.15, the percentage differences between calculations and experiments having been reported in Tables 3.3 through 3.14. Also shown there are the locations and values of the greatest percentage difference by which the experimentally measured local power density exceeds the calculated value. The former is important because of safety considerations related to the "hot spot" power density. The latter is important for determining maximum bias factors which could be applied to calculations to insure conservatism regarding thermal-hydraulic limits.

**Table 3.3. HFIR Critical Experiment 4.1
Control Blades at 44.45 cm
Inner Annulus Relative Power Distribution
(100*(Experiment-Calculation)/Experiment)**

Axial Height (cm)	Radius (cm)						
	7.14	8.00	9.00	10.00	11.00	12.00	12.60
25.40	-70.95	-31.10	-27.38	-31.35	-36.26	-35.47	-41.21
24.00	-39.67	-39.74	-38.49	-35.80	-30.71	-33.24	-27.57
22.00	-17.66	-27.02	-18.43	-13.02	-8.42	-11.87	-10.36
20.00	-5.88	-15.14	-10.27	-8.79	-5.43	-6.53	-3.65
18.00	1.13	-7.49	-4.73	-3.25	-1.32	-2.04	1.65
16.00	5.42	-3.59	-2.37	.14	.98	1.24	4.62
14.00	9.02	-.89	.98	2.70	3.55	3.69	7.59
12.00	11.33	1.20	2.88	4.80	5.68	5.74	10.09
10.00	13.30	3.62	5.19	7.31	7.50	7.48	12.87
8.00	15.08	5.73	7.16	8.75	9.71	8.95	15.27
6.00	15.84	7.04	8.87	10.62	10.95	10.81	17.37
4.00	16.19	7.68	10.39	12.24	11.98	11.82	18.71
2.00	16.10	7.68	10.48	13.02	12.81	12.03	18.87
.00	16.02	7.61	10.44	13.02	12.84	12.09	18.41
-2.00	15.92	6.85	9.59	12.18	12.65	12.56	17.80
-4.00	15.35	5.96	8.54	11.11	11.60	10.97	16.45
-6.00	13.78	4.91	6.54	8.35	8.85	8.34	14.21
-8.00	12.10	2.38	3.42	5.82	6.29	6.60	12.16
-10.00	9.66	-1.32	-.33	2.71	3.94	4.36	9.60
-12.00	7.44	-4.13	-3.10	-1.15	.97	1.53	7.19
-14.00	4.06	-7.63	-6.59	-3.90	-2.73	-1.06	4.22
-16.00	-.33	-12.22	-9.96	-7.43	-5.18	-5.38	.51
-18.00	-6.58	-18.75	-14.72	-12.23	-9.78	-8.79	-4.47
-20.00	-18.88	-27.73	-20.93	-16.80	-14.21	-14.81	-12.64
-22.00	-36.19	-41.44	-29.70	-22.22	-16.67	-19.95	-19.54
-24.00	-40.91	-51.98	-49.74	-46.86	-38.89	-43.05	-38.06
-25.40	-61.00	-39.08	-41.68	-46.45	-49.22	-47.33	-52.50

Table 3.4. HFIR Critical Experiment 4.1
 Control Blades at 44.45 cm
 Outer Annulus Relative Power Distribution
 (100*(Experiment-Calculation)/Experiment)

Axial Height (cm)	Radius (cm)						
	15.15	16.00	17.00	18.00	19.00	20.00	21.00
25.40	-14.73	-46.77	-68.67	-72.66	-58.14	-83.88	-216.95
24.00	-22.40	-28.99	-43.14	-54.00	-73.57	-97.61	-182.91
22.00	-6.47	-16.68	-16.84	-27.94	-49.22	-84.19	-161.43
20.00	-5.25	-15.15	-14.51	-22.16	-38.54	-67.00	-138.20
18.00	-1.72	-9.76	-8.12	-12.67	-24.59	-41.09	-77.08
16.00	2.47	-5.44	-2.54	-4.59	-10.28	-18.70	-33.23
14.00	5.71	-1.12	2.02	1.85	-1.00	-2.46	-7.27
12.00	8.44	2.47	6.59	7.82	7.93	8.49	7.10
10.00	10.76	5.43	9.43	11.46	13.37	16.76	17.33
8.00	12.71	7.83	12.96	15.50	17.88	22.29	24.77
6.00	14.92	9.79	15.73	17.82	21.69	26.64	29.57
4.00	16.32	12.03	17.38	19.50	23.79	29.54	32.57
2.00	16.50	12.25	18.19	20.24	23.57	30.58	34.69
.00	16.63	12.42	18.41	20.51	23.78	30.55	34.37
-2.00	16.13	11.91	18.08	21.10	24.22	29.82	32.80
-4.00	15.46	11.21	16.95	20.28	23.28	28.38	30.93
-6.00	13.34	8.83	14.61	18.04	21.29	25.36	26.71
-8.00	10.69	5.75	11.37	14.62	16.97	21.10	21.45
-10.00	7.34	1.73	6.93	9.65	11.46	14.40	13.09
-12.00	4.64	-2.61	1.82	3.57	4.41	5.59	1.83
-14.00	.36	-7.22	-5.09	-5.02	-5.94	-7.56	-10.65
-16.00	-4.03	-13.04	-12.81	-15.22	-20.96	-26.06	-35.10
-18.00	-8.67	-20.58	-21.20	-28.98	-40.95	-59.15	-105.64
-20.00	-17.61	-28.57	-31.23	-44.26	-66.23	-121.22	-292.25
-22.00	-35.37	-42.33	-41.98	-54.01	-84.40	-147.11	-440.43
-24.00	-60.60	-74.48	-76.55	-92.14	-114.63	-162.33	-530.98
-25.40	-32.12	-67.93	-94.96	-105.96	-99.98	-168.71	-1982.93

**Table 3.5. HFIR Critical Experiment 4.2
Control Blades at 49.28 cm
Inner Annulus Relative Power Distribution
(100*(Experiment-Calculations)/Experiment)**

Axial Height (cm)	Radius (cm)						
	7.14	8.00	9.00	10.00	11.00	12.00	12.60
25.40	-49.04	-14.47	-9.30	-11.81	-16.05	-20.59	-29.08
24.00	-29.12	-33.58	-28.69	-27.53	-29.04	-33.69	-32.44
22.00	-17.52	-27.42	-18.46	-13.48	-12.78	-17.20	-15.13
20.00	-6.49	-18.42	-16.48	-11.41	-7.53	-8.04	-6.04
18.00	-2.28	-12.10	-9.15	-7.00	-3.58	-5.14	-2.11
16.00	.70	-8.40	-4.67	-3.47	-1.54	-3.16	-.40
14.00	2.71	-5.88	-3.40	-2.01	-.26	-1.09	1.41
12.00	4.26	-4.80	-1.69	-.12	1.44	.38	2.67
10.00	5.61	-3.94	-1.17	1.36	1.94	.68	4.35
8.00	6.90	-3.16	.80	2.59	3.06	1.61	5.06
6.00	8.22	-2.38	-.42	3.68	4.07	2.45	6.39
4.00	8.56	-1.59	-.10	3.96	4.28	2.54	7.02
2.00	8.68	-1.26	.37	3.69	3.98	2.18	7.90
.00	8.99	-1.47	.91	4.22	3.79	1.98	7.72
-2.00	8.50	-1.55	.04	4.12	3.72	1.97	7.12
-4.00	8.18	-2.19	-.81	3.34	3.75	2.11	6.03
-6.00	7.04	-3.37	-1.56	1.89	3.19	.98	5.13
-8.00	5.33	-4.65	-2.46	.21	.88	-.32	4.13
-10.00	2.88	-6.06	-4.45	-1.80	-.09	-1.04	2.91
-12.00	.77	-8.65	-5.95	-4.36	-1.45	-3.05	2.14
-14.00	-1.03	-10.94	-8.02	-6.64	-3.39	-3.77	-.04
-16.00	-3.49	-14.13	-10.99	-9.92	-5.07	-6.30	-2.14
-18.00	-6.22	-17.63	-14.06	-11.92	-7.86	-7.73	-5.55
-20.00	-11.33	-23.96	-19.68	-14.41	-10.01	-11.49	-10.60
-22.00	-19.92	-32.88	-24.18	-18.98	-17.99	-20.41	-23.34
-24.00	-27.40	-35.63	-32.91	-33.83	-35.32	-42.10	-42.74
-25.40	-49.20	-20.27	-16.65	-20.98	-25.95	-31.09	-42.25

Table 3.6. HFIR Critical Experiment 4.2
 Control Blades at 49.28 cm
 Outer Annulus Relative Power Distribution
 (100*(Experiment-Calculation)/Experiment)

Axial Height (cm)	Radius (cm)						
	15.15	16.00	17.00	18.00	19.00	20.00	21.00
25.40	-4.92	-25.87	-37.00	-38.67	-31.31	-56.69	-190.85
24.00	-19.23	-27.40	-28.12	-34.53	-50.11	-77.70	-141.01
22.00	-7.51	-14.79	-11.27	-16.27	-31.92	-46.04	-94.83
20.00	-6.69	-14.43	-10.97	-12.52	-15.06	-18.66	-37.51
18.00	-2.80	-9.59	-5.05	-2.82	-3.44	-1.13	-9.18
16.00	2.46	-5.06	-.55	3.01	5.60	8.30	6.36
14.00	3.76	-2.04	3.25	7.51	10.87	15.32	15.48
12.00	4.55	-.79	5.74	9.36	13.69	19.70	21.58
10.00	5.02	-.05	6.54	10.86	15.51	22.11	24.64
8.00	4.65	.37	7.55	11.40	15.84	23.04	26.75
6.00	4.29	.68	7.54	11.43	15.36	23.89	29.05
4.00	4.67	1.01	7.56	11.48	14.99	22.55	29.29
2.00	5.40	1.75	9.41	12.28	15.13	21.19	27.25
.00	5.82	2.85	9.76	11.85	14.47	20.84	26.61
-2.00	5.96	2.36	9.37	12.25	15.05	21.56	26.45
-4.00	5.80	2.26	8.87	12.18	14.97	21.75	25.89
-6.00	5.36	1.18	8.25	11.69	14.38	21.19	23.14
-8.00	2.76	-1.59	6.02	10.37	14.64	21.74	23.47
-10.00	1.21	-3.34	3.74	9.60	14.20	20.66	22.30
-12.00	-.95	-5.92	1.12	6.33	11.49	17.13	18.58
-14.00	-3.08	-9.75	-2.00	2.99	7.04	11.88	10.95
-16.00	-6.35	-14.18	-7.07	-2.88	.35	3.28	-2.43
-18.00	-8.99	-16.70	-12.09	-9.38	-9.62	-10.48	-23.16
-20.00	-13.21	-22.14	-20.84	-20.73	-25.06	-33.70	-62.36
-22.00	-19.65	-27.33	-24.79	-34.64	-52.67	-75.68	-170.66
-24.00	-34.83	-43.53	-46.76	-56.78	-75.52	-126.03	-492.17
-25.40	-19.88	-43.22	-58.59	-62.74	-54.92	-123.89	-2946.89

Table 3.7. HFIR Critical Experiment 4.3
 Control Blades at 54.09 cm
 Inner Annulus Relative Power Distribution
 (100*(Experiment-Calculation)/Experiment)

Axial Height (cm)	Radius (cm)						
	7.14	8.00	9.00	10.00	11.00	12.00	12.60
25.40	-39.60	-9.05	-5.14	-6.41	-9.62	-11.91	-17.98
24.00	-20.85	-22.01	-14.45	-11.86	-13.04	-13.47	-15.57
22.00	-19.93	-23.51	-12.48	-8.21	-5.84	-11.26	-9.11
20.00	-8.91	-15.86	-11.94	-8.97	-3.65	-6.83	-3.44
18.00	.55	-12.88	-10.93	-6.65	-4.58	-3.86	-2.00
16.00	1.83	-10.67	-8.97	-6.13	-5.59	-3.06	-1.40
14.00	2.39	-9.50	-8.05	-5.24	-6.03	-3.10	-.65
12.00	2.69	-8.83	-6.61	-3.83	-5.76	-3.48	1.39
10.00	2.99	-7.44	-6.45	-3.69	-3.75	-3.90	3.08
8.00	3.35	-7.04	-5.50	-2.76	-2.08	-3.47	4.57
6.00	3.30	-6.53	-4.59	-1.02	-1.33	-3.77	4.73
4.00	2.93	-6.62	-4.45	-.91	-.48	-3.84	3.77
2.00	2.82	-6.54	-4.21	-.70	-1.11	-3.74	3.06
.00	3.11	-6.12	-3.72	-.23	-1.44	-4.08	2.74
-2.00	3.05	-6.28	-3.95	-1.24	-.84	-4.25	2.64
-4.00	3.98	-6.86	-4.75	-2.03	-1.55	-4.89	2.21
-6.00	4.59	-7.31	-6.40	-2.76	-2.17	-5.39	1.99
-8.00	4.89	-8.44	-7.16	-3.45	-3.59	-5.74	1.24
-10.00	4.80	-8.70	-7.00	-4.19	-6.13	-5.07	.56
-12.00	2.71	-9.06	-6.98	-4.14	-4.95	-4.42	.66
-14.00	1.02	-9.61	-8.31	-4.30	-4.95	-2.83	.66
-16.00	-.44	-10.71	-9.18	-4.99	-3.10	-2.62	.18
-18.00	-1.96	-12.92	-11.16	-6.74	-3.10	-3.34	-1.38
-20.00	-6.42	-17.48	-12.27	-7.61	-2.07	-6.35	-4.16
-22.00	-18.49	-23.93	-12.89	-8.46	-7.43	-10.89	-11.87
-24.00	-19.28	-20.44	-14.55	-10.10	-9.42	-17.92	-16.57
-25.40	-39.91	-8.16	-4.81	-6.71	-9.86	-12.35	-20.20

Table 3.8. HFIR Critical Experiment 4.3
 Control Blades at 54.09 cm
 Outer Annulus Relative Power Distribution
 (100*(Experiment-Calculation)/Experiment)

Axial Height (cm)	Radius (cm)						
	15.15	16.00	17.00	18.00	19.00	20.00	21.00
25.40	10.81	-7.76	-17.33	-16.39	-4.86	-18.51	-91.14
24.00	-5.75	-11.42	-5.27	-3.46	-5.67	-6.76	-46.27
22.00	-3.41	-7.71	-2.76	-1.40	-2.91	-9.36	-18.64
20.00	-2.50	-7.14	-.84	2.82	4.51	4.66	1.14
18.00	-1.69	-6.14	-.89	4.44	8.16	15.66	9.93
16.00	-1.74	-7.05	-.39	4.87	8.40	22.66	11.89
14.00	-2.57	-6.66	.01	3.81	7.56	22.23	12.61
12.00	-2.79	-5.86	.66	2.94	6.43	18.06	11.37
10.00	-3.87	-6.12	1.94	2.90	6.99	16.44	11.82
8.00	-4.81	-5.46	2.37	3.88	7.84	15.05	14.99
6.00	-4.67	-4.61	3.07	4.40	8.48	14.04	16.84
4.00	-4.24	-3.49	3.35	4.58	8.28	13.92	17.24
2.00	-2.83	-3.60	3.23	4.39	7.88	13.23	16.81
.00	-2.46	-3.23	3.57	4.73	8.13	12.71	17.29
-2.00	-2.54	-3.30	4.21	4.65	8.09	12.74	16.86
-4.00	-3.64	-3.63	3.92	5.11	8.00	13.55	16.79
-6.00	-4.52	-4.44	3.21	4.47	8.44	13.81	15.83
-8.00	-5.14	-5.78	2.07	3.48	6.53	12.27	12.66
-10.00	-5.58	-6.97	.31	2.06	4.29	9.24	6.17
-12.00	-4.19	-8.28	-1.59	1.79	3.38	7.66	3.18
-14.00	-3.73	-8.91	-1.90	1.26	4.45	9.25	7.37
-16.00	-3.80	-9.26	-2.15	1.44	5.71	10.95	9.20
-18.00	-3.88	-9.74	-2.80	.65	5.19	9.64	7.95
-20.00	-5.05	-9.86	-4.66	-.30	2.04	4.15	1.18
-22.00	-6.29	-10.86	-5.73	-5.84	-7.21	-6.88	-18.18
-24.00	-9.76	-15.91	-11.15	-11.14	-14.27	-28.74	-92.33
-25.40	.72	-19.30	-29.34	-29.47	-19.37	-44.55	-259.39

**Table 3.9. HFIR Critical Experiment 4.4
Control Blades at 61.72 cm
Inner Annulus Relative Power Distribution
(100*(Experiment-Calculation)/Experiment)**

Axial Height (cm)	Radius (cm)						
	7.14	8.00	9.00	10.00	11.00	12.00	12.60
25.40	-36.79	.50	8.09	7.95	4.68	.04	-6.95
24.00	-24.41	-21.23	-9.25	-8.30	-8.28	-15.00	-14.24
22.00	-16.87	-26.11	-11.69	-4.58	-4.37	-10.38	-9.97
20.00	-7.91	-24.99	-17.47	-8.50	-6.58	-8.82	-6.79
18.00	-3.28	-19.18	-15.84	-9.14	-6.13	-8.51	-4.11
16.00	-2.41	-17.21	-14.36	-8.15	-6.93	-8.38	-4.42
14.00	-2.16	-15.11	-12.59	-6.76	-7.04	-8.90	-4.21
12.00	-2.92	-14.76	-11.49	-7.02	-6.35	-9.65	-4.26
10.00	-3.59	-14.55	-10.71	-6.33	-6.88	-9.36	-4.33
8.00	-3.43	-14.47	-9.16	-4.89	-5.52	-9.19	-4.42
6.00	-3.87	-13.46	-8.79	-4.57	-5.26	-8.11	-4.47
4.00	-2.62	-13.23	-7.41	-3.26	-4.88	-7.83	-3.48
2.00	-1.27	-12.08	-7.01	-3.77	-4.51	-7.52	-3.26
.00	.86	-10.87	-7.50	-4.25	-5.00	-8.03	-2.95
-2.00	.15	-11.09	-7.80	-4.54	-5.29	-9.19	-3.15
-4.00	-.38	-12.10	-8.10	-4.84	-5.55	-9.41	-4.07
-6.00	-.74	-13.09	-9.40	-6.11	-6.78	-9.61	-4.10
-8.00	-.82	-13.96	-10.71	-6.38	-6.99	-10.65	-4.81
-10.00	-.76	-13.91	-11.16	-6.75	-7.27	-10.76	-5.55
-12.00	-.66	-15.05	-11.86	-7.35	-7.75	-11.00	-5.43
-14.00	-1.34	-16.51	-12.90	-8.22	-7.24	-10.19	-4.26
-16.00	-2.37	-18.71	-14.64	-8.35	-7.04	-9.63	-4.34
-18.00	-5.28	-22.36	-17.74	-9.29	-6.14	-8.36	-3.89
-20.00	-10.34	-28.90	-17.75	-10.27	-6.51	-7.04	-3.61
-22.00	-21.81	-26.35	-13.71	-6.28	-5.86	-9.95	-9.46
-24.00	-22.57	-21.26	-12.70	-9.80	-11.31	-17.95	-18.92
-25.40	-34.64	1.11	8.08	7.36	4.19	.50	-7.83

Table 3.10. HFIR Critical Experiment 4.4
 Control Blades at 61.72 cm
 Outer Annulus Relative Power Distribution
 (100*(Experiment-Calculation)/Experiment)

Axial Height (cm)	Radius (cm)						
	15.15	16.00	17.00	18.00	19.00	20.00	21.00
25.40	13.74	4.51	3.56	9.54	18.20	14.21	-10.60
24.00	-3.96	-8.94	-1.08	2.80	5.31	8.24	-.76
22.00	-1.70	-6.36	.36	3.24	6.15	7.95	9.35
20.00	-5.28	-8.06	.62	4.50	8.17	15.44	17.69
18.00	-7.31	-7.85	1.52	4.97	8.96	15.57	19.04
16.00	-8.16	-7.74	1.33	4.48	8.69	14.85	17.75
14.00	-9.44	-8.12	.83	3.82	7.43	14.29	16.86
12.00	-9.75	-8.59	.34	4.18	7.35	13.36	16.52
10.00	-10.01	-8.94	.00	2.91	6.70	12.91	16.08
8.00	-10.24	-9.25	-.27	2.65	7.03	12.73	16.00
6.00	-9.50	-9.44	.37	2.52	6.73	12.15	15.67
4.00	-8.57	-8.52	.43	2.61	6.72	11.93	16.34
2.00	-7.57	-7.53	1.37	2.81	6.84	11.92	16.70
.00	-7.27	-7.23	.89	3.10	6.37	11.45	16.24
-2.00	-7.45	-8.23	-.06	2.13	5.45	11.34	14.53
-4.00	-9.17	-9.12	-.93	2.03	4.63	10.74	14.16
-6.00	-9.99	-9.93	-.91	2.02	4.68	11.00	13.44
-8.00	-10.63	-9.63	-.64	2.26	5.01	11.61	14.34
-10.00	-11.25	-10.15	-.25	2.62	5.52	12.52	14.99
-12.00	-10.91	-9.71	.23	3.10	7.12	13.01	16.06
-14.00	-10.51	-9.13	.90	3.85	8.30	14.85	17.15
-16.00	-9.09	-8.62	.57	4.83	8.98	14.91	16.79
-18.00	-8.11	-8.57	-.18	4.69	8.84	13.42	13.31
-20.00	-7.25	-10.05	-2.37	2.04	3.49	6.64	9.47
-22.00	-3.39	-8.16	-1.00	2.60	4.85	5.96	5.80
-24.00	-6.64	-10.18	-3.31	3.06	6.54	12.07	.59
-25.40	7.95	.51	-.73	5.21	15.39	10.16	-14.75

Table 3.11. HFIR Critical Experiment 4.5
 Control Blades at 67.31 cm
 Inner Annulus Relative Power Distribution
 (100*(Experiment-Calculation)/Experiment)

Axial Height (cm)	Radius (cm)						
	7.14	8.00	9.00	10.00	11.00	12.00	12.60
25.40	-37.90	-2.88	1.79	.47	-4.57	-10.01	-17.49
24.00	-29.68	-25.75	-20.99	-19.26	-17.68	-22.74	-21.70
22.00	-19.13	-25.71	-18.01	-13.07	-11.41	-14.44	-14.11
20.00	-10.43	-22.21	-18.89	-11.96	-10.36	-13.08	-9.48
18.00	-5.96	-17.68	-16.40	-11.58	-8.77	-10.12	-8.33
16.00	-3.42	-16.63	-15.74	-11.13	-8.75	-10.46	-7.59
14.00	-2.66	-15.22	-14.55	-11.41	-8.11	-10.18	-6.46
12.00	-2.21	-14.38	-13.99	-9.62	-7.90	-10.27	-6.82
10.00	-2.63	-13.83	-12.62	-8.35	-7.95	-10.55	-6.30
8.00	-2.22	-13.44	-10.53	-7.39	-7.11	-10.92	-6.85
6.00	-2.46	-12.17	-9.79	-5.65	-6.45	-10.35	-6.47
4.00	-1.85	-11.87	-8.20	-5.06	-5.89	-9.85	-5.22
2.00	-1.11	-11.53	-8.65	-4.56	-6.34	-10.35	-4.88
.00	-.10	-11.02	-8.06	-4.91	-5.76	-9.77	-4.38
-2.00	-.40	-12.40	-8.62	-5.47	-6.31	-10.32	-3.99
-4.00	-1.10	-12.72	-8.14	-5.01	-6.79	-9.79	-3.44
-6.00	-.95	-13.02	-9.70	-5.56	-7.35	-10.26	-3.69
-8.00	-1.37	-13.32	-10.40	-6.23	-6.99	-9.77	-3.94
-10.00	-.94	-12.65	-10.19	-7.08	-6.71	-9.32	-4.21
-12.00	-.43	-13.09	-11.34	-7.07	-6.57	-8.95	-4.57
-14.00	-1.59	-13.81	-12.98	-7.34	-6.65	-7.59	-5.13
-16.00	-3.18	-16.35	-13.99	-8.07	-5.85	-7.62	-4.91
-18.00	-9.05	-23.45	-17.72	-9.69	-6.98	-8.37	-6.63
-20.00	-21.52	-33.06	-20.40	-9.84	-8.30	-11.00	-9.01
-22.00	-25.69	-31.51	-19.61	-10.68	-9.07	-13.84	-13.49
-24.00	-19.52	-25.22	-20.43	-16.62	-16.97	-19.92	-20.82
-25.40	-37.30	-4.65	-1.48	-2.58	-8.87	-15.04	-23.59

Table 3.12. HFIR Critical Experiment 4.5
 Control Blades at 67.31 cm
 Outer Annulus Relative Power Distribution
 (100*(Experiment-Calculation)/Experiment)

Axial Height (cm)	Radius (cm)						
	15.15	16.00	17.00	18.00	19.00	20.00	21.00
25.40	9.64	-2.10	-5.22	-1.29	8.73	5.16	-3.91
24.00	-2.95	-10.93	-4.38	-.55	4.05	6.57	1.70
22.00	-3.53	-6.17	.08	4.22	6.76	9.26	4.52
20.00	-7.42	-9.48	.38	4.23	7.67	12.87	12.21
18.00	-8.46	-8.18	1.24	5.08	7.33	13.21	14.95
16.00	-8.41	-8.28	1.09	5.03	6.33	12.88	15.82
14.00	-8.91	-8.83	.61	4.67	6.08	13.10	16.27
12.00	-8.58	-8.52	.95	5.08	6.55	12.38	15.90
10.00	-9.35	-9.29	1.17	4.50	6.03	12.39	16.16
8.00	-9.15	-9.09	.50	4.76	6.31	12.40	16.44
6.00	-8.96	-8.90	.71	4.99	6.56	12.43	16.79
4.00	-8.72	-9.54	.14	4.46	5.27	11.86	16.12
2.00	-9.30	-9.24	-.37	3.98	4.81	10.71	15.03
.00	-8.81	-9.61	.09	3.65	4.49	10.40	14.74
-2.00	-9.27	-9.21	-.35	3.22	4.83	10.73	15.05
-4.00	-8.66	-9.48	1.00	5.29	5.32	11.90	16.15
-6.00	-7.98	-8.80	1.61	5.07	6.63	13.15	17.39
-8.00	-8.11	-8.05	1.46	4.87	6.41	13.16	17.66
-10.00	-8.22	-8.16	1.32	4.64	6.16	13.21	17.45
-12.00	-7.38	-8.31	1.14	5.25	6.71	13.26	17.27
-14.00	-6.55	-7.51	1.83	4.89	6.28	13.25	17.06
-16.00	-6.95	-7.96	1.38	5.31	6.59	13.08	16.70
-18.00	-6.82	-7.78	.45	4.32	5.45	13.49	15.99
-20.00	-5.58	-7.55	-.42	2.16	4.49	12.30	14.52
-22.00	-1.53	-5.45	2.27	6.48	7.74	9.00	9.17
-24.00	-1.97	-9.74	-2.96	2.63	7.45	10.12	-1.66
-25.40	7.73	-4.76	-8.37	-3.01	6.67	.66	-17.36

Table 3.13. HFIR Critical Experiment 4.6
 Control Blades at 42.16 cm
 Inner Annulus Relative Power Distribution
 (100*(Experiment-Calculation)/Experiment)

Axial Height (cm)	Radius (cm)						
	7.14	8.00	9.00	10.00	11.00	12.00	12.60
25.40	-67.68	-32.72	-29.99	-31.94	-33.00	-27.64	-30.27
24.00	-35.56	-32.52	-23.26	-20.27	-19.94	-21.82	-15.10
22.00	-29.97	-27.02	-14.03	-9.79	-7.08	-7.18	-4.04
20.00	-13.93	-20.75	-13.34	-9.74	-8.45	-6.87	-2.53
18.00	-5.57	-12.97	-10.30	-9.79	-7.67	-4.11	1.71
16.00	.85	-9.60	-8.38	-8.17	-6.47	-3.41	2.82
14.00	1.36	-7.68	-6.49	-6.39	-5.94	-3.33	3.29
12.00	2.82	-6.44	-5.14	-5.05	-4.76	-2.59	4.31
10.00	3.34	-5.49	-4.02	-3.09	-2.91	-1.88	4.65
8.00	3.80	-3.93	-1.54	-1.33	-1.22	-1.15	5.09
6.00	3.82	-3.02	-.52	.44	.52	.45	5.76
4.00	4.01	-2.68	-.79	.20	.95	.83	6.62
2.00	4.35	-2.89	-.95	.07	.16	.72	7.07
.00	4.38	-2.84	-1.58	-.54	-.41	.87	7.21
-2.00	5.13	-2.68	-1.43	-1.08	-.21	.48	7.51
-4.00	5.56	-2.30	-1.09	-1.45	-.51	.29	7.48
-6.00	5.54	-1.83	-1.42	-2.58	-1.53	.17	6.95
-8.00	5.03	-2.67	-2.48	-2.96	-2.58	-.60	5.21
-10.00	3.93	-4.29	-3.61	-4.18	-2.85	-1.35	4.10
-12.00	3.26	-4.64	-4.17	-4.80	-3.28	-1.45	3.56
-14.00	1.44	-6.22	-5.06	-4.76	-3.95	-1.71	2.83
-16.00	-1.39	-8.75	-6.61	-6.21	-4.10	-2.37	2.53
-18.00	-5.23	-11.99	-9.49	-7.63	-5.06	-2.95	2.33
-20.00	-13.83	-19.94	-15.38	-10.07	-8.26	-5.81	.03
-22.00	-29.06	-31.10	-15.96	-19.22	-7.92	-7.09	-2.31
-24.00	-54.25	-42.62	-32.20	-26.82	-21.21	-20.91	-13.51
-25.40	-107.58	-47.85	-38.62	-37.00	-34.97	-27.22	-29.83

Table 3.14. HFIR Critical Experiment 4.6
 Control Blades at 42.16 cm
 Outer Annulus Relative Power Distribution
 (100*(Experiment-Calculation)/Experiment)

Axial Height (cm)	Radius (cm)						
	15.15	16.00	17.00	18.00	19.00	20.00	21.00
25.40	-4.28	-28.67	-39.42	-32.42	-9.20	-3.67	-71.15
24.00	-5.97	-16.38	-14.45	-12.17	-11.82	11.21	-19.49
22.00	2.88	-5.09	-3.62	-7.39	-9.39	-5.71	-18.68
20.00	1.11	-9.04	-7.18	-7.52	-9.65	-5.41	-8.43
18.00	1.22	-7.44	-5.98	-4.79	-3.98	2.32	-1.99
16.00	2.18	-6.66	-4.15	-1.63	1.16	6.53	4.45
14.00	2.51	-5.60	-3.16	.16	3.79	9.91	9.69
12.00	2.72	-5.66	-1.63	2.16	5.93	13.75	13.28
10.00	2.34	-4.87	-.33	3.67	9.12	15.54	17.24
8.00	2.13	-4.05	.89	5.93	11.18	19.45	21.45
6.00	2.87	-3.70	3.04	8.32	13.64	23.01	28.06
4.00	3.83	-2.42	4.57	8.66	13.37	21.94	25.97
2.00	5.55	-.32	5.55	9.25	13.56	21.67	25.97
.00	7.49	.66	6.02	10.00	14.69	23.26	28.32
-2.00	6.17	.41	6.46	11.23	16.01	23.73	28.65
-4.00	5.60	-.36	6.93	12.29	16.93	24.34	30.50
-6.00	5.11	-.42	6.69	12.60	18.60	25.15	24.52
-8.00	5.35	-1.13	4.18	9.89	15.01	19.90	13.38
-10.00	5.77	-1.79	2.27	6.08	9.42	12.61	3.38
-12.00	5.51	-2.60	-.05	1.44	2.66	7.69	-1.22
-14.00	5.14	-3.72	-2.12	-2.70	-.51	4.40	-4.89
-16.00	3.55	-5.48	-4.12	-4.92	-4.10	1.56	-9.15
-18.00	.78	-8.56	-4.92	-6.03	-5.60	-.43	-21.58
-20.00	-.47	-9.28	-6.44	-6.18	-8.71	-6.03	-24.89
-22.00	2.87	-7.31	-5.47	-7.99	-8.49	-6.56	-13.87
-24.00	-6.99	-18.81	-17.97	-19.95	-20.64	-5.02	-16.88
-25.40	-8.26	-32.69	-43.57	-36.17	-11.00	-14.01	-328.38

Table 3.15. Peak Power Locations for Critical Experiments

Expt. No.	Max. Relative Power Density			Max. % Expt. Over Calc.		
	Value	<u>Location (cm)</u>		Value	<u>Location (cm)</u>	
		Radial	Axial		Radial	Axial
4.1	2.38	17.00	25.40	34.69	21.00	2.00
4.2	1.64	7.14	0.00	29.29	21.00	4.00
4.3	1.62	7.14	0.00	22.66	20.00	16.00
4.4	1.56	7.14	0.00	19.04	21.00	18.00
4.5	1.50	7.14	0.00	17.66	21.00	-8.00
4.6	2.11	10.00	25.40	30.50	21.00	-4.00

The impact on calculated power distribution of increasing the number of mesh points is shown in Tables 3.16 and 3.17. These power densities are from the fine mesh case for experiment 4.6 which is noted in Table 3.2. A comparison of Tables 3.16 to 3.13 and 3.17 to 3.14 shows that the fine mesh calculation exhibits poorer agreement with experiment. The fine mesh calculation appears to yield a more strongly buckled flux distribution than experimental measurements yield.

For calculation of margin to incipient boiling a parameter of special interest is the quantity of energy deposited in the water coolant (and subsequent temperature increase) as it flows downward through the core. Consequently, it is desirable to accurately estimate the quantity of heat generated along any axial pathway inside the core. Table 3.18 provides a comparison of experimentally measured and calculated, axially averaged relative power densities for each of the six critical experiments. In many cases, the level of agreement exceeds the experimental uncertainty (5%).

The accuracy of calculated local power densities for these critical experiments is summarized in a slightly different manner in Table 3.19. The second column in the table contains the calculation-to-experiment (c/e) ratio for the point in the core at which the percentage by which the experimental value exceeds the calculated value is largest. That is, the point at which the computational method would most underpredict the power on a percentage basis. The third and fourth columns provide data for the hottest axial coolant path in the core. The third column shows the axially averaged c/e ratio. The fourth column shows c/e ratios for the point in the hottest axial path at which the computational method would most underpredict the power on a percentage basis.

The variation in the max. local c/e ratio for whole core casts some doubt on the ability to accurately determine the worth of a perturbation. A reassessment of the manner in which the irradiated foil data were transformed to power density maps seems desirable since no details of the procedure are contained in Ref. 1. A significant impact on experiment/calculation agreement could occur due to the procedure used to count the foil activity. Since the length of these foils is greater than the mesh spacing for which the experimentally derived data is reported, the manner in which the foils were analyzed must be known to correctly interpret the values reported in Ref. 1. The foils were, in fact, counted integrally, and the reported "experimental" values in Ref. 1 determined by an unknown procedure.

Table 3.16. HFIR Critical Experiment 4.6
 Inner Annulus Relative Power Distribution with Finer Computational Mesh
 $100^*(\text{Experiment-Calculation})/\text{Experiment}$

Axial Height (cm)	Radius (cm)						
	7.14	8.00	9.00	10.00	11.00	12.00	12.60
25.40	-65.31	-19.56	-15.09	-16.66	-20.04	-20.42	-30.44
24.00	-41.36	-25.61	-19.64	-17.79	-20.09	-24.15	-30.71
22.00	-32.95	-18.22	-8.94	-5.63	-5.16	-6.38	-14.51
20.00	-13.75	-10.55	-7.02	-4.54	-5.11	-3.97	-9.75
18.00	-3.44	-1.92	-2.70	-3.15	-2.75	.47	-3.10
16.00	2.71	2.54	.70	.11	.30	3.12	.22
14.00	6.17	5.60	4.01	3.53	2.77	5.26	2.91
12.00	8.73	7.94	6.70	6.42	5.74	7.94	6.06
10.00	10.23	9.88	8.99	9.63	9.06	10.38	8.31
8.00	11.54	12.16	12.27	12.44	11.98	12.57	10.37
6.00	12.17	13.60	13.94	14.88	14.52	15.07	12.22
4.00	12.73	14.32	14.22	15.27	15.58	16.16	13.84
2.00	13.21	14.36	14.35	15.47	15.26	16.47	14.68
.00	13.11	14.28	13.72	14.88	14.71	16.54	14.79
-2.00	13.44	14.05	13.46	14.02	14.47	15.79	14.63
-4.00	13.17	13.68	12.99	12.87	13.34	14.73	13.67
-6.00	12.27	13.14	11.65	10.74	11.20	13.31	11.81
-8.00	10.65	11.20	9.33	8.86	8.58	10.86	8.29
-10.00	8.18	8.26	6.57	5.80	6.18	7.91	4.78
-12.00	5.92	6.24	4.09	3.00	3.32	5.21	1.43
-14.00	2.33	2.90	1.07	.57	-.03	2.08	-2.44
-16.00	-2.52	-1.47	-2.73	-3.39	-3.00	-1.55	-5.99
-18.00	-8.74	-6.68	-7.92	-7.35	-6.74	-5.04	-9.38
-20.00	-20.57	-16.65	-16.05	-12.05	-12.50	-10.70	-15.15
-22.00	-40.88	-30.37	-18.73	-23.36	-14.42	-15.14	-22.06
-24.00	-72.56	-45.27	-38.35	-34.43	-31.86	-34.38	-40.68
-25.40	-120.28	-43.70	-32.88	-31.62	-32.82	-31.30	-42.31

Table 3.17. HFIR Critical Experiment 4.6
 Outer Annulus Relative Power Distribution with Finer Computational Mesh
 100*(Experiment-Calculation)/Experiment

Axial Height (cm)	Radius (cm)						
	15.15	16.00	17.00	18.00	19.00	20.00	21.00
25.40	-10.90	-29.49	-43.70	-46.57	-37.49	-60.76	-263.61
24.00	-22.30	-25.62	-30.89	-38.19	-56.48	-51.83	-162.37
22.00	-7.68	-9.77	-15.21	-28.34	-48.41	-75.56	-153.64
20.00	-6.58	-11.49	-16.85	-25.39	-43.35	-66.04	-118.04
18.00	-4.16	-7.47	-12.61	-18.31	-30.02	-44.69	-89.79
16.00	-.72	-3.95	-7.26	-10.36	-17.39	-28.93	-61.44
14.00	2.17	-.02	-2.62	-3.75	-7.72	-14.18	-35.21
12.00	4.87	2.79	2.46	2.98	1.32	.84	-12.45
10.00	6.76	6.09	6.87	8.64	10.48	11.75	6.65
8.00	8.51	8.99	10.59	14.00	16.76	21.64	19.61
6.00	10.61	10.85	14.32	18.31	21.74	28.47	30.67
4.00	12.43	12.98	16.83	19.97	23.17	29.52	31.23
2.00	14.50	15.32	18.31	21.25	24.29	30.45	32.70
.00	16.23	16.16	18.78	22.02	25.50	32.18	35.27
-2.00	14.59	15.50	18.72	22.67	26.25	32.21	35.18
-4.00	13.08	13.83	18.10	22.55	25.92	31.54	35.53
-6.00	11.12	12.21	16.26	21.09	25.50	30.11	27.30
-8.00	9.28	9.37	11.54	15.90	19.01	21.27	11.12
-10.00	6.99	5.79	6.27	8.09	8.19	6.52	-10.76
-12.00	3.57	1.44	-.42	-2.37	-7.21	-12.19	-40.50
-14.00	-.31	-3.67	-7.57	-13.49	-20.48	-32.31	-79.39
-16.00	-5.64	-9.58	-14.81	-22.69	-34.28	-51.35	-119.56
-18.00	-12.29	-16.84	-20.56	-30.28	-45.04	-68.42	-177.83
-20.00	-17.18	-21.24	-26.62	-36.08	-57.93	-92.51	-218.57
-22.00	-17.49	-22.65	-29.14	-43.38	-66.05	-109.12	-221.03
-24.00	-35.80	-41.56	-50.14	-66.46	-94.26	-118.20	-250.99
-25.40	-27.52	-48.62	-66.20	-71.55	-62.59	-115.45	-1150.18

Table 3.18. Comparison of Experimental and Calculated Axially
Averaged Relative Power Densities
 $100^*(\text{Expt.}-\text{Calc.})/\text{Expt.}$

Radius (cm)	Experiment Number					
	4.1	4.2	4.3	4.4	4.5	4.6
7.14	4.56	.66	-.25	-4.31	-5.09	-2.88
8.0	-4.80	-9.06	-10.14	-15.82	-15.70	-9.37
9.0	-2.48	-6.29	-7.49	-10.73	-12.38	-6.70
10.0	-.26	-3.58	-4.18	-6.11	-8.05	-6.00
11.0	.91	-2.39	-3.82	-6.12	-7.80	-4.72
12.0	.55	-4.07	-5.25	-9.35	-10.79	-3.30
12.6	5.70	-.61	-.34	-5.16	-7.02	2.58
15.15	3.32	-.63	-3.77	-8.09	-7.28	3.03
16.0	-3.59	-6.15	-6.52	-8.54	-8.54	-4.91
17.0	-.51	-.38	.13	.07	.40	-.93
18.0	-.76	2.41	2.22	3.19	4.30	2.20
19.0	-1.64	4.75	5.40	6.78	6.06	6.23
20.0	-1.58	9.67	11.19	12.27	11.93	14.16
21.0	-6.76	10.42	9.41	14.67	14.70	14.17

Table 3.19. Local Power Density Ratios for HFIR
Critical Experiments

Control Blade Position (cm)	Calculation-to-Experiment Ratio		
	Max. Local for Whole Core	"Hot Streak" Axial Ave.	Max. Local
42.16	0.695	1.029	0.944
44.45	0.653	0.954	0.838
49.28	0.707	0.993	0.910
54.09	0.773	1.002	0.966
61.72	0.810	1.043	0.991
67.31 (out)	0.823	0.853	0.823

While the worst position for the whole core has a c/e ratio much lower than desired (experimental error $\pm 5\%$), the axially averaged values for the hot streak are acceptable in all but one case. However, the 67.31 cm case is the only critical configuration in which the "hot streak" lies along the outside edge of the outer fuel element. This region lies at the point of transition between a weakly absorbing region (Be, Al, water) and a strongly absorbing region (highly enriched uranium). The assumptions underlying diffusion theory would be least applicable at that point in the model.

The ability to accurately calculate axially averaged power densities is important because the local power at the exit of the "hot streak" determines the margin to incipient boiling and therefore the maximum steady-state overpower limit. These calculations indicate that reactor physics calculation input to the thermal-hydraulic computer codes should yield accurate (within experimental uncertainties) "hot streak" exit temperatures for all except the "rods full out" position. At that configuration, more sophisticated methods of analysis are necessary.

As a result of these studies, Research Reactors Division authorized analyses of these experiments with discrete ordinates methods. Furthermore, the results of those calculations were to be compared with the actual experimental data from Ref. 1 rather than the interpolated values which were the basis for the comparisons in this section. It is those studies, rather than the information reported in this chapter which will form the basis of the Safety Analysis Report reactor physics parameters.

4. TWO DIMENSIONAL FLUX - EIGENVALUE CALCULATION

This section provides a description of the method and model used to calculate reactor physics parameters for the HFIR operating at a power level of 85 MW. Comparisons are made to experimental measurements when data are available. Physics parameters for both beginning- and end-of-life are presented. Unless stated otherwise, the fast flux is defined to be composed of those neutrons with energy greater than 0.1 MeV. Epithermal neutrons have energies between 0.625 eV and 100 eV. Thermal neutrons are those having energies less than or equal to 0.625 eV.

4.1. Method of Analysis

The BOLD-VENTURE system for nuclear reactor analysis is used to determine time dependent fluxes and power distributions (Ref. 7). The system has two major components - a neutronics module, based on the diffusion theory solution to the transport equation, and a depletion module. The depletion module uses fluxes calculated in the neutronics module to estimate nuclide concentrations after irradiation for a user-selected time interval. A variety of utility modules are also available for manipulating files and extracting information.

4.2. VENTURE Input

The input to the VENTURE system was based on data provided in Figs. A.8 through A.10 and Table A.6 of Ref. 1. An R - Z model was created with 17 annular fuel zones, target, reflector and control blade regions. The VENTURE dataset is provided in Appendix A. This section will describe those parts of the input dataset which differed from the description given in Ref. 1.

4.2.1. Target Region

The hydraulic tube was assumed to be empty. As stated in Section 2.2, there were 15 Cm rods and 16 irradiation rods in campaign 65. The irradiation rods were assumed to be the same size as the target rods but composed of solid Al-6061. The values of Cm-244 and Cm-246 loaded into the reactor for campaign 65 were reported by Alexander to be 68.6 and 47.3 grams, respectively. The values tallied by VENTURE from the input dataset were exactly the same.

Since the VENTURE model of the core was an R - Z geometry, the three zones in the central target were homogenized to form 3 concentric cylinders. The outer radius of the hydraulic tube zone was 0.887 cm, the outer radius of the Cm rod zone was 3.547 cm and the outer radius of the material irradiation zone was 6.4 cm.

4.2.2. Fuel Region

Deviating from the description in Ref. 1, the fuel element sideplates were explicitly represented in the VENTURE model. Also the radial mesh was modified from that provided

in Ref. 1. Thin (0.1 mm) zones were included on the inner and outer edges of each of the two elements. This change was made to be consistent with discrete ordinates models which were under development at the time these calculations were performed.

The fuel concentration for each zone was calculated from the fuel distribution data given in Figs. A.9 and A.10 of Ref. 1. The Al filler and clad were both assumed to be Al-6061. Because of the variation in mesh from Ref. 1 values and because of the alloying agents in Al-6061, the atom densities in the VENTURE dataset provided in Appendix A differ from those of Ref. 1. However, the total quantity of U-235 as tallied from the input was found to be 9.47 kg. The value quoted in Ref. 1 is 9.40 kg.

Even though the fuel concentration is constant in the axial direction for any particular radial location, the core was divided into five axial zones. The lower two zones were symmetric about the axial midpoint to the upper two zones. The outermost zones were 1.35 cm thick and the penultimate zones were 5.36 cm thick.

The additional two zones at the top and bottom of the core were added so that fuel in those regions could be depleted with the appropriate flux spectra and intensity. It was expected that the presence of water above and below the core would have a significant local impact on power generation. Depletion with axially averaged flux values would probably not yield accurate power distributions at the edges of the elements.

4.2.3. Control Blades

In Ref. 1, the outer element sideplate and inner control blade and water gap between these structures were all homogenized into one region. In the VENTURE model these structures were represented separately. However, for the control blade, the Al clad was homogenized with the control poison material.

Blackness coefficients were used to modify the diffusion coefficient in the europium. The procedure was the same as that described in Section 3.

4.3. Fission Product Treatment

The depletion module of the VENTURE system is a computer program called BURNER (Ref. 8). The program requires as input a list of the fission product nuclides whose quantities are to be estimated at user-input time intervals. As a part of this study, the input to the BURNER program was updated to include ENDF/B-V data. The selection of fission products to be calculated was also examined.

The selection process for determining "explicitly represented" fission products is described in Ref. 9. The chosen nuclides are presented in Fig. 4.1. (This figure is a correction to a similar one presented in Ref. 9.) The fission product production chains shown in Fig. 4.1 were input to the BURNER program and this input is included in the VENTURE dataset provided in Appendix A with identifying labels for each chain.

ORNL-DWG 12509

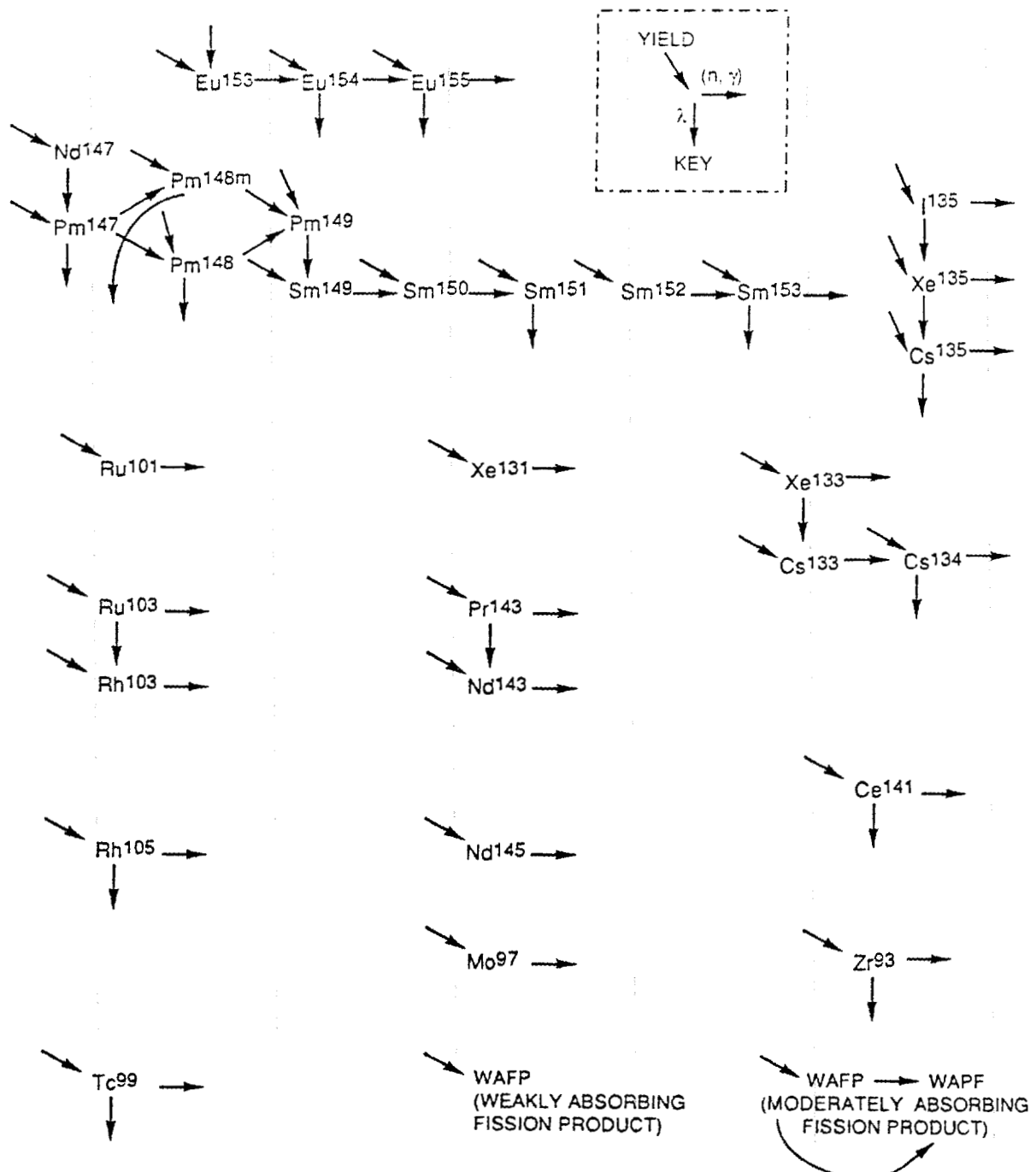


Fig. 4.1. Fission Product Chains Explicitly Represented in the Burner Input.

All fission yields and decay constants were from ENDF/B-V data or more recent values. Data for fission yields were not only updated for U-235 and U-238 but also for Th-232, U-233, U-236, Pu-239, Pu-240 and Pu-241. Where choices were available, data for thermal reactors were selected.

As noted in Ref. 9, each of the other fission product nuclides were combined (using the fission yield as a weighting function) into either a moderately absorbing fission product (MAFP) or a weakly absorbing fission product (WAFP) depending on its calculated reaction rate at the end of the fuel cycle. The constituents of the MAFP are shown in Table 4.1 and the components of the WAFP are shown in Table 4.2.

Table 4.1. Constituents of the Moderately Absorbing Lumped Fission Product^a

Nuclide	Yield	Nuclide	Yield	Nuclide	Yield
Kr-82	1.25E-6	Ru-102	4.20E-2	Ba-140	6.32E-2
Kr-83	5.27E-3	Ru-104	1.82E-2	La-139	5.17E-2
Rb-85	1.31E-2	Pd-105	9.83E-11	La-140	5.67E-3
Zr-92	5.97E-2	Pd-107	1.63E-3	Ce-143	5.97E-2
Zr-95	6.47E-2	Pd-108	7.10E-4	Ce-144	5.45E-2
Zr-96	6.25E-2	Ag-109	2.98E-4	Pr-141	5.89E-2
Nb-95	1.64E-6	Cd-113	1.24E-4	Nd-146	2.99E-2
Mo-98	5.78E-2	I-129	6.59E-3	Nd-148	1.69E-2
Mo-99	6.13E-2	I-131	2.83E-2	Nd-150	6.46E-3
Mo-100	6.31E-2	Xe-132	3.20E-2	Pm-151	4.20E-3
Ru-100	2.38E-7	Xe-134	7.68E-2	Eu-156	1.35E-4

^aTotal Yield=0.945

4.4. Actinide Production

In order to calculate the contents of the Cm target rods after irradiation, it was necessary to generate the BURNER input for the production paths for the transcurium actinides. These paths are shown in Figs. 4.2 and 4.3. This input is included in the VENTURE dataset provided in Appendix A with identifying labels for each chain.

4.5. Control Blade Position

Figure 4.4 shows control blade position as a function of energy released from the core for four HFIR cycles. These data were supplied by R. M. Stinnett, Research Reactors Division and were prepared during April, 1986. Since at that time the HFIR was operating at 100 MW, the abscissa can also be read as days of operation since startup.

Table 4.2. Constituents of Weakly Absorbing Lumped Fission Product

Nuclide	% Yield*	Nuclide	% Yield	Nuclide	% Yield	Nuclide	% Yield
Ge-73	1.06E-4	Pd-110	2.23E-2	Te-122	4.45E-8	Nd-144	1.07E-3
Ge-76	3.59E-3	Ag-111	1.97E-2	Te-123	9.88E-11	Sm-147	0.0
As-75	1.12E-3	Cd-110	2.82E-9	Te-124	6.17E-6	Sm-148	5.73E-6
Se-77	8.37E-3	Cd-111	1.55E-11	Te-125	7.12E-8	Sm-154	7.57E-2
Se-78	1.66E-2	Cd-112	1.28E-2	Te-126	2.49E-6	Gd-156	5.65E-8
Se-80	0.123	Cd-114	1.13E-2	Te-127m	6.01E-5	Gd-157	6.47E-3
Br-81	0.210	Cd-115m	2.37E-6	Te-128	0.350	Gd-158	3.22E-3
Kr-84	0.969	Cd-116	1.06E-2	Te-129m	0.316	Tb-159	1.04E-3
Kr-85	2.33E-3	In-115	1.03E-2	Te-130	1.45	Tb-160	3.26E-8
Kr-86	1.95	Sn-115	5.39E-10	Te-132	4.22		
Rb-86	7.57E-5	Sn-116	2.22E-12	I-127	0.130		
Rb-87	2.55	Sn-117	1.08E-2	I-130	2.46E-4		
Sr-89	4.85	Sn-118	1.21E-2	Xe-128	1.43E-5		
Sr-90	5.91	Sn-119	9.59E-3	Xe-129	0.659		
Y-89	5.84E-7	Sn-120	1.17E-2	Xe-130	2.46E-4		
Y-90	2.35E-4	Sn-122	1.23E-2	Xe-136	4.28		
Zr-91	1.58E-7	Sn-123	1.93E-4	Cs-136	5.31E-3		
Zr-94	6.42	Sn-124	2.20E-2	Cs-137	6.27		
Mo-95	1.64E-4	Sn-125	1.94E-2	Ba-134	3.52E-8		
Mo-96	5.99E-4	Sb-121	1.29E-2	Ba-138	6.58		
Ru-105	b	Sb-123	1.42E-2	Ce-140	6.37E-7		
Ru-106	0.391	Sb-124	6.17E-6	Ce-142	5.92		
Pd-104	6.56E-8	Sb-125	1.03E-2	Pr-142	c		
Pd-106	6.92E-7	Sb-126	5.70E-2	Nd-142	2.88E-8		

*% Yield = atoms produced per atom fissioned $\times 100$, Total % Yield = 53.9541.

*Immediately decays to Rh-105.

*Half-life = 19 hr.

The differences between the control blade position curves are believed to be due to differences in the quantity and type of materials being irradiated for the three cycles. Since the VENTURE model presented in Appendix A was prepared under the assumption that the material irradiation positions were empty (contained blanks), an expected lifetime of 23 days, corresponding to the value contained in Ref. 1, seemed reasonable.

ORNL-DWG 91M-12510

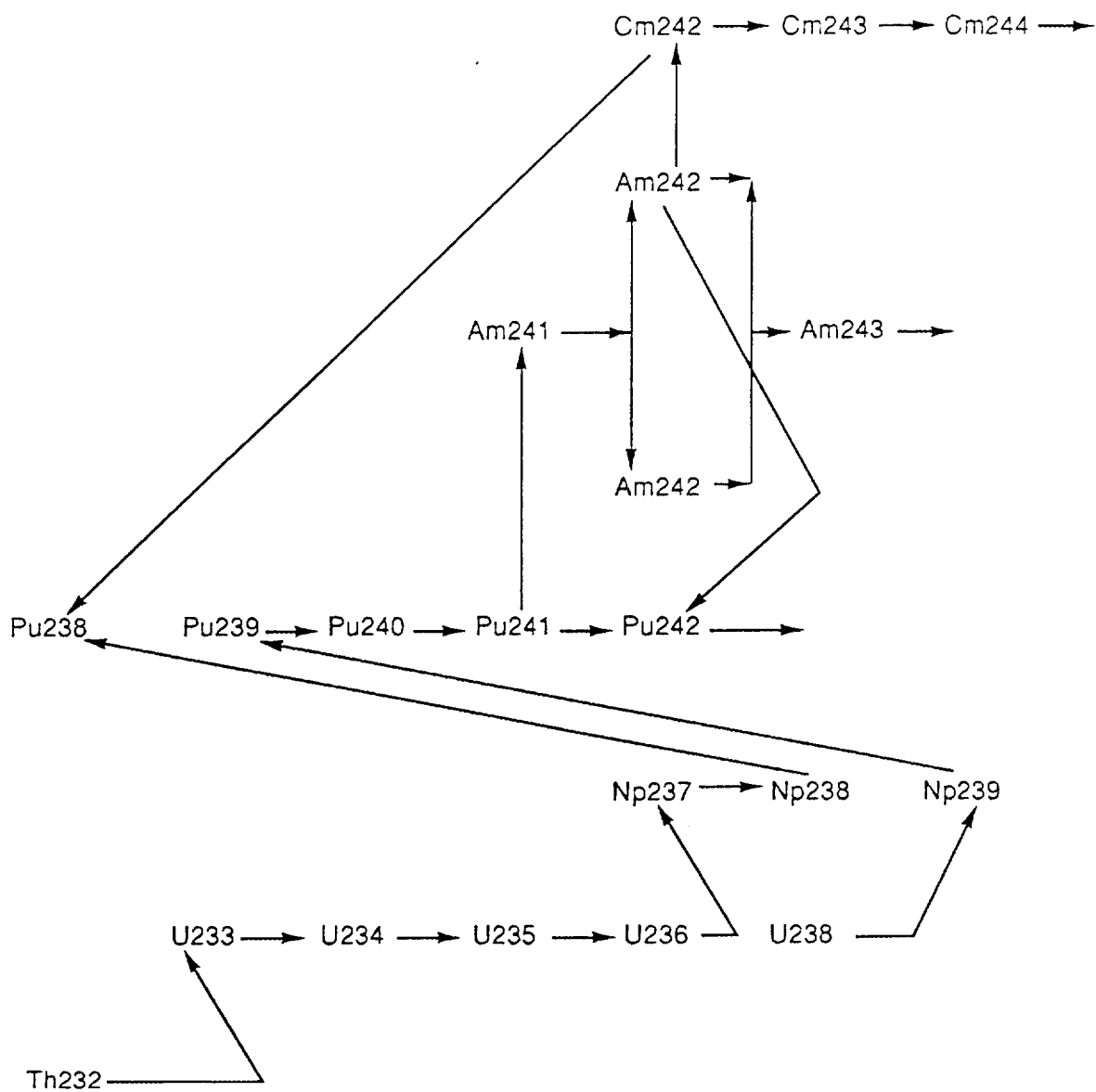


Fig. 4.2. Actinide Production Chains (Part I).

ORNL-DWG 91M-12511

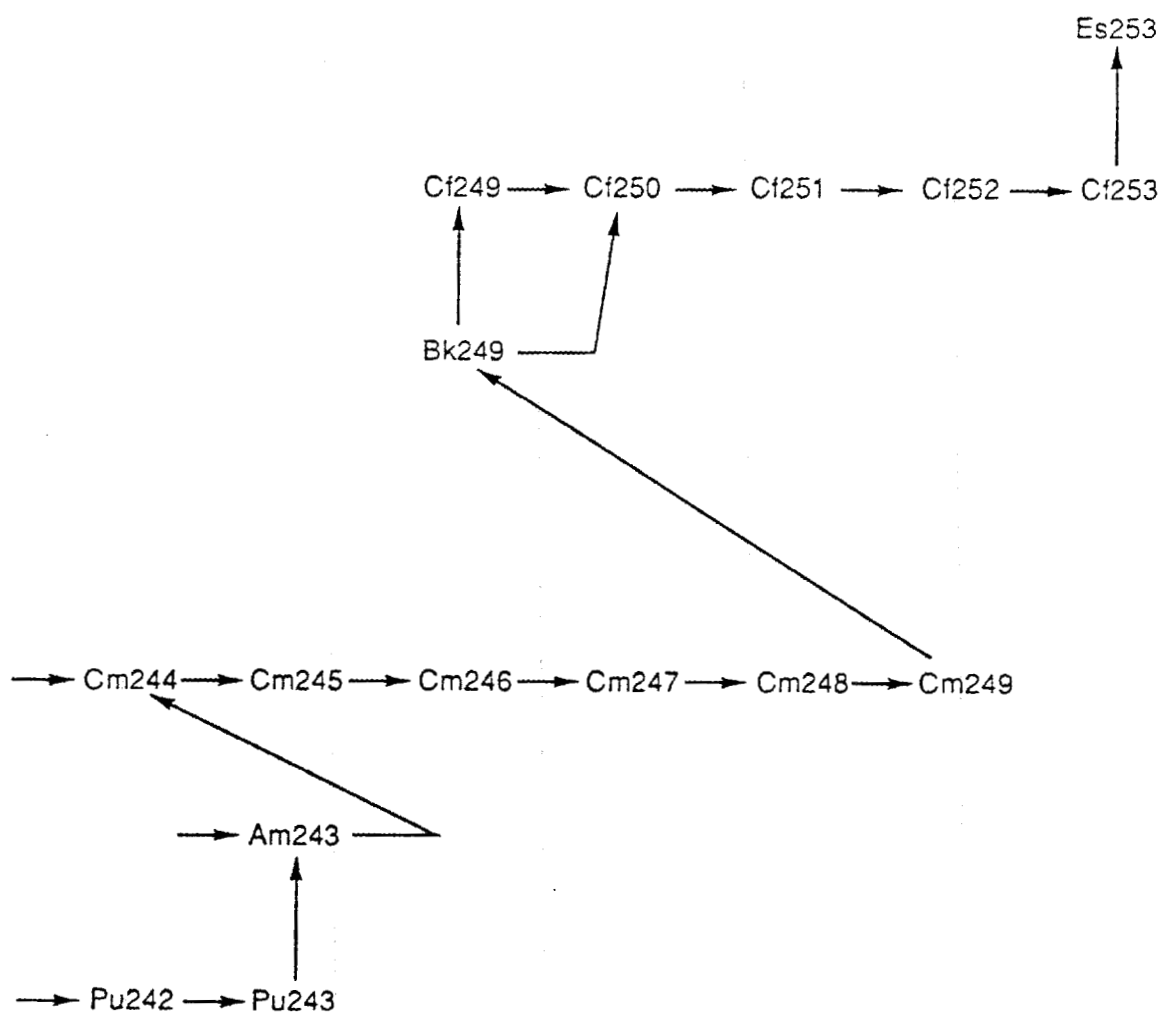


Fig. 4.3. Actinide Production Chains (Part II).

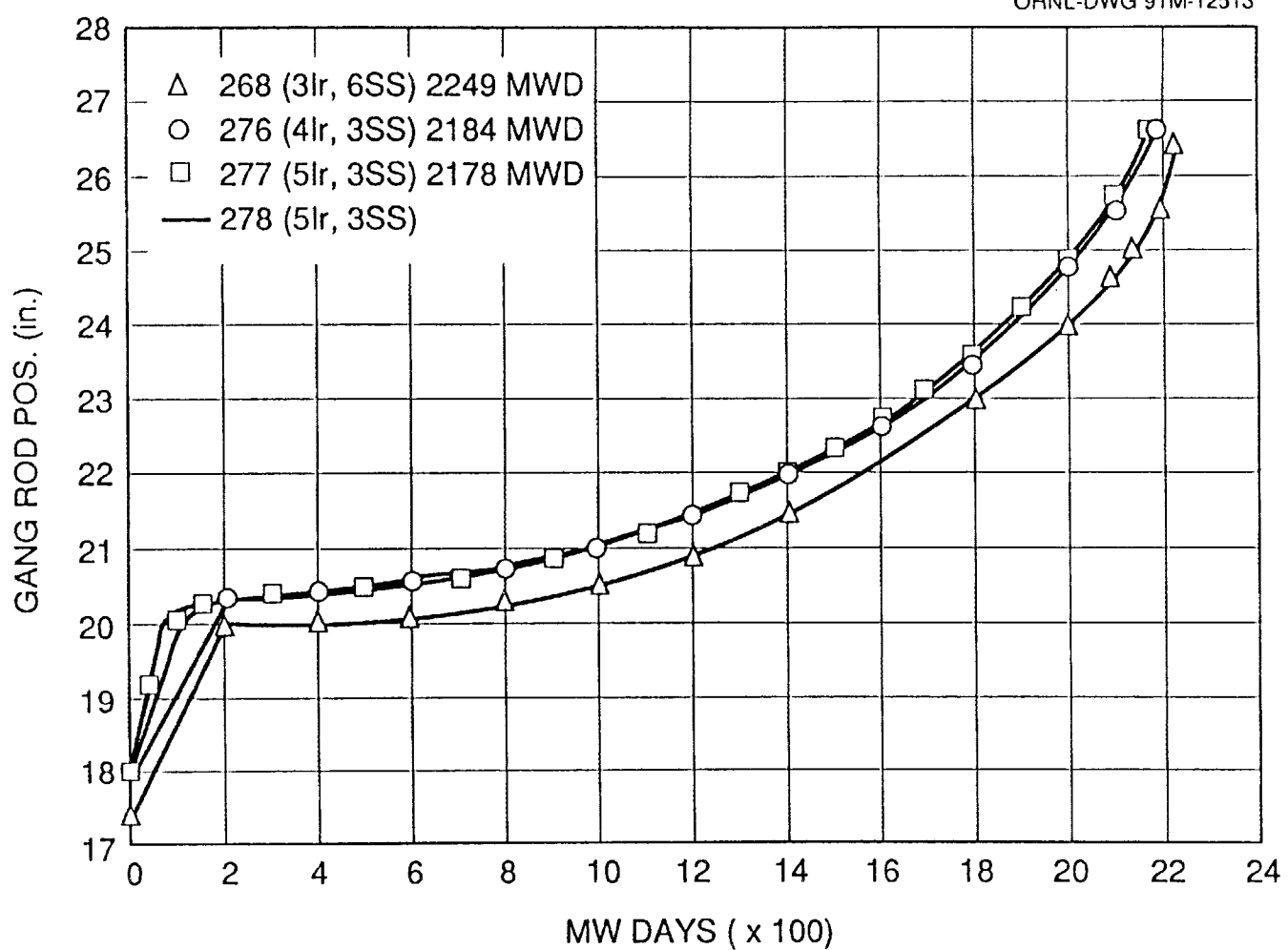


Fig. 4.4. HFIR Control Blade Position

Figure 4.5 is a comparison of the control blade position/irradiation interval pairs which were input to VENTURE with one of the actual control blade position curves from Fig. 4.4. The asterisks on the figure indicate the positions/times at which k-effectives were calculated.

It is apparent that for calculations at 1200, 1600, 1800, and 2000 megawatt-days the calculated k-effective would probably be greater than 1.0 (control blade in VENTURE model is more withdrawn than actual condition). However, these particular positions are believed to be the correct calculation points because they provide for the correct control rod position for the irradiation intervals following these days. Local parameters around the control blade (nuclide concentrations, power densities) are more accurately estimated by this technique.

Note though, that at beginning- and end-of-life (0, 50, 100 and 2300 MW-days) the k-effective calculation was performed with the VENTURE model corresponding to the actual control blade position for those times. Thus accurate estimates of k-effective, flux and power distribution should be obtainable at those times. Not by coincidence these are the times for which experimental measurements are available (beginning-of-life) and for which safety analyses are to be performed using discrete ordinates codes (beginning- and end-of-life).

4.6. Results of Calculations

The calculated k-effectives for several exposure times are shown in Table 4.3. The same data are presented graphically in Fig. 4.6. Note that beginning-of-cycle k-effectives exceed 1.0 by approximately the same degree as found in the beginning-of-cycle-typical critical experiments 4.1 and 4.6. Note also that, as in the critical experiments, k-effective first falls and then rises as the control blades are withdrawn. The high end-of-cycle k-effectives are not readily explainable.

Table 4.3. Calculated k-effectives for
HFIR Fuel Cycles

Time (d)	k-effective
0.0	1.0323
0.588	1.0140
1.176	0.9931
14.117	0.9901
18.823	0.9985
21.176	1.0093
23.529	1.0198
27.058	1.0170
30.587	1.0054

The time at which calculated k-effective reaches 1.0 for constant cycle power of 85 MW is 32.2 days. The actual cycle length for 1990-1991 time frame varies from 21 to 23 days. The Experiment Coordinator for HFIR estimates that the cycle length for a core with no experiments - corresponding to the VENTURE computer model - would have a cycle length of 24 +/- 2 days. Whereas the estimated cycle length reported in Ref. 1 was 40% less than the actual value, the currently calculated cycle length is 34.2% longer than the actual value.

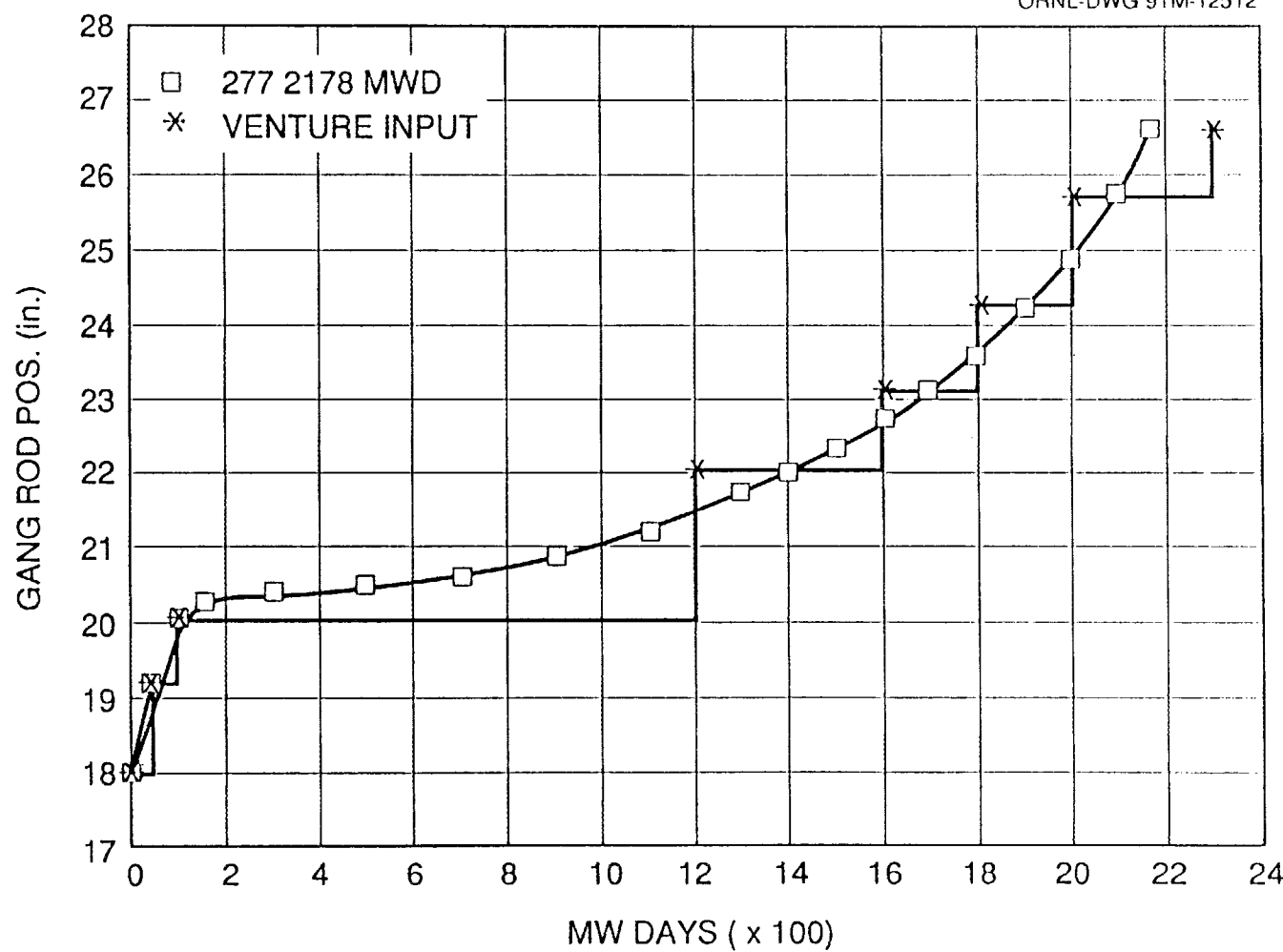


Fig. 4.5. Comparison of VENTURE Mode to Actual HFIR Control Blade Position.

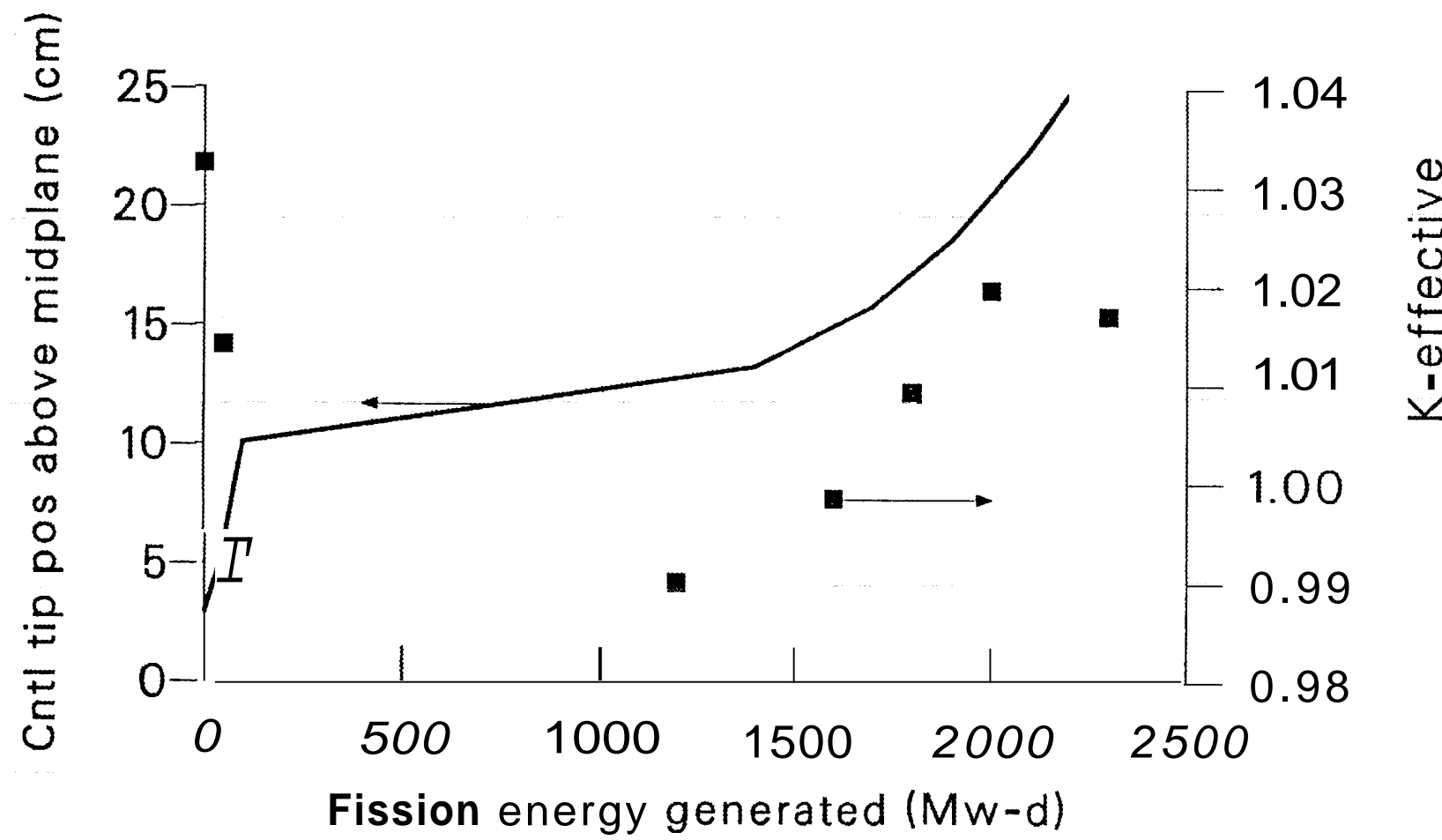


Fig. 4.6. Calculated k-effectives during HFIR fuel cycle.

During 1986, the HFIR operated at 100 MW and the cycle length (as shown in Fig. 4.4) varied from 22 to 22.5 days. It is stated in Ref. 1 (published after 5 years of HFIR operation) that the cycle length is 23 days. If the 23 day figure is multiplied by the ratio of the old-to-new power, an estimated cycle length of 27.1 days is obtained. The current estimate of lifetime would then be 19% longer than expected.

A particular cycle length is strongly dependent on the experiments in the Be reflector during that cycle. During the past five years, no core configurations exist which correspond to the computational model. Considering the information which is available, the 34.2% figure mentioned previously can be considered a maximum deviation.

Pertinent flux values are given in Table 4.4. Also shown in Table 4.4 are values from Ref. 1 adjusted to a power level of 85 MW. Note that the thermal flux in Ref. 1 is defined to be the flux less than or equal to .414 eV. The two current values in Table 4.4 bracket the Ref. 1 thermal flux definition.

The values from the current study are in reasonably good agreement with those from Ref. 1. The maximum unperturbed flux in the island is now estimated to be about 20% lower than the previous value. However, the average in the island target is about 20% higher. Note that the Ref. 1 target is 300 grams of Pu-242 whereas the current target is curium, the composition being that described in Section 2.

The large disagreement at the Be-water interface is likely due to the steep decline in thermal flux in the water region. The value for the current estimate is at a point 0.5 mm inside the outer Be edge. It should be noted that the accuracy of diffusion theory at interfaces between materials is frequently poor.

A radial flux distribution slightly above the axial centerline of the reactor, at the point of peak thermal flux, is shown in Fig. 4.7. The data shown are for beginning-of-life. End-of-life data are shown in Fig. 4.8. The thermal flux depression inside the two fuel elements is readily apparent. The Be reflector outer edge is at 540 mm. and the transition to water rapidly decreases the thermal flux.

Radial profiles of flux ratios are shown in Figs. 4.9 and 4.10. The change in ratios from beginning- to end-of-life is generally small.

Axial flux profiles at seven irradiation positions are shown in Figs. 4.11 through 4.24. The radial locations in the VENTURE model corresponding to these positions are the (empty) island hydraulic tube (4.4 mm), the curium target location (20.8 mm), the large and small removable Be facilities (276.2 mm), the control rod access plug facilities (321.8 mm), the inner small Vertical Experimental Facility (VXF) (387.1 mm), the outer small VXF (442.1 mm), and the large VXF (462.3 mm).

4.6.1. Power Distribution Profiles

To predict time-dependent thermal-hydraulic performance, time dependent power distributions are required as input. In past thermal-hydraulic studies, these distributions were taken from Ref. 1. The following extract from Ref. 1 describes the manner in which these distributions were derived.

Table 4.4. Summary of Neutronics Parameters

	Neutron Flux (*10 ¹⁵ n/cm ² s)			
	Ref 1 (100 MW)	Ref 1 (85 MW)	Current Estimate $\phi_{Th} < .33\text{eV}$	Current Estimate $\phi_{Th} < .625\text{eV}$
Thermal^a				
Maximum unperturbed in island	5.5	4.675	3.906 ^b	3.969 ^b
Average in typical 300-g ²⁴² Pu island ^c	2.0	1.70	2.048	2.116
Maximum unperturbed in Be reflector				
Beginning of fuel cycle	1.1	0.94	1.013	1.045
End of fuel cycle	1.6	1.36	1.523	1.545
Maximum unperturbed at Be-H ₂ O reflector interface				
Beginning of fuel cycle	0.14	0.12	0.235	0.236
End of fuel cycle	0.17	0.14	0.326	0.327
Average in fuel region				
Beginning of cycle	0.33	0.28	0.301	0.301
End of fuel cycle	0.45	0.38	0.428	0.428
Total nonthermal				
Average in island target	2.4	2.04	2.320 ^d	2.252 ^d
Maximum in fuel region	4.0	3.40	3.585 ^d	3.516 ^d
Length of typical fuel cycle, days	23	27 ^e	30.6	--

^aThermal in Ref. 1 is defined as flux <.414eV.^bFrom critical exp. with control blades at 44.45cm with power adjusted to 85 MW.^cCurium target used in current estimate.^dBeginning of life.^eHFIR experiment coordinator estimates the length of a fuel cycle with no experiments to be 24 + -2 days.

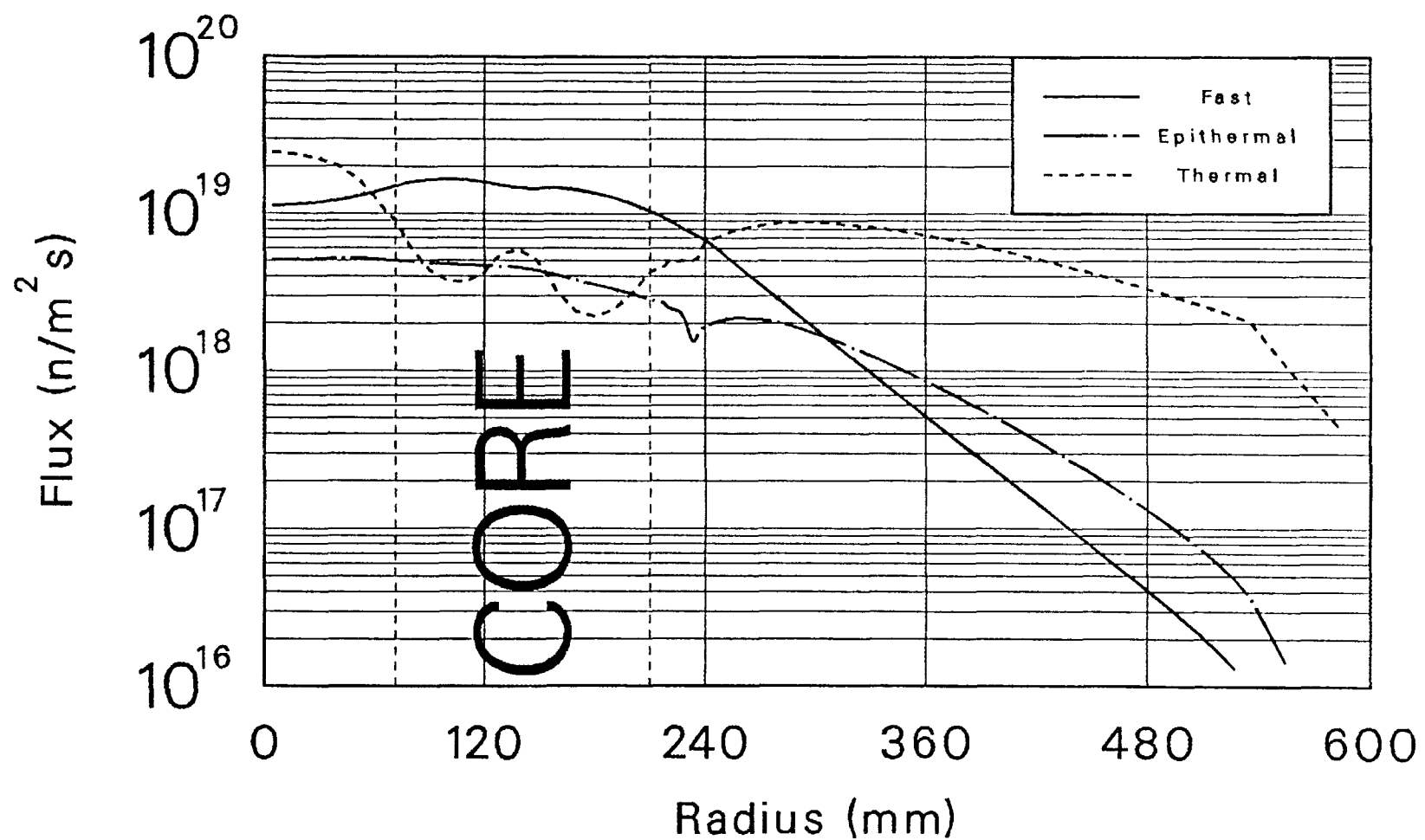


Fig. 4.7. Radial flux profile at axial location of 43.4 mm, beginning-of-life.

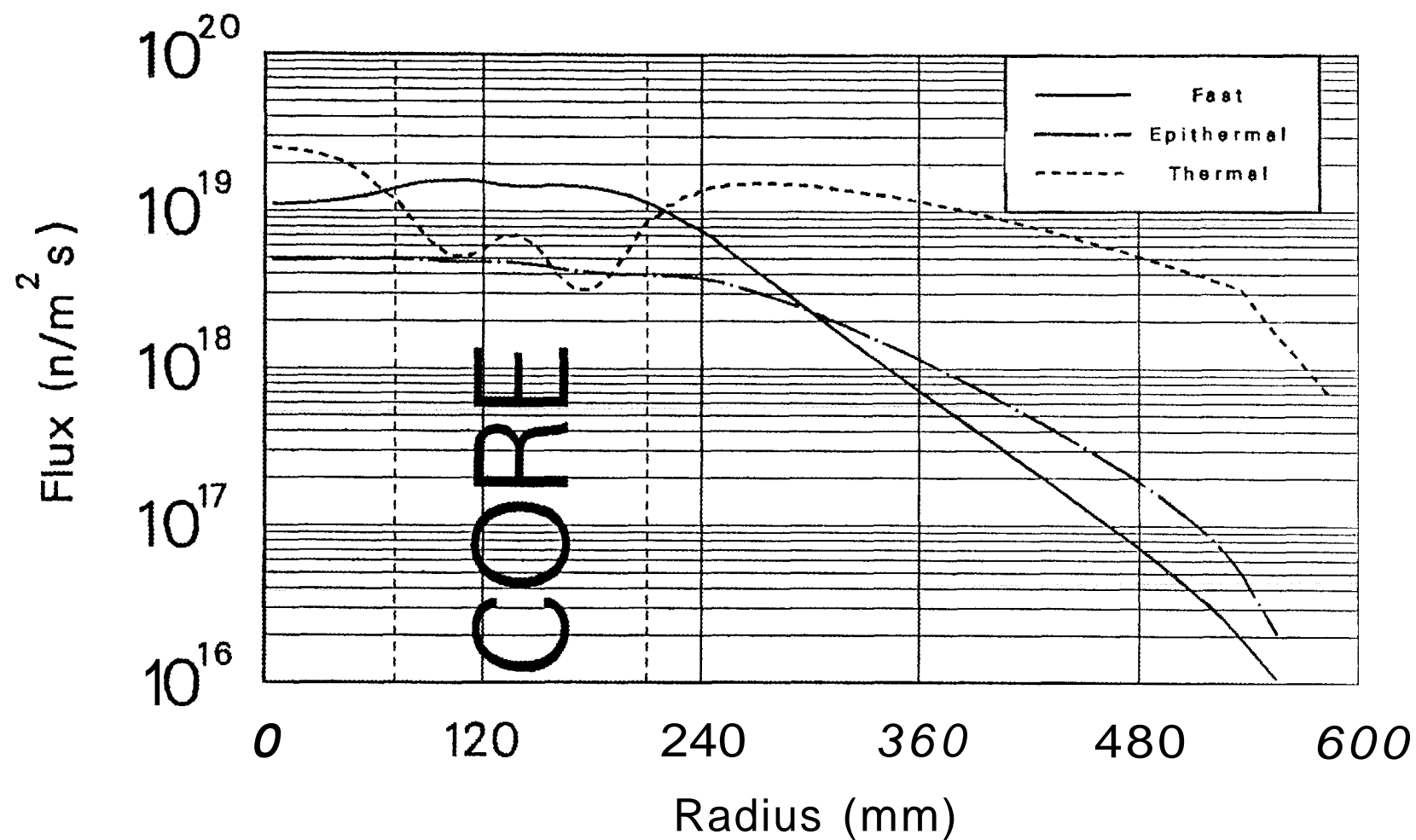


Fig. 4.8. Radial flux profile at axial location of 43.4 mm, end-of-life.

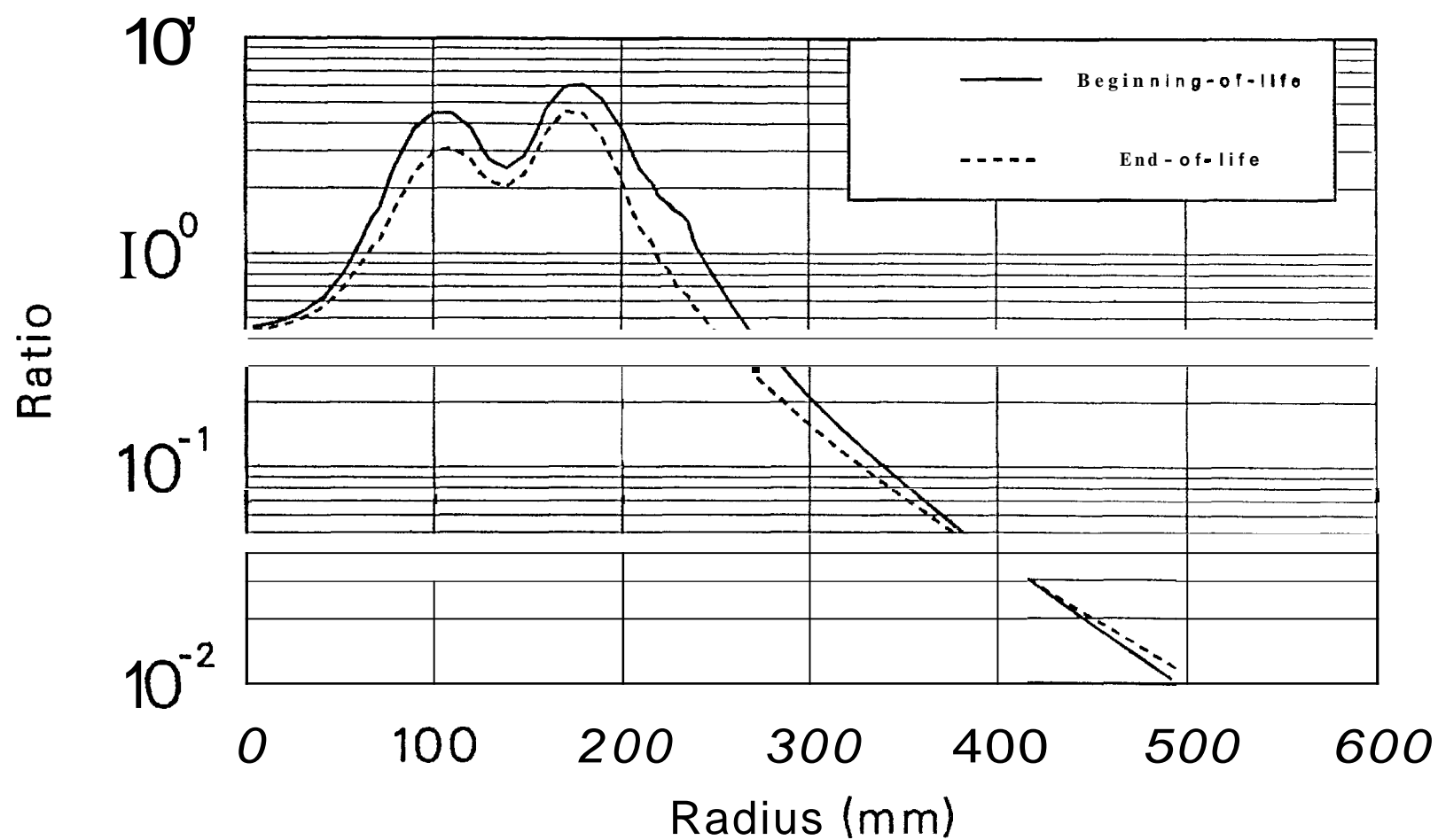


Fig. 4.9. Radial fast/thermal flux ratio profile at axial location of 43.4 mm.

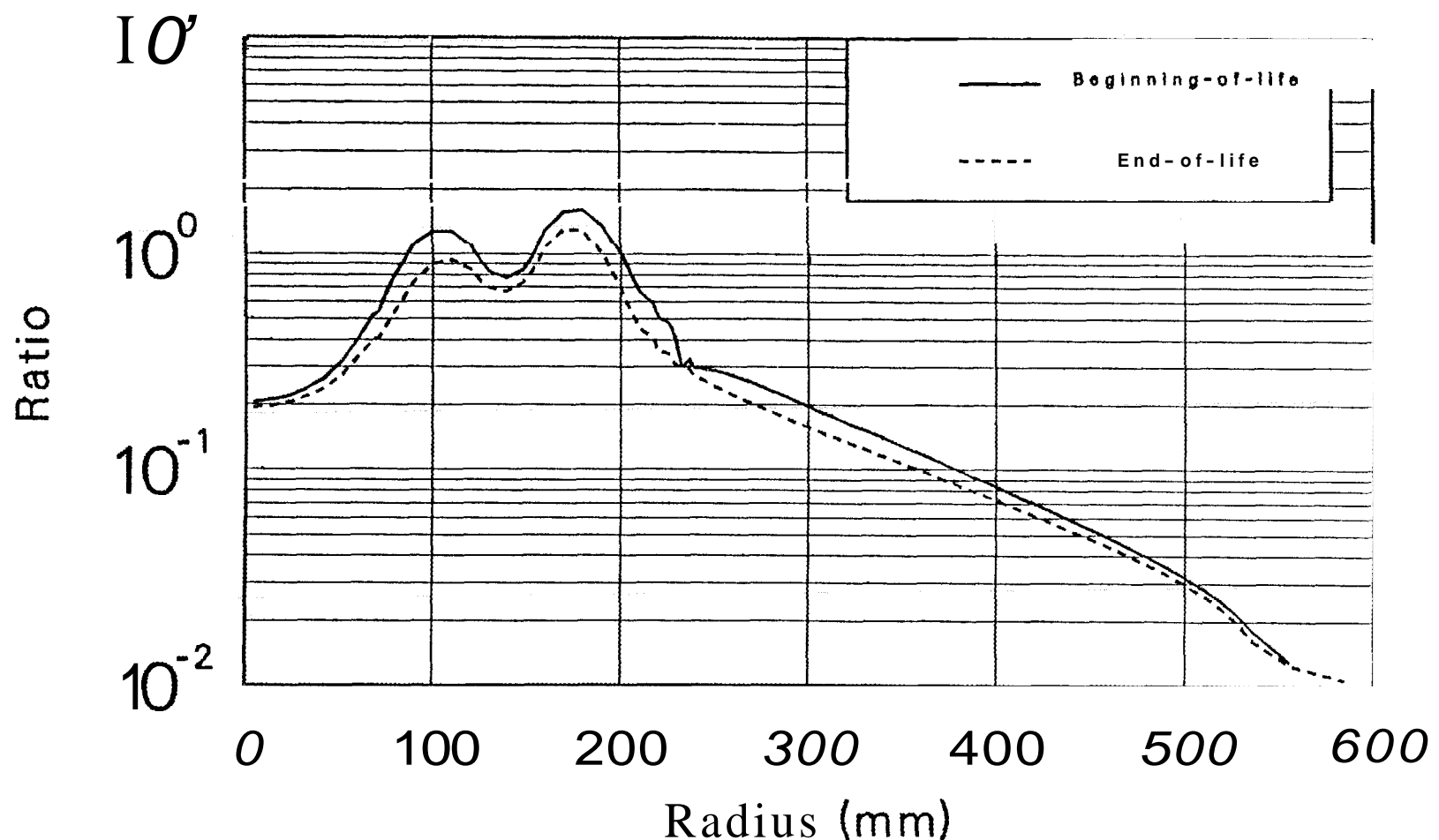


Fig. 4.10. Radial epithermal/thermal flux ratio profile at axial location of 43.4 mm.

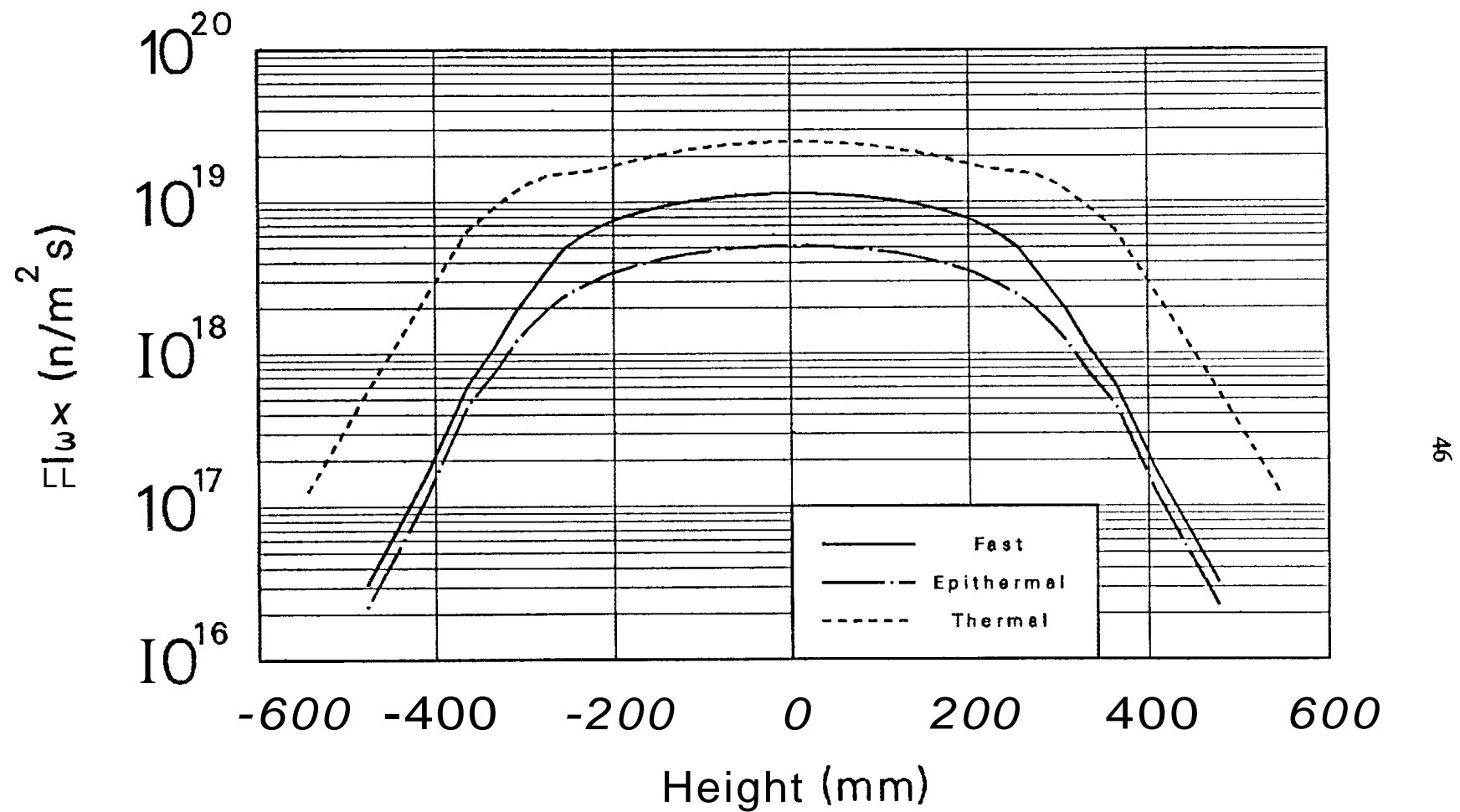


Fig. 4.11. Axial flux profile at island hydraulic tube, beginning-of-life.

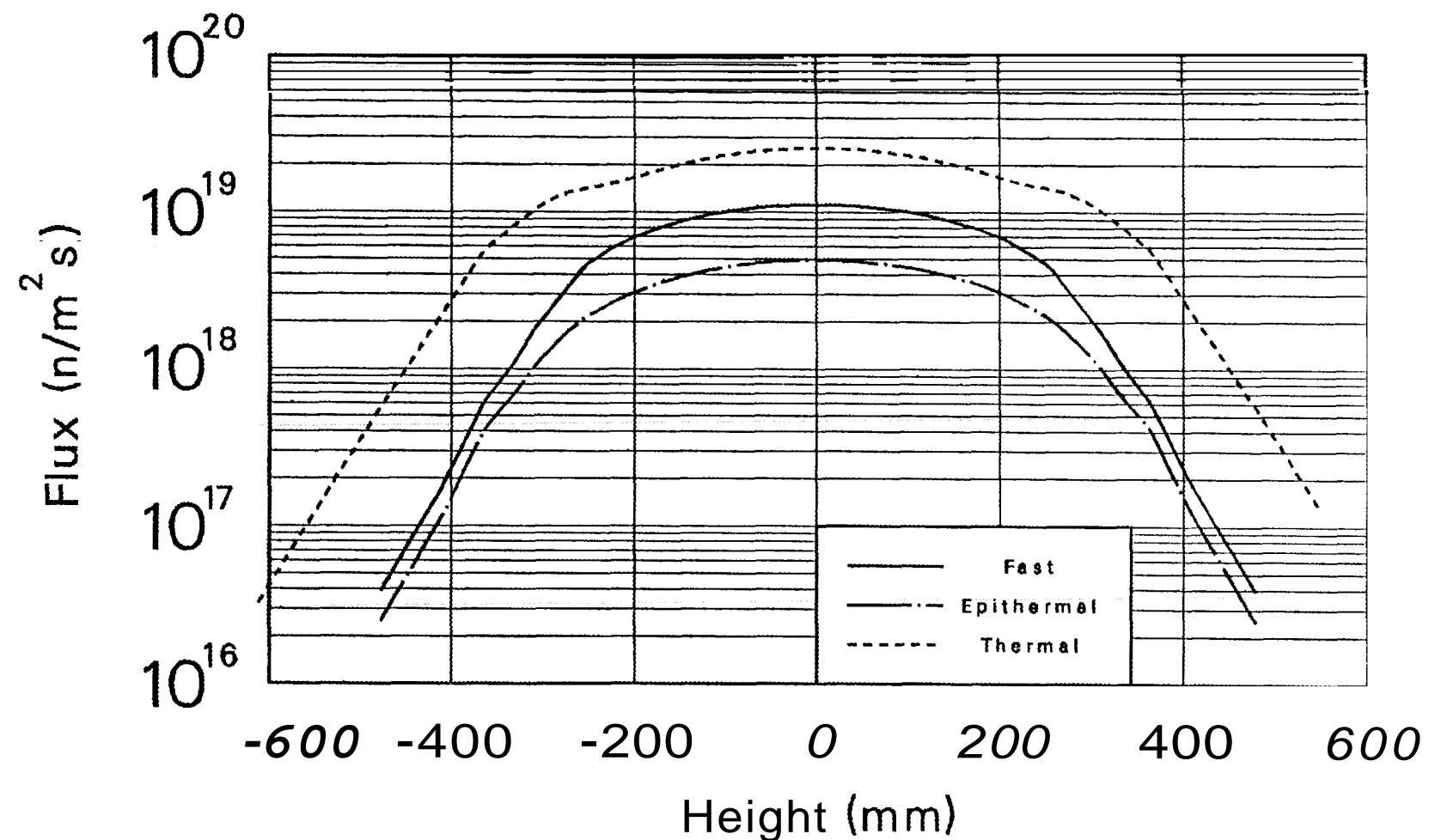


Fig. 4.12. Axial flux profile at island hydraulic tube, end-of-life.

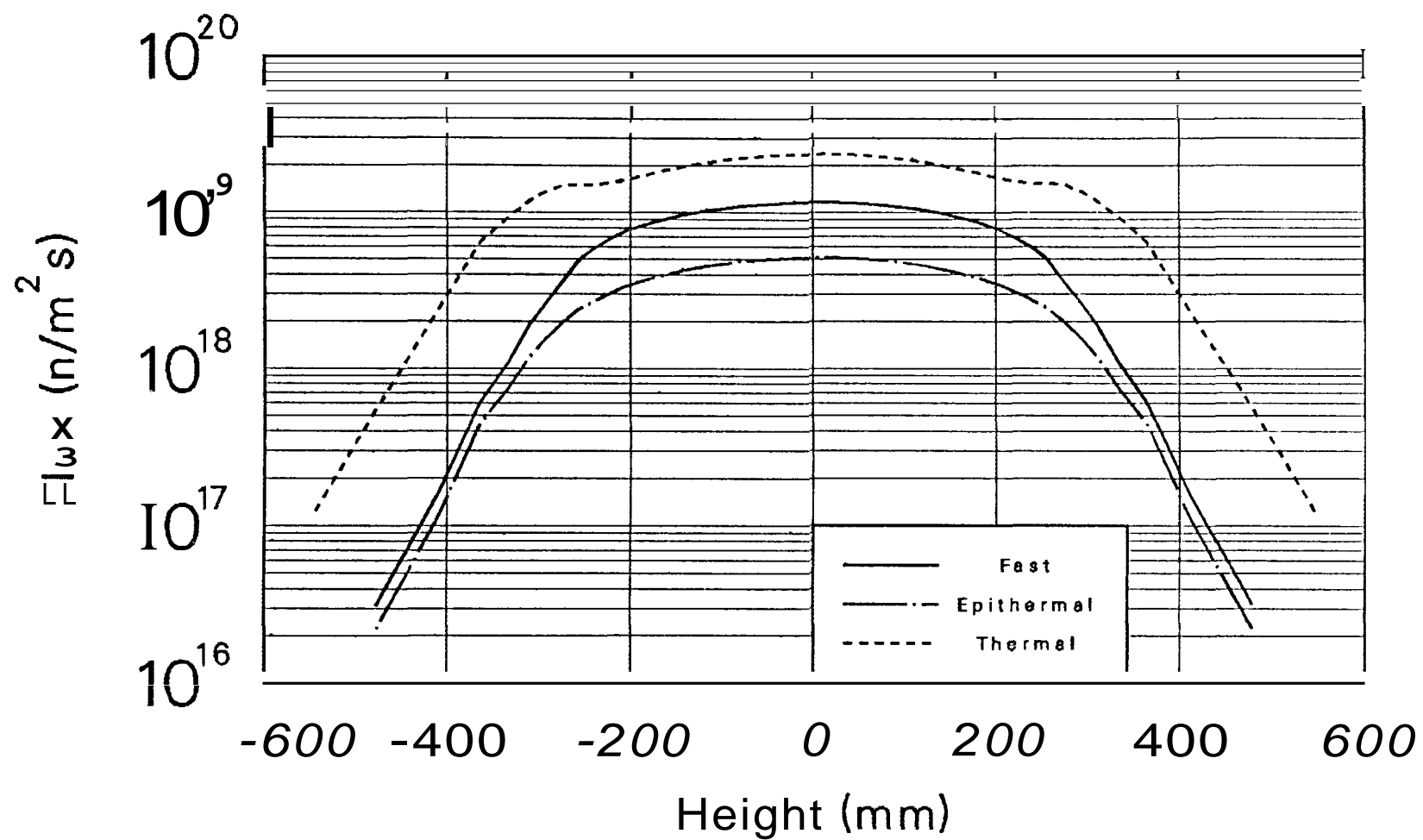


Fig. 4.13. Axial flux profile at curium target rods, beginning-of-life.

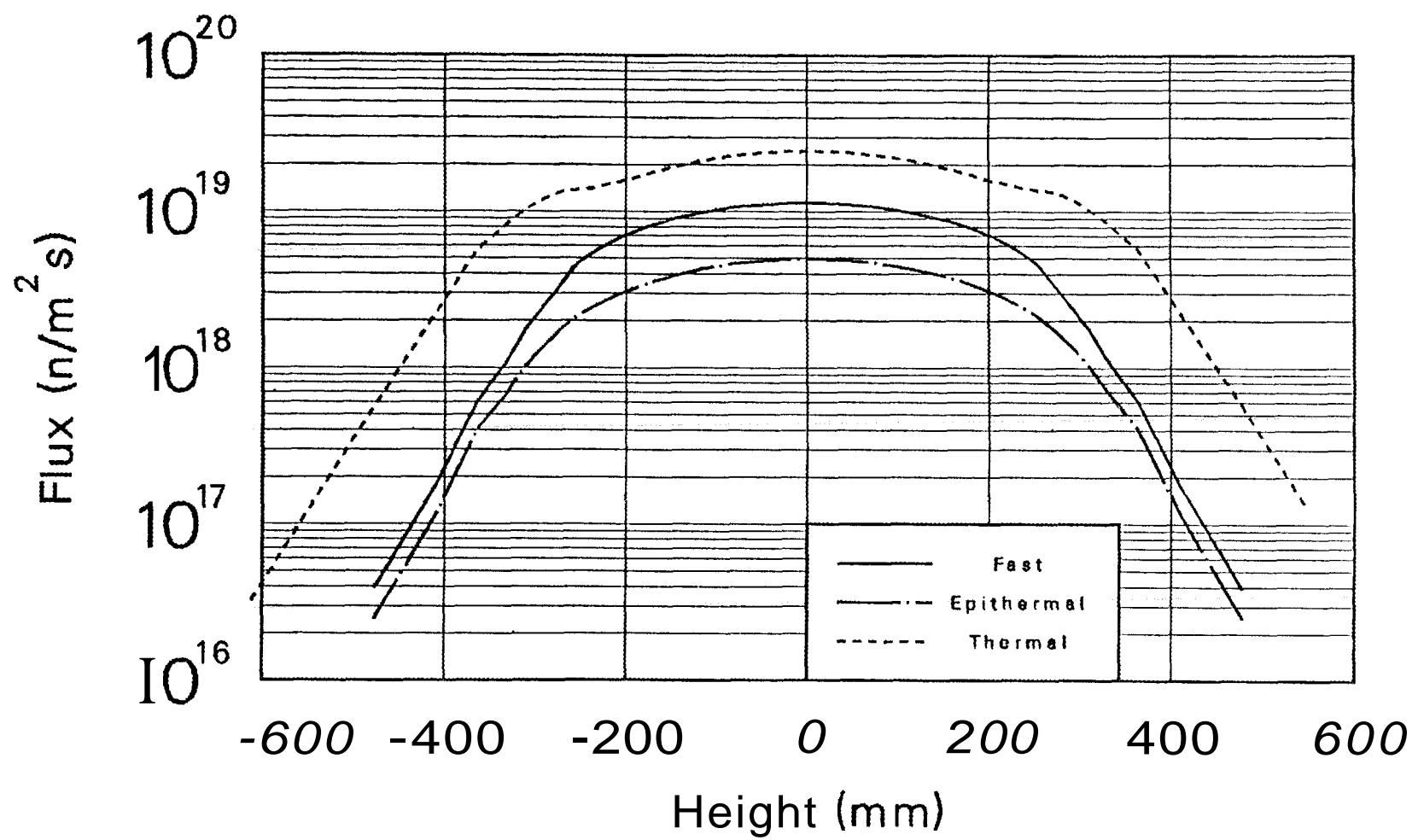


Fig. 4.14. Axial flux profile at curium target rods, end-of-life.

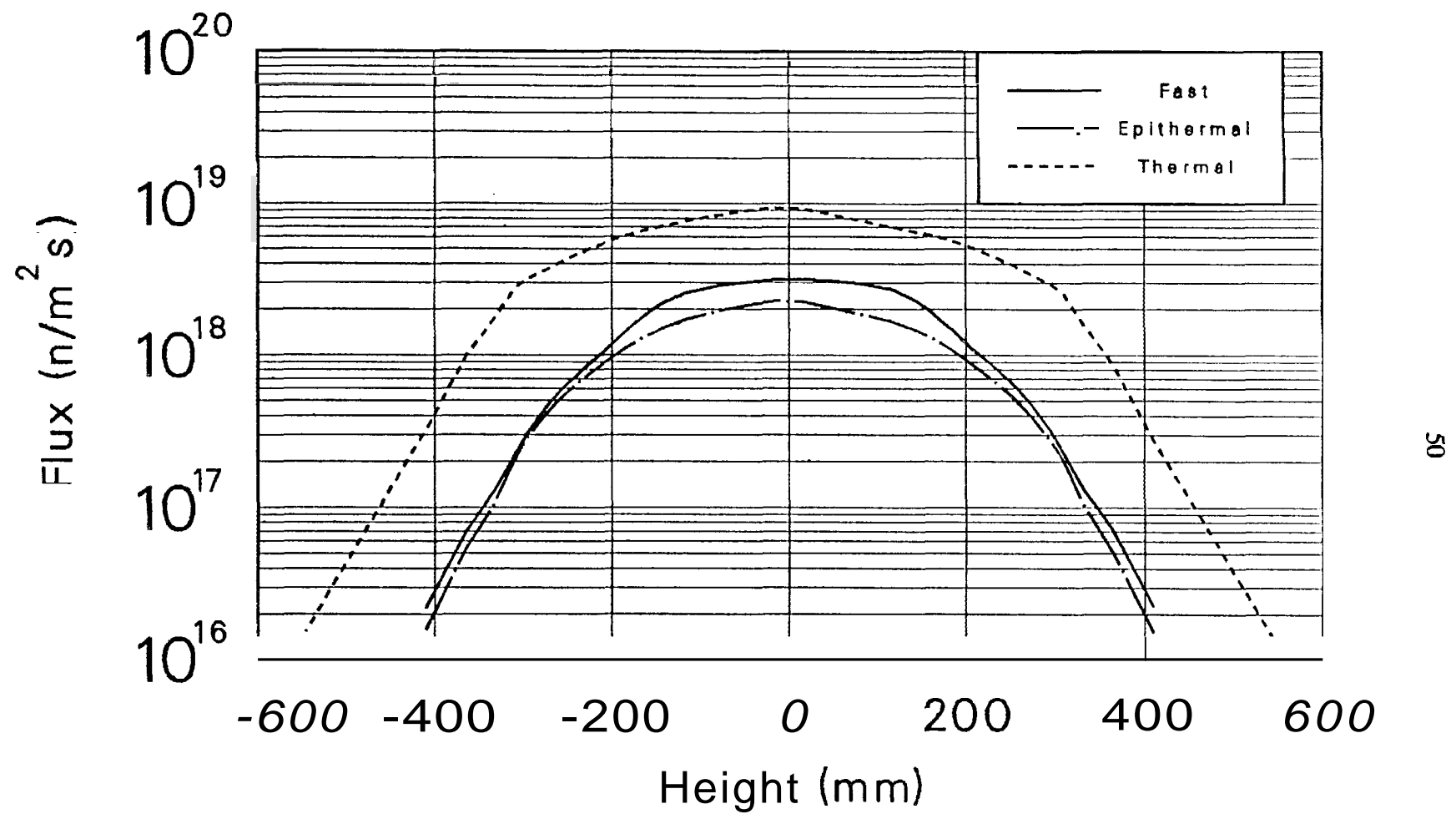


Fig. 4.15. Axial flux profile at removable Be facilities, beginning-of-life.

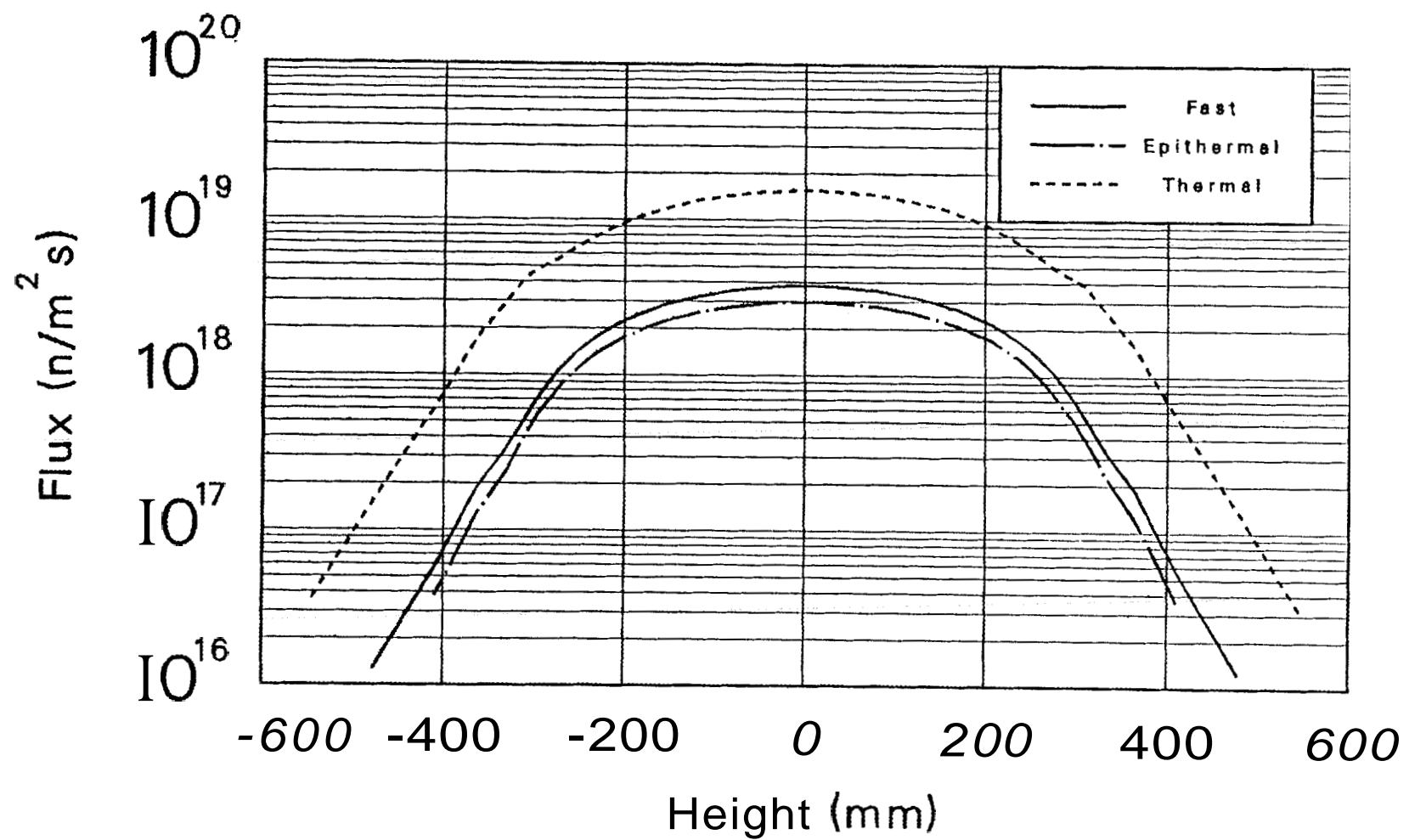


Fig. 4.16. Axial flux profile at removable Be facilities, end-of-life.

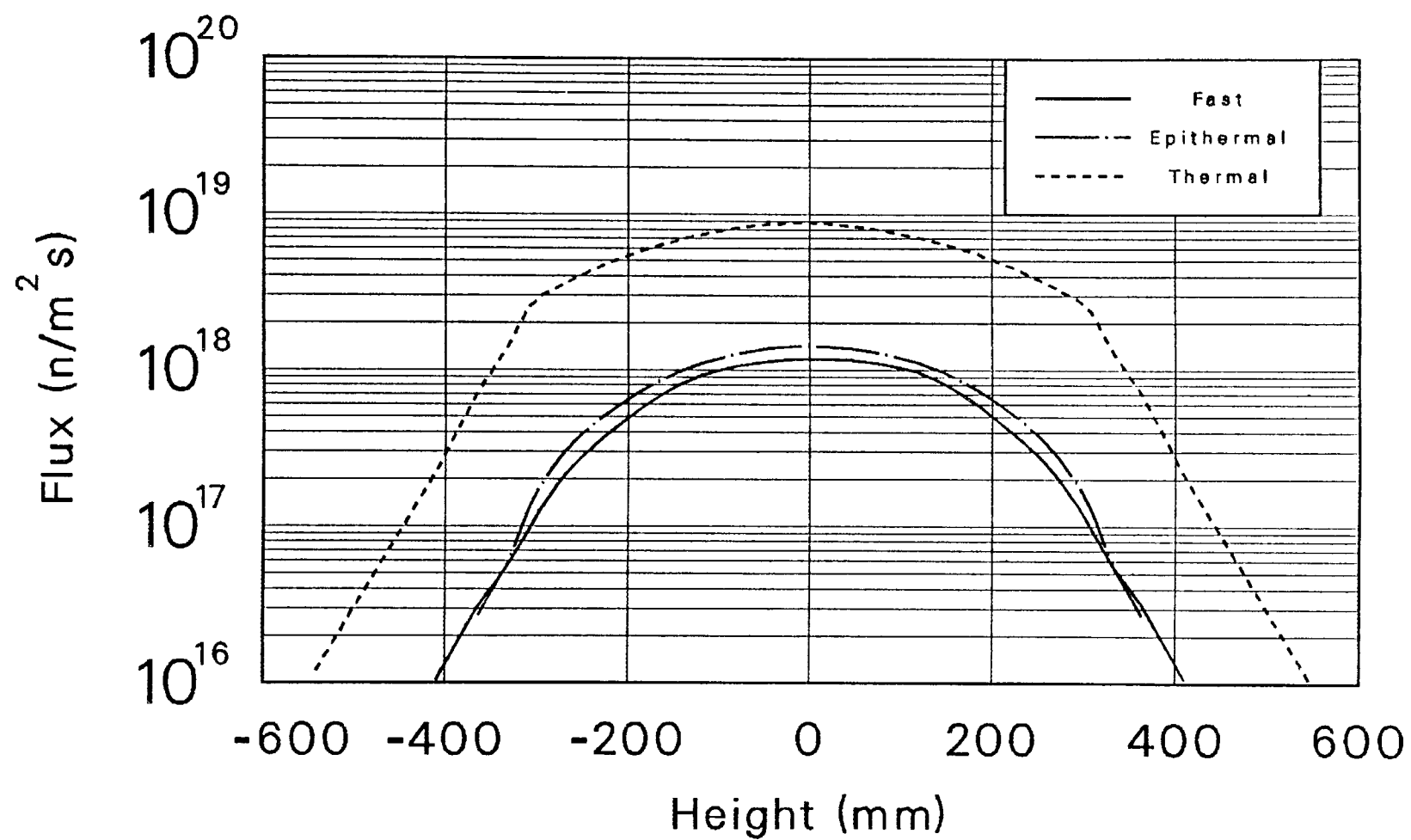


Fig. 4.17. Axial flux profile at control rod access plug facilities, beginning-of-life.

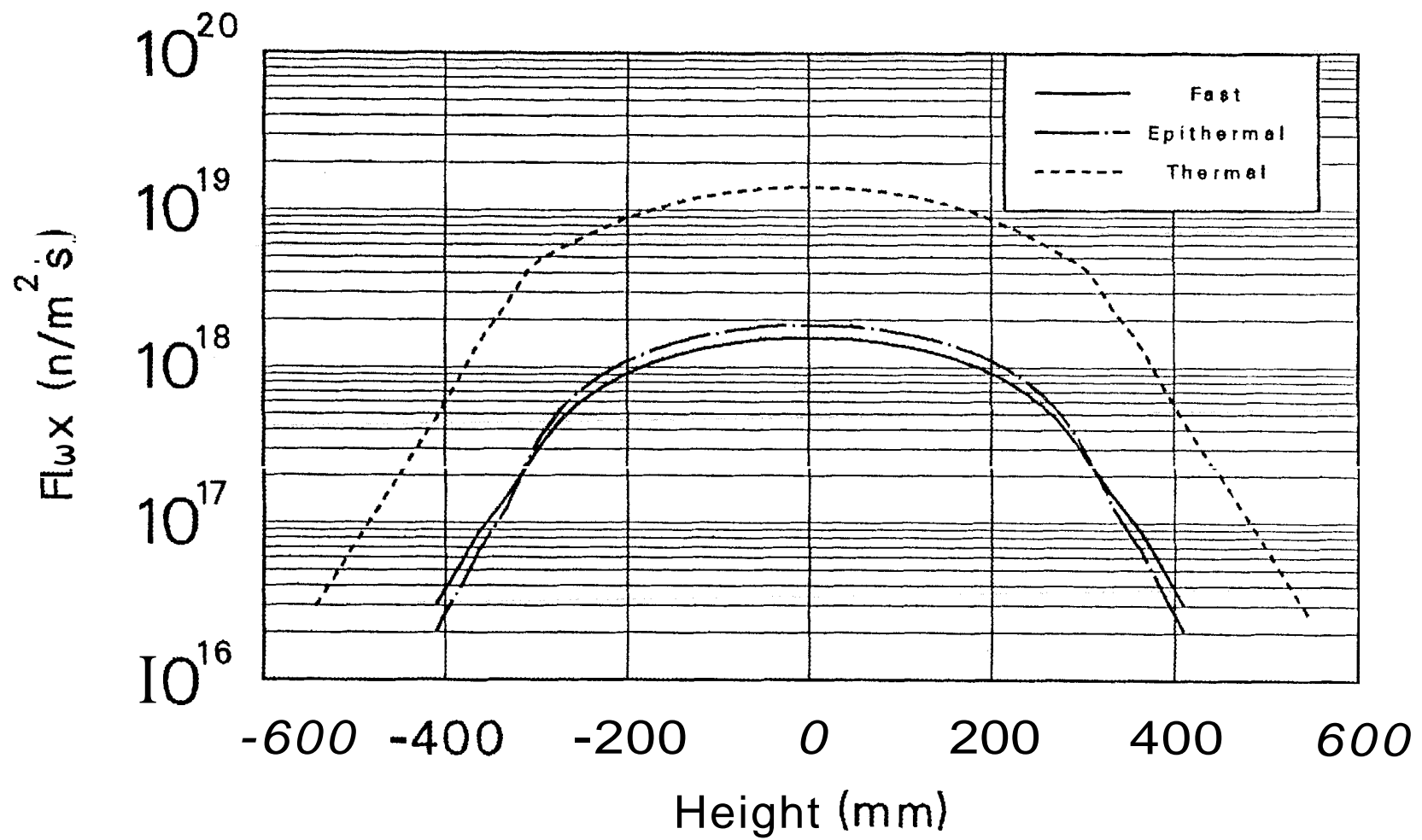


Fig. 4.18. Axial flux profile at control rod access plug facilities, end-of-life.

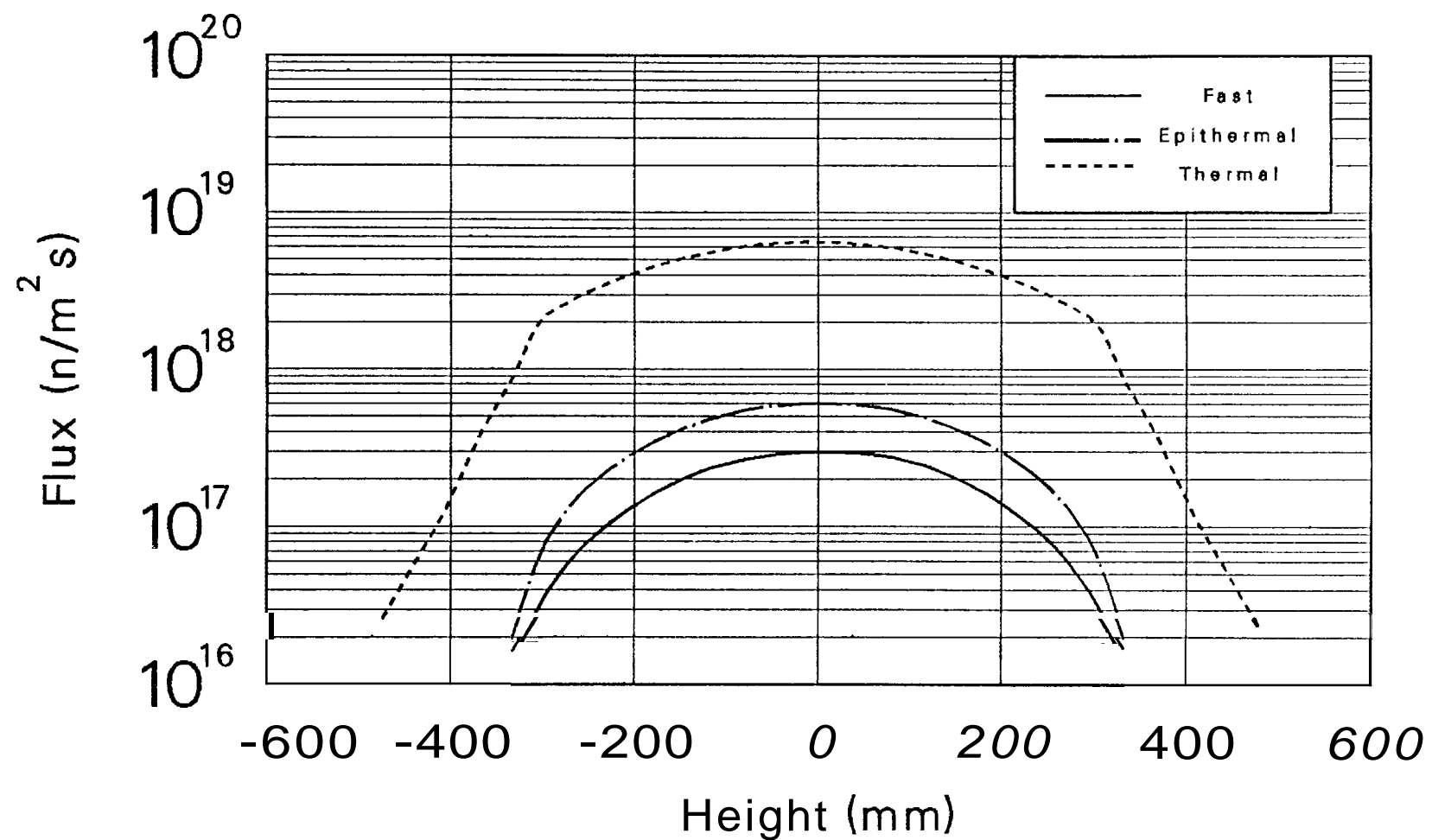


Fig. 4.19. Axial flux profile at inner small VXF facilities, beginning-of-life.

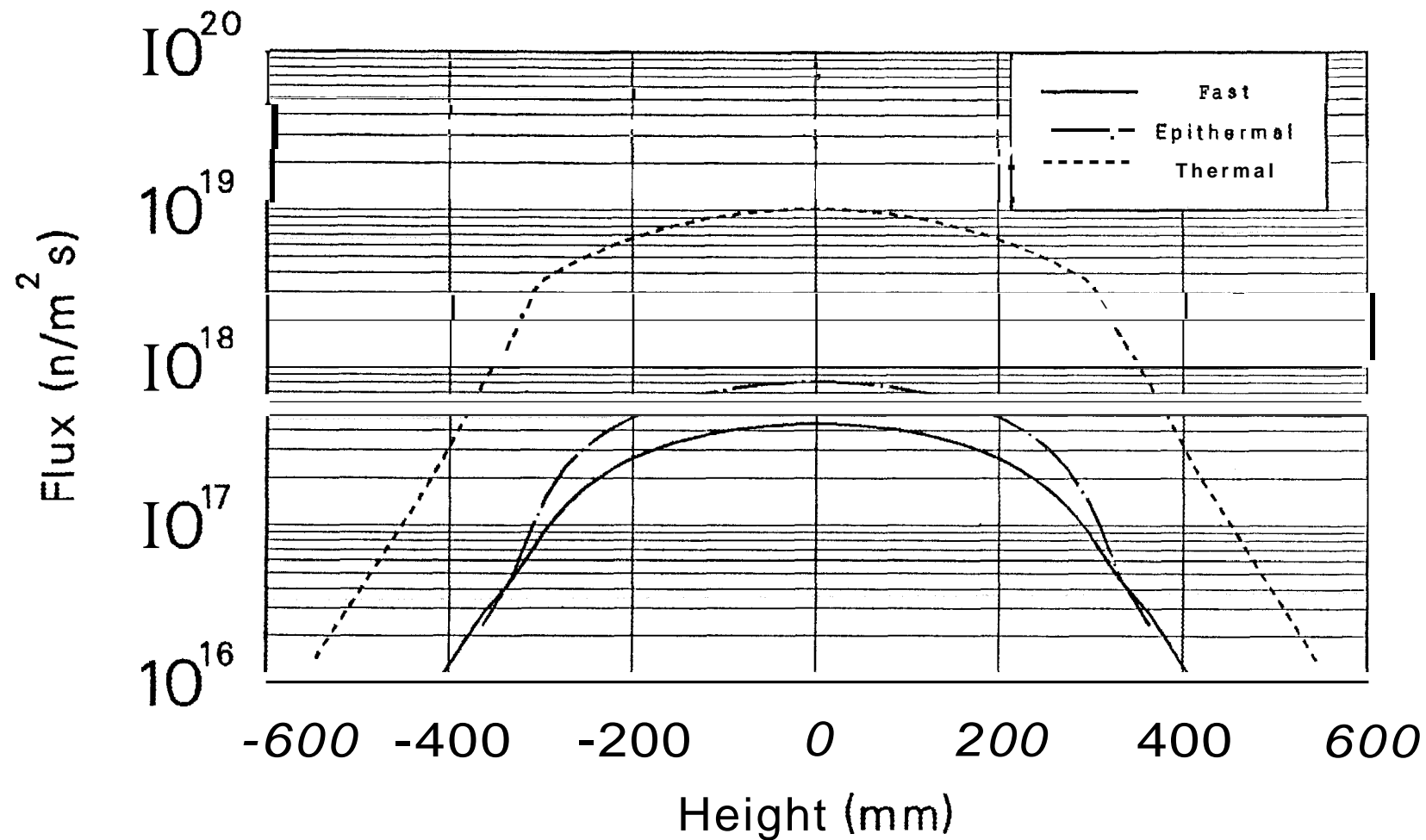


Fig. 4.20. Axial flux profile at inner small VXF facilities, end-of-life.

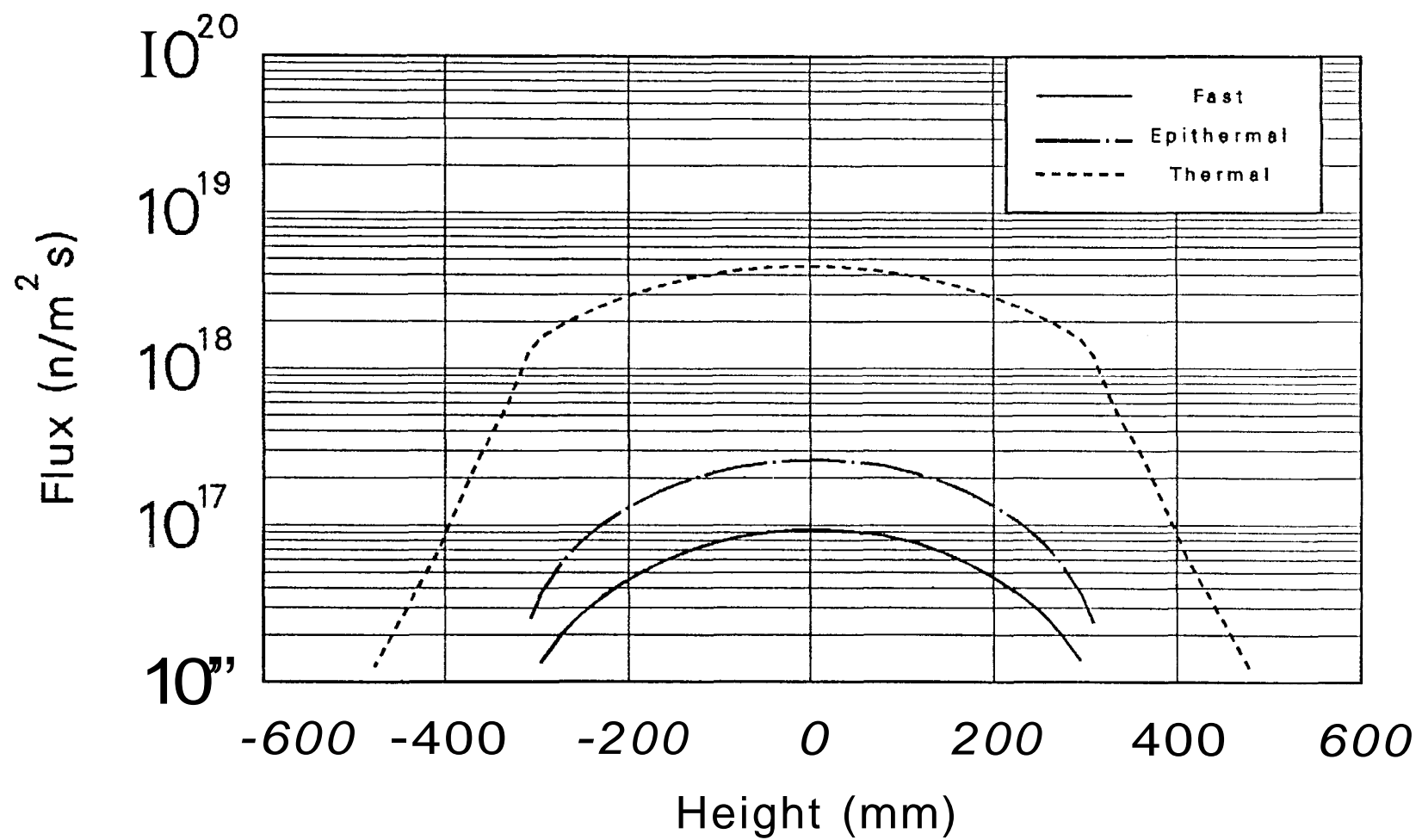


Fig. 4.21. Axial flux profile at outer small VXF facilities, beginning-of-life.

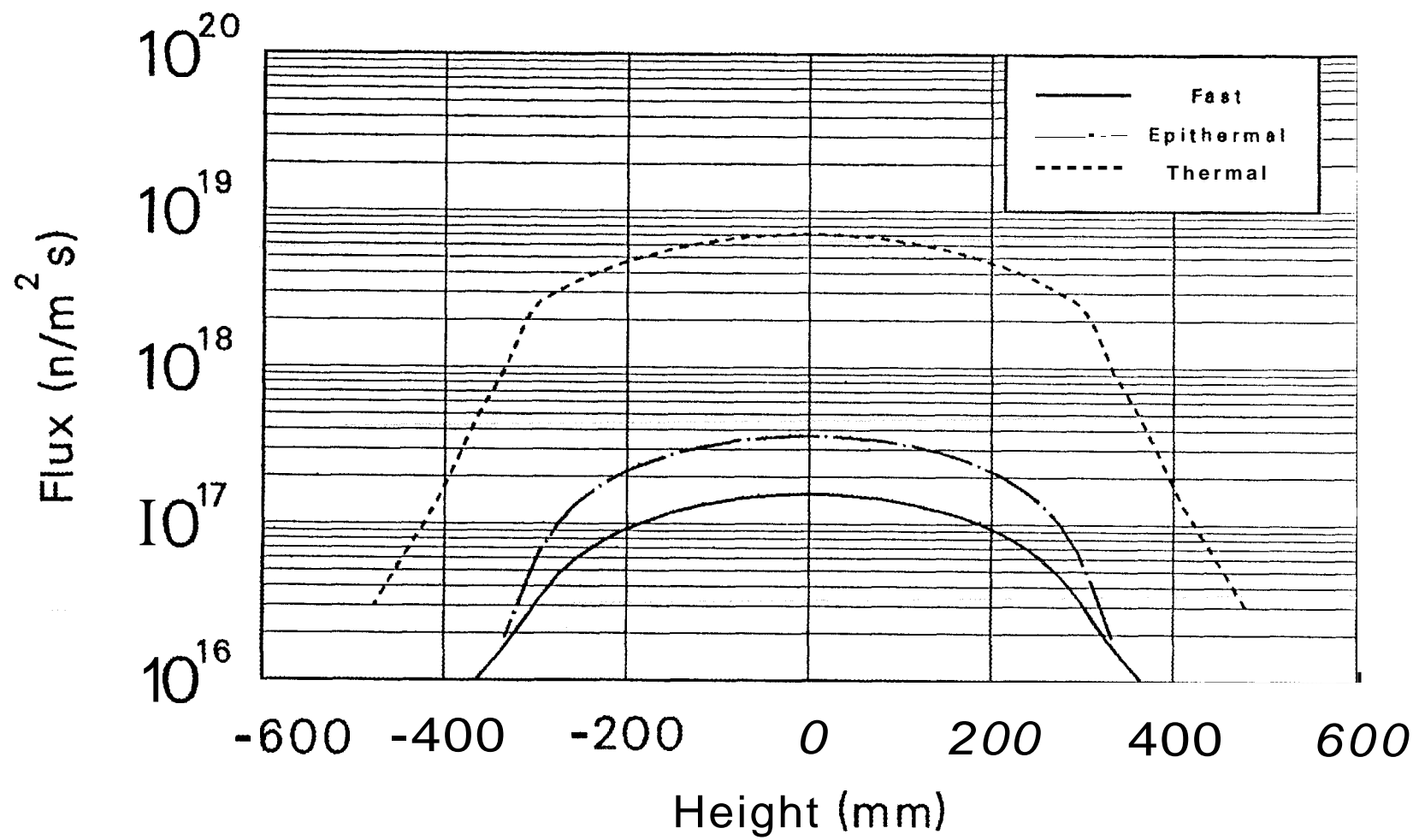


Fig. 4.22. Axial flux profiles at outer small VXF facilities, end-of-life.

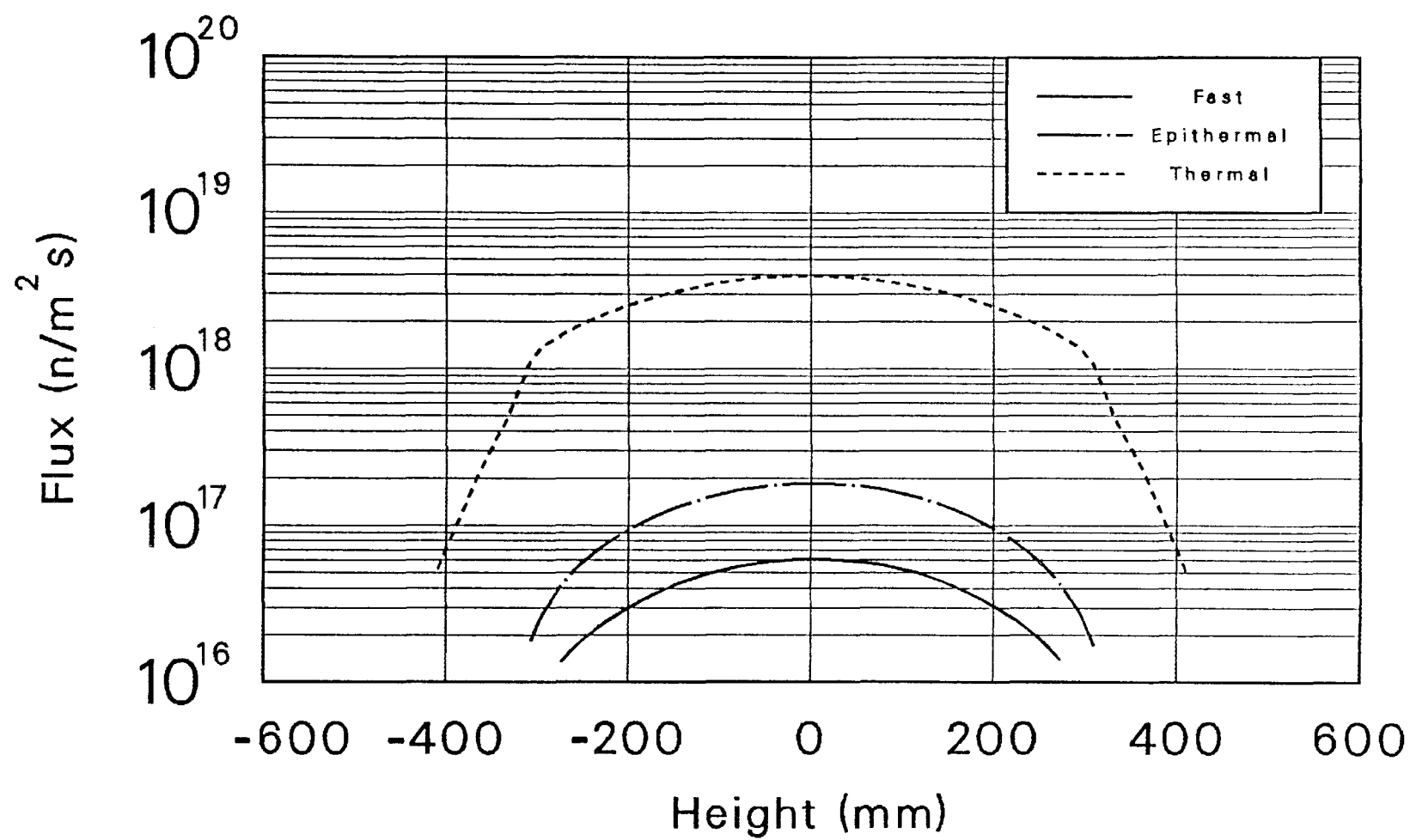


Fig. 4.23. Axial flux profile at large VXF facilities, beginning-of-life.

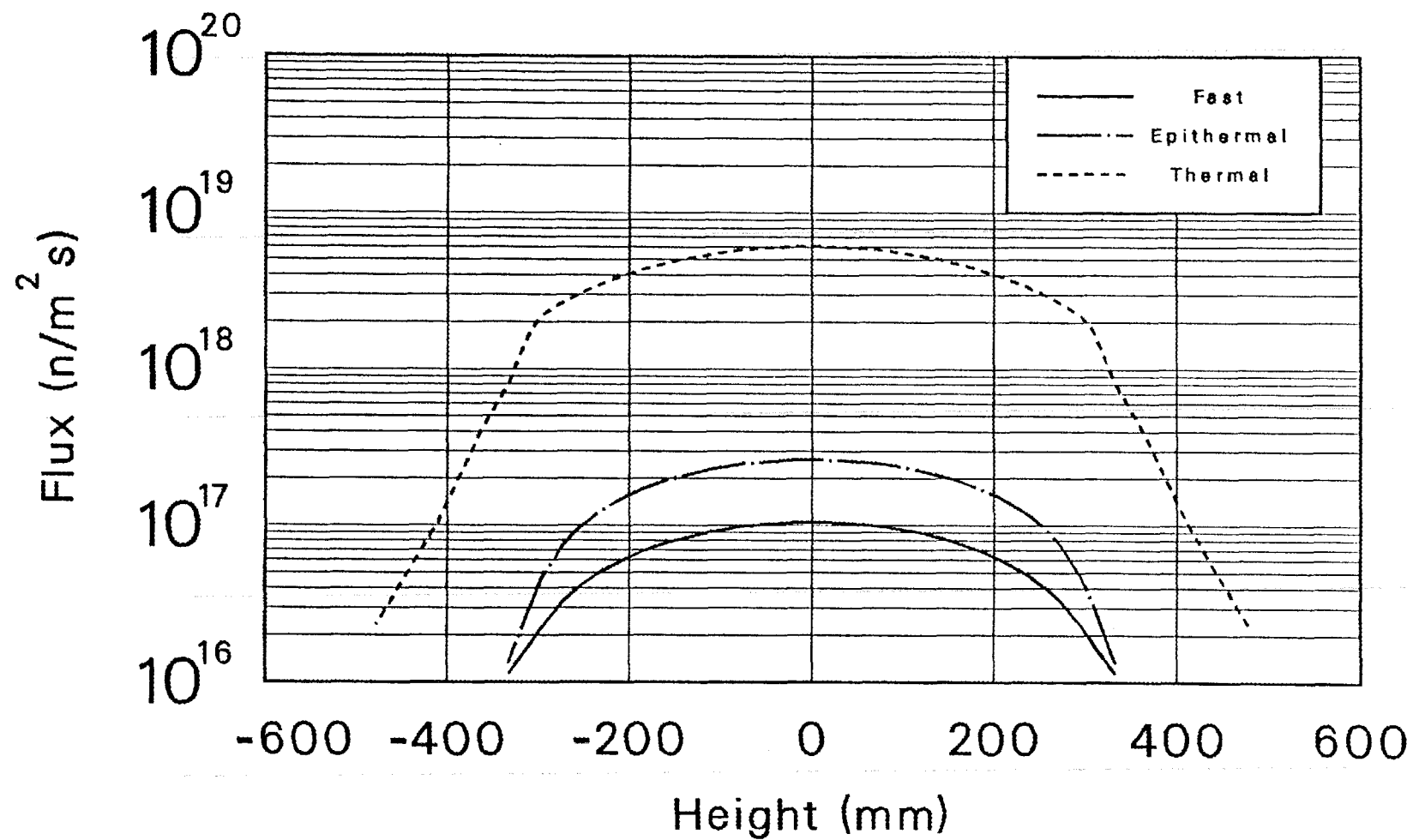


Fig. 4.24. Axial flux profile at large VXF facilities, end-of-life.

"Power distributions for other than clean core conditions were obtained by adjusting the one-dimensional fuel-cycle calculation results with the critical-experiment data to obtain a normalized two-dimensional power distribution. In order to match a calculated partially depleted core with a partially poisoned (moderator soluble poison) critical-experiment core, an appropriate relationship between control-rod position and control-region smeared-poison concentration was obtained from one-dimensional calculations of the experimental cores. . . . This technique does not consider the different relationship that would be obtained if calculations were made for actual partially burned cores containing nonuniformly distributed fission products and nonuniformly depleted fuel. . . . Two-dimensional calculations were not relied upon for predicting power distributions."

The power distributions for the eight time steps at which k-effectives were calculated are given in Tables 4.5 through 4.20. It is emphasized that, unlike the data contained in Ref. 1, these data are from two dimensional R - Z calculations and therefore should provide a more accurate prediction of thermal-hydraulic performance. To maintain consistency with previous calculations, the data presented are interpolated from the spatial mesh in the VENTURE calculation as the VENTURE mesh did not precisely match the mesh structure in Ref. 1.

It would be possible to use the experiment-to-calculation differences presented in Section 3 to normalize the data presented in Tables 4.5 through 4.20. Such a procedure should improve both the accuracy and precision of the power distributions but is beyond the scope of this study.

4.6.2. Specification of End-of-Life Conditions

The HFIR Safety Analysis Report is currently being revised to include safety parameters for the reduced rated power of 85 MW. Inputs to this report include end-of-life reactivity coefficients. These coefficients are being calculated with transport theory programs, but the end-of-cycle conditions are defined using the VENTURE diffusion theory system.

The cumulative burnup in various regions of the HFIR core are shown in Fig. 4.25. The inner edge of the inner element has the highest percentage burnup. This region is the most distant from the control blade locations which are along the outside edge of the outer element. That fact along with the proximity of the water in the central target region contribute to a high thermal flux (see Fig. 4.7). That, in turn, results in high local power generation along the inside edge.

The impact of the water reflector can also be seen along the top edges of the two elements and along the inner and outer radial edges. The percentage depletion in those zones is greater than for fuel regions a few millimeters inside the elements.

Table 4.5. Inner Annulus Relative Power Distribution
Time = 0.0 Days

Axial Height (cm)	Radius (cm)						
	7.14	8.00	9.00	10.00	11.00	12.00	12.60
25.40	1.22	1.41	1.52	1.60	1.61	1.52	1.47
24.00	1.05	1.07	1.03	1.04	1.06	1.09	1.14
22.00	.99	.97	.89	.88	.90	.95	1.01
20.00	.99	.97	.89	.88	.90	.93	.99
18.00	1.04	1.03	.95	.94	.96	.99	1.04
16.00	1.10	1.09	1.01	1.00	1.02	1.05	1.10
14.00	1.16	1.15	1.07	1.05	1.07	1.10	1.15
12.00	1.22	1.21	1.12	1.10	1.12	1.15	1.20
10.00	1.26	1.25	1.16	1.14	1.16	1.19	1.24
8.00	1.31	1.29	1.19	1.18	1.19	1.22	1.28
6.00	1.33	1.32	1.22	1.20	1.21	1.24	1.30
4.00	1.35	1.34	1.23	1.22	1.23	1.26	1.32
2.00	1.36	1.35	1.24	1.22	1.24	1.27	1.33
.00	1.36	1.35	1.24	1.22	1.24	1.27	1.33
-2.00	1.36	1.34	1.24	1.22	1.24	1.27	1.32
-4.00	1.34	1.33	1.22	1.20	1.22	1.25	1.30
-6.00	1.31	1.30	1.20	1.18	1.20	1.22	1.28
-8.00	1.29	1.27	1.17	1.15	1.17	1.20	1.25
-10.00	1.24	1.23	1.13	1.12	1.13	1.16	1.21
-12.00	1.20	1.18	1.09	1.08	1.09	1.12	1.17
-14.00	1.14	1.13	1.04	1.03	1.04	1.07	1.12
-16.00	1.08	1.07	.99	.97	.99	1.02	1.06
-18.00	1.02	1.01	.93	.91	.93	.96	1.01
-20.00	.97	.95	.87	.86	.88	.91	.96
-22.00	.97	.95	.87	.86	.88	.93	.99
-24.00	1.03	1.05	1.01	1.02	1.04	1.06	1.12
-25.40	1.19	1.38	1.49	1.57	1.58	1.49	1.44

Table 4.6. Outer Annulus Relative Power Distribution
Time = 0.0 Days

Axial Height (cm)	Radius (cm)						
	15.15	16.00	17.00	18.00	19.00	20.00	21.00
25.40	1.50	1.73	1.73	1.60	1.39	1.10	.85
24.00	1.16	1.17	1.08	1.00	.92	.82	.73
22.00	1.03	1.00	.90	.83	.78	.72	.66
20.00	1.00	.99	.90	.82	.77	.70	.63
18.00	1.05	1.04	.94	.86	.79	.71	.63
16.00	1.10	1.10	.99	.89	.81	.72	.63
14.00	1.16	1.15	1.03	.92	.83	.73	.64
12.00	1.20	1.19	1.07	.95	.85	.74	.65
10.00	1.24	1.23	1.10	.98	.88	.77	.68
8.00	1.28	1.27	1.13	1.01	.91	.80	.71
6.00	1.30	1.29	1.16	1.04	.94	.85	.77
4.00	1.32	1.31	1.18	1.07	.98	.90	.84
2.00	1.33	1.33	1.20	1.09	1.03	.96	.93
.00	1.33	1.33	1.20	1.09	1.03	.98	.95
-2.00	1.32	1.31	1.18	1.08	1.01	.95	.92
-4.00	1.30	1.29	1.15	1.03	.94	.85	.78
-6.00	1.27	1.26	1.12	.99	.89	.79	.70
-8.00	1.24	1.22	1.08	.95	.84	.73	.64
-10.00	1.20	1.19	1.05	.92	.81	.70	.61
-12.00	1.16	1.15	1.02	.89	.78	.67	.58
-14.00	1.12	1.10	.98	.87	.76	.65	.56
-16.00	1.07	1.06	.95	.84	.74	.63	.52
-18.00	1.02	1.01	.91	.81	.72	.61	.49
-20.00	.97	.96	.87	.78	.70	.60	.48
-22.00	1.00	.98	.87	.79	.72	.62	.51
-24.00	1.14	1.14	1.05	.96	.86	.72	.59
-25.40	1.47	1.69	1.69	1.55	1.31	1.01	.73

Table 4.8. Outer Annulus Relative Power Distribution
Time = 0.588 Days

Axial Height (cm)	Radius (cm)						
	15.15	16.00	17.00	18.00	19.00	20.00	21.00
25.40	1.47	1.68	1.68	1.55	1.34	1.06	.83
24.00	1.13	1.13	1.04	.96	.88	.79	.71
22.00	1.00	.97	.86	.79	.75	.69	.64
20.00	.98	.96	.86	.79	.74	.67	.60
18.00	1.03	1.01	.91	.83	.76	.68	.59
16.00	1.09	1.07	.96	.86	.78	.68	.58
14.00	1.14	1.12	1.00	.90	.80	.69	.59
12.00	1.19	1.17	1.05	.93	.83	.72	.61
10.00	1.24	1.22	1.09	.97	.88	.77	.67
8.00	1.28	1.26	1.13	1.01	.92	.82	.74
6.00	1.31	1.30	1.17	1.07	1.00	.94	.90
4.00	1.34	1.33	1.21	1.12	1.08	1.05	1.05
2.00	1.36	1.35	1.23	1.15	1.12	1.11	1.14
.00	1.36	1.35	1.23	1.15	1.13	1.12	1.16
-2.00	1.35	1.34	1.22	1.14	1.11	1.11	1.14
-4.00	1.33	1.31	1.19	1.10	1.06	1.04	1.06
-6.00	1.29	1.27	1.14	1.03	.96	.90	.86
-8.00	1.25	1.23	1.09	.96	.86	.75	.64
-10.00	1.20	1.18	1.04	.92	.81	.69	.58
-12.00	1.16	1.13	1.00	.87	.76	.64	.53
-14.00	1.11	1.08	.96	.84	.73	.61	.50
-16.00	1.05	1.04	.92	.82	.72	.59	.47
-18.00	1.00	.98	.88	.79	.70	.58	.46
-20.00	.95	.93	.84	.75	.67	.57	.46
-22.00	.98	.94	.84	.76	.69	.60	.50
-24.00	1.11	1.10	1.01	.92	.83	.70	.58
-25.40	1.44	1.64	1.64	1.50	1.28	.98	.72

Table 4.9. Inner Annulus Relative Power Distribution
Time = 1.176 Days

Axial Height (cm)	Radius (cm)						
	7.14	8.00	9.00	10.00	11.00	12.00	12.60
25.40	1.04	1.21	1.30	1.35	1.34	1.25	1.19
24.00	.91	.94	.90	.89	.89	.90	.94
22.00	.87	.87	.79	.77	.77	.80	.85
20.00	.88	.88	.80	.78	.79	.81	.85
18.00	.95	.95	.87	.85	.86	.88	.92
16.00	1.02	1.03	.95	.93	.94	.96	1.00
14.00	1.09	1.10	1.02	1.00	1.01	1.04	1.09
12.00	1.16	1.18	1.09	1.07	1.09	1.12	1.16
10.00	1.22	1.24	1.15	1.13	1.15	1.18	1.23
8.00	1.28	1.30	1.20	1.19	1.21	1.24	1.30
6.00	1.31	1.33	1.24	1.22	1.24	1.28	1.34
4.00	1.34	1.36	1.27	1.25	1.28	1.32	1.38
2.00	1.36	1.38	1.29	1.27	1.29	1.34	1.40
.00	1.36	1.38	1.29	1.27	1.30	1.34	1.40
-2.00	1.35	1.38	1.28	1.26	1.29	1.33	1.39
-4.00	1.33	1.35	1.26	1.24	1.27	1.31	1.37
-6.00	1.30	1.32	1.22	1.21	1.23	1.27	1.32
-8.00	1.26	1.28	1.18	1.17	1.19	1.22	1.28
-10.00	1.20	1.21	1.12	1.10	1.12	1.15	1.20
-12.00	1.13	1.15	1.06	1.04	1.06	1.08	1.13
-14.00	1.06	1.07	.99	.97	.98	1.01	1.05
-16.00	.99	1.00	.92	.89	.90	.92	.96
-18.00	.92	.92	.84	.82	.83	.85	.88
-20.00	.85	.85	.77	.75	.75	.77	.81
-22.00	.83	.83	.76	.73	.74	.76	.81
-24.00	.88	.90	.86	.85	.85	.86	.89
-25.40	1.00	1.16	1.24	1.28	1.27	1.18	1.13

Table 4.7. Inner Annulus Relative Power Distribution
Time = 0.588 Days

Axial Height (cm)	Radius (cm)						
	7.14	8.00	9.00	10.00	11.00	12.00	12.60
25.40	1.19	1.38	1.49	1.56	1.57	1.48	1.43
24.00	1.03	1.05	1.01	1.01	1.03	1.06	1.12
22.00	.97	.95	.87	.85	.87	.92	.99
20.00	.97	.96	.87	.85	.87	.91	.96
18.00	1.03	1.02	.93	.91	.93	.97	1.02
16.00	1.09	1.08	.99	.97	.99	1.03	1.08
14.00	1.15	1.15	1.05	1.03	1.05	1.08	1.14
12.00	1.21	1.20	1.11	1.08	1.10	1.14	1.19
10.00	1.26	1.25	1.15	1.13	1.14	1.18	1.24
8.00	1.31	1.30	1.19	1.17	1.18	1.22	1.28
6.00	1.33	1.32	1.21	1.19	1.21	1.25	1.31
4.00	1.36	1.35	1.24	1.21	1.23	1.27	1.33
2.00	1.37	1.36	1.25	1.22	1.24	1.28	1.35
.00	1.37	1.36	1.25	1.22	1.24	1.28	1.35
-2.00	1.36	1.35	1.24	1.22	1.24	1.28	1.34
-4.00	1.35	1.34	1.23	1.20	1.22	1.26	1.32
-6.00	1.32	1.31	1.20	1.18	1.19	1.23	1.29
-8.00	1.29	1.28	1.17	1.15	1.16	1.19	1.25
-10.00	1.24	1.23	1.13	1.10	1.12	1.15	1.21
-12.00	1.19	1.18	1.08	1.06	1.08	1.11	1.16
-14.00	1.13	1.12	1.03	1.01	1.02	1.05	1.11
-16.00	1.07	1.06	.97	.95	.97	1.00	1.05
-18.00	1.01	1.00	.91	.89	.91	.94	.99
-20.00	.95	.94	.85	.83	.85	.89	.94
-22.00	.95	.93	.85	.83	.86	.90	.97
-24.00	1.01	1.03	.99	.99	1.01	1.04	1.09
-25.40	1.17	1.35	1.46	1.53	1.54	1.45	1.41

Table 4.10. Outer Annulus Relative Power Distribution
Time = 1.176 Days

Axial Height (cm)	Radius (cm)						
	15.15	16.00	17.00	18.00	19.00	20.00	21.00
25.40	1.19	1.35	1.32	1.18	.96	.71	.49
24.00	.94	.93	.83	.73	.63	.51	.40
22.00	.85	.81	.71	.63	.55	.47	.38
20.00	.85	.83	.73	.65	.57	.49	.41
18.00	.92	.91	.81	.72	.64	.55	.46
16.00	1.01	1.00	.89	.79	.71	.62	.53
14.00	1.09	1.08	.97	.88	.80	.70	.61
12.00	1.17	1.17	1.06	.96	.89	.81	.73
10.00	1.25	1.25	1.14	1.06	1.02	.97	.95
8.00	1.32	1.33	1.22	1.16	1.15	1.15	1.18
6.00	1.36	1.37	1.27	1.21	1.22	1.24	1.30
4.00	1.40	1.42	1.32	1.26	1.28	1.32	1.40
2.00	1.43	1.44	1.34	1.29	1.31	1.36	1.45
.00	1.43	1.44	1.35	1.30	1.32	1.37	1.46
-2.00	1.42	1.43	1.34	1.29	1.31	1.36	1.45
-4.00	1.39	1.40	1.31	1.25	1.27	1.31	1.40
-6.00	1.34	1.35	1.26	1.20	1.21	1.23	1.30
-8.00	1.29	1.30	1.20	1.13	1.13	1.14	1.18
-10.00	1.21	1.21	1.11	1.02	.97	.92	.89
-12.00	1.13	1.13	1.01	.91	.83	.73	.63
-14.00	1.05	1.04	.93	.82	.73	.63	.52
-16.00	.96	.95	.84	.74	.65	.55	.45
-18.00	.88	.86	.76	.67	.58	.48	.40
-20.00	.81	.78	.69	.60	.52	.43	.35
-22.00	.80	.77	.66	.57	.49	.39	.30
-24.00	.88	.87	.77	.66	.55	.41	.27
-25.40	1.12	1.26	1.22	1.08	.86	.60	.36

Table 4.11. Inner Annulus Relative Power Distribution
Time = 14.117 Days

Axial Height (cm)	Radius (cm)						
	7.14	8.00	9.00	10.00	11.00	12.00	12.60
25.40	.73	1.01	1.15	1.20	1.17	1.06	.93
24.00	.71	.91	.93	.91	.89	.85	.80
22.00	.65	.84	.84	.80	.79	.77	.74
20.00	.67	.87	.86	.83	.81	.79	.75
18.00	.73	.94	.94	.91	.89	.86	.82
16.00	.78	1.02	1.02	.99	.97	.94	.89
14.00	.84	1.10	1.11	1.07	1.05	1.02	.97
12.00	.90	1.17	1.18	1.15	1.13	1.10	1.04
10.00	.94	1.23	1.25	1.21	1.19	1.17	1.10
8.00	.99	1.29	1.31	1.27	1.26	1.23	1.17
6.00	1.02	1.33	1.35	1.31	1.30	1.27	1.20
4.00	1.04	1.36	1.38	1.34	1.33	1.30	1.24
2.00	1.06	1.38	1.40	1.36	1.35	1.32	1.25
.00	1.06	1.38	1.40	1.37	1.35	1.33	1.26
-2.00	1.05	1.38	1.40	1.36	1.35	1.32	1.25
-4.00	1.04	1.35	1.37	1.34	1.32	1.29	1.23
-6.00	1.01	1.32	1.33	1.30	1.28	1.26	1.19
-8.00	.98	1.28	1.29	1.25	1.24	1.21	1.15
-10.00	.93	1.21	1.23	1.19	1.17	1.15	1.08
-12.00	.88	1.15	1.16	1.12	1.10	1.08	1.02
-14.00	.82	1.07	1.08	1.04	1.02	1.00	.94
-16.00	.76	.99	1.00	.96	.94	.91	.86
-18.00	.70	.91	.91	.88	.86	.83	.79
-20.00	.65	.84	.83	.80	.78	.75	.71
-22.00	.63	.81	.81	.77	.75	.73	.70
-24.00	.68	.87	.89	.86	.84	.81	.76
-25.40	.70	.97	1.10	1.14	1.11	1.00	.87

Table 4.12. Outer Annulus Relative Power Distribution
Time = 14.117 Days

Axial Height (cm)	Radius (cm)						
	15.15	16.00	17.00	18.00	19.00	20.00	21.00
25.40	.92	1.12	1.11	.96	.75	.51	.32
24.00	.79	.85	.77	.66	.55	.42	.29
22.00	.73	.77	.68	.59	.51	.40	.28
20.00	.74	.80	.72	.63	.54	.43	.31
18.00	.81	.88	.80	.71	.62	.50	.37
16.00	.89	.97	.89	.80	.72	.61	.47
14.00	.97	1.06	.99	.90	.84	.74	.62
12.00	1.05	1.16	1.08	1.02	.98	.93	.85
10.00	1.11	1.23	1.16	1.10	1.09	1.06	1.00
8.00	1.18	1.31	1.24	1.19	1.19	1.18	1.14
6.00	1.22	1.35	1.29	1.24	1.25	1.25	1.21
4.00	1.25	1.39	1.33	1.28	1.30	1.30	1.27
2.00	1.27	1.41	1.35	1.30	1.33	1.33	1.30
.00	1.27	1.42	1.35	1.31	1.33	1.34	1.31
-2.00	1.27	1.41	1.34	1.30	1.32	1.33	1.30
-4.00	1.24	1.38	1.32	1.27	1.29	1.30	1.27
-6.00	1.20	1.34	1.27	1.23	1.24	1.24	1.21
-8.00	1.16	1.29	1.22	1.17	1.18	1.18	1.14
-10.00	1.09	1.21	1.14	1.08	1.07	1.05	1.00
-12.00	1.02	1.13	1.05	.99	.95	.90	.84
-14.00	.94	1.03	.95	.86	.78	.67	.53
-16.00	.86	.93	.85	.75	.65	.52	.37
-18.00	.78	.84	.76	.66	.55	.43	.29
-20.00	.70	.75	.67	.58	.48	.36	.24
-22.00	.69	.72	.64	.54	.44	.33	.22
-24.00	.74	.79	.71	.60	.48	.34	.22
-25.40	.85	1.04	1.01	.86	.65	.42	.23

Table 4.13. Inner Annulus Relative Power Distribution
Time = 18.823 Days

Axial Height (cm)	Radius (cm)						
	7.14	8.00	9.00	10.00	11.00	12.00	12.60
25.40	.63	.92	1.08	1.13	1.11	.99	.85
24.00	.63	.86	.91	.89	.87	.83	.76
22.00	.57	.79	.82	.80	.78	.75	.69
20.00	.59	.82	.85	.82	.80	.77	.71
18.00	.63	.89	.93	.90	.88	.84	.77
16.00	.68	.96	1.01	.98	.96	.92	.84
14.00	.73	1.03	1.09	1.06	1.04	1.00	.92
12.00	.78	1.10	1.16	1.13	1.12	1.07	.98
10.00	.82	1.16	1.22	1.20	1.18	1.13	1.04
8.00	.86	1.22	1.28	1.26	1.24	1.19	1.10
6.00	.88	1.25	1.32	1.29	1.28	1.23	1.13
4.00	.91	1.28	1.35	1.33	1.31	1.26	1.16
2.00	.92	1.30	1.37	1.34	1.33	1.28	1.17
.00	.92	1.30	1.37	1.35	1.33	1.28	1.18
-2.00	.92	1.30	1.37	1.34	1.32	1.27	1.17
-4.00	.90	1.28	1.35	1.32	1.30	1.25	1.15
-6.00	.88	1.24	1.31	1.28	1.27	1.22	1.12
-8.00	.85	1.21	1.27	1.24	1.23	1.18	1.08
-10.00	.81	1.15	1.21	1.18	1.16	1.12	1.03
-12.00	.77	1.09	1.14	1.12	1.10	1.05	.97
-14.00	.72	1.02	1.07	1.04	1.02	.98	.90
-16.00	.67	.94	.99	.96	.94	.90	.82
-18.00	.62	.87	.91	.88	.86	.82	.75
-20.00	.57	.80	.83	.80	.78	.74	.68
-22.00	.55	.77	.80	.77	.75	.72	.67
-24.00	.61	.83	.88	.86	.84	.79	.72
-25.40	.61	.89	1.04	1.09	1.06	.94	.80

Table 4.14. Outer Annulus Relative Power Distribution
Time = 18.823 Days

Axial Height (cm)	Radius (cm)						
	15.15	16.00	17.00	18.00	19.00	20.00	21.00
25.40	.84	1.07	1.07	.93	.73	.50	.30
24.00	.75	.84	.76	.66	.55	.41	.28
22.00	.69	.76	.69	.60	.51	.41	.29
20.00	.70	.79	.72	.64	.56	.46	.33
18.00	.77	.87	.81	.74	.67	.57	.44
16.00	.85	.97	.91	.84	.79	.72	.61
14.00	.92	1.06	1.01	.95	.92	.88	.79
12.00	1.00	1.14	1.09	1.05	1.04	1.01	.94
10.00	1.05	1.21	1.17	1.12	1.13	1.11	1.04
8.00	1.11	1.28	1.24	1.20	1.21	1.20	1.13
6.00	1.15	1.32	1.28	1.24	1.26	1.25	1.18
4.00	1.18	1.36	1.31	1.28	1.30	1.29	1.22
2.00	1.19	1.38	1.33	1.30	1.32	1.32	1.25
.00	1.20	1.38	1.34	1.30	1.33	1.32	1.25
-2.00	1.19	1.37	1.33	1.29	1.32	1.31	1.25
-4.00	1.17	1.35	1.31	1.27	1.29	1.29	1.22
-6.00	1.14	1.31	1.27	1.23	1.25	1.25	1.18
-8.00	1.10	1.27	1.22	1.19	1.20	1.19	1.13
-10.00	1.04	1.20	1.15	1.11	1.12	1.10	1.04
-12.00	.98	1.12	1.08	1.03	1.03	1.01	.94
-14.00	.90	1.03	.98	.93	.91	.87	.79
-16.00	.82	.94	.88	.81	.75	.67	.56
-18.00	.75	.84	.78	.69	.61	.50	.36
-20.00	.68	.75	.68	.59	.50	.38	.25
-22.00	.66	.72	.64	.55	.45	.33	.21
-24.00	.71	.79	.71	.60	.48	.34	.21
-25.40	.79	1.00	.98	.84	.64	.41	.23

Table 4.15. Inner Annulus Relative Power Distribution
Time = 21.176 Days

Axial Height (cm)	Radius (cm)						
	7.14	8.00	9.00	10.00	11.00	12.00	12.60
25.40	.58	.87	1.04	1.09	1.07	.95	.80
24.00	.59	.83	.89	.88	.86	.81	.73
22.00	.52	.76	.81	.79	.77	.74	.67
20.00	.54	.79	.84	.81	.79	.76	.69
18.00	.58	.85	.91	.89	.87	.83	.75
16.00	.63	.92	.99	.96	.95	.90	.82
14.00	.67	.99	1.06	1.04	1.02	.97	.88
12.00	.72	1.05	1.13	1.11	1.09	1.04	.94
10.00	.75	1.11	1.19	1.17	1.15	1.10	1.00
8.00	.79	1.16	1.25	1.23	1.21	1.15	1.05
6.00	.81	1.19	1.28	1.26	1.24	1.19	1.08
4.00	.83	1.22	1.31	1.29	1.27	1.22	1.10
2.00	.84	1.23	1.33	1.31	1.29	1.23	1.12
.00	.84	1.24	1.33	1.31	1.29	1.24	1.12
-2.00	.84	1.23	1.33	1.31	1.29	1.23	1.12
-4.00	.83	1.21	1.31	1.29	1.27	1.21	1.10
-6.00	.81	1.18	1.28	1.26	1.24	1.18	1.07
-8.00	.78	1.15	1.24	1.22	1.20	1.15	1.04
-10.00	.75	1.10	1.18	1.16	1.14	1.09	.99
-12.00	.71	1.04	1.12	1.10	1.08	1.03	.93
-14.00	.67	.98	1.05	1.03	1.01	.96	.87
-16.00	.62	.91	.97	.95	.93	.89	.80
-18.00	.57	.84	.89	.87	.85	.81	.73
-20.00	.53	.77	.82	.79	.77	.74	.67
-22.00	.51	.74	.79	.77	.75	.71	.65
-24.00	.57	.81	.87	.86	.83	.78	.71
-25.40	.56	.85	1.01	1.06	1.03	.91	.77

Table 4.16. Outer Annulus Relative Power Distribution
Time = 21.176 Days

Axial Height (cm)	Radius (cm)						
	15.15	16.00	17.00	18.00	19.00	20.00	21.00
25.40	.81	1.04	1.05	.92	.72	.50	.30
24.00	.73	.83	.76	.67	.56	.43	.30
22.00	.67	.76	.69	.62	.54	.44	.32
20.00	.69	.79	.73	.67	.61	.53	.42
18.00	.76	.87	.83	.78	.75	.69	.61
16.00	.83	.96	.92	.88	.87	.84	.76
14.00	.90	1.05	1.01	.98	.98	.96	.88
12.00	.96	1.13	1.09	1.06	1.07	1.06	.98
10.00	1.01	1.19	1.16	1.12	1.14	1.13	1.05
8.00	1.07	1.25	1.22	1.19	1.21	1.20	1.12
6.00	1.10	1.29	1.25	1.22	1.25	1.24	1.16
4.00	1.12	1.32	1.29	1.26	1.28	1.28	1.20
2.00	1.14	1.34	1.30	1.27	1.30	1.30	1.21
.00	1.14	1.34	1.31	1.28	1.31	1.30	1.22
-2.00	1.14	1.34	1.30	1.27	1.30	1.29	1.21
-4.00	1.12	1.32	1.28	1.25	1.28	1.27	1.19
-6.00	1.09	1.28	1.25	1.22	1.24	1.24	1.16
-8.00	1.06	1.24	1.21	1.18	1.20	1.20	1.12
-10.00	1.01	1.18	1.15	1.12	1.14	1.13	1.05
-12.00	.95	1.11	1.08	1.05	1.06	1.05	.98
-14.00	.88	1.03	1.00	.96	.97	.95	.88
-16.00	.81	.94	.91	.87	.86	.83	.77
-18.00	.74	.85	.81	.76	.72	.67	.60
-20.00	.67	.76	.71	.63	.56	.47	.35
-22.00	.65	.73	.66	.57	.48	.37	.24
-24.00	.70	.79	.72	.61	.50	.36	.22
-25.40	.77	.98	.98	.84	.64	.41	.23

Table 4.17. Inner Annulus Relative Power Distribution
Time = 23.529 Days

Axial Height (cm)	Radius (cm)						
	7.14	8.00	9.00	10.00	11.00	12.00	12.60
25.40	.54	.83	1.00	1.07	1.05	.93	.78
24.00	.55	.80	.88	.88	.86	.81	.72
22.00	.48	.73	.80	.78	.77	.73	.66
20.00	.50	.76	.82	.80	.79	.75	.67
18.00	.54	.82	.89	.87	.86	.81	.73
16.00	.58	.88	.96	.95	.93	.88	.79
14.00	.62	.94	1.03	1.02	1.00	.95	.85
12.00	.66	1.00	1.10	1.08	1.06	1.01	.90
10.00	.69	1.05	1.15	1.14	1.12	1.06	.95
8.00	.72	1.09	1.20	1.19	1.17	1.11	.99
6.00	.74	1.12	1.23	1.22	1.20	1.14	1.02
4.00	.75	1.15	1.26	1.25	1.23	1.16	1.04
2.00	.76	1.16	1.28	1.26	1.24	1.18	1.05
.00	.76	1.16	1.28	1.27	1.25	1.18	1.06
-2.00	.76	1.16	1.28	1.26	1.24	1.18	1.05
-4.00	.75	1.14	1.26	1.25	1.23	1.16	1.04
-6.00	.73	1.12	1.23	1.22	1.20	1.14	1.01
-8.00	.71	1.09	1.20	1.19	1.17	1.11	.99
-10.00	.68	1.04	1.15	1.13	1.11	1.06	.94
-12.00	.65	.99	1.09	1.08	1.06	1.00	.90
-14.00	.61	.93	1.02	1.01	.99	.94	.84
-16.00	.57	.87	.95	.94	.92	.87	.78
-18.00	.53	.81	.88	.87	.85	.80	.72
-20.00	.50	.75	.81	.79	.78	.74	.66
-22.00	.48	.72	.79	.77	.76	.72	.65
-24.00	.54	.79	.87	.86	.84	.79	.71
-25.40	.53	.82	.99	1.05	1.03	.91	.76

Table 4.18. Outer Annulus Relative Power Distribution
Time = 23.529 Days

Axial Height (cm)	Radius (cm)						
	15.15	16.00	17.00	18.00	19.00	20.00	21.00
25.40	.79	1.04	1.07	.96	.78	.56	.36
24.00	.72	.84	.79	.71	.63	.51	.39
22.00	.66	.77	.72	.67	.64	.58	.49
20.00	.68	.80	.76	.73	.72	.69	.62
18.00	.74	.88	.85	.82	.82	.80	.73
16.00	.80	.95	.93	.90	.92	.90	.82
14.00	.86	1.03	1.01	.98	1.00	.99	.91
12.00	.92	1.10	1.08	1.05	1.07	1.06	.98
10.00	.97	1.16	1.13	1.11	1.13	1.12	1.04
8.00	1.01	1.21	1.19	1.16	1.19	1.18	1.09
6.00	1.04	1.24	1.22	1.20	1.22	1.21	1.12
4.00	1.06	1.27	1.25	1.22	1.25	1.24	1.15
2.00	1.08	1.29	1.27	1.24	1.27	1.26	1.17
.00	1.08	1.29	1.27	1.24	1.27	1.26	1.17
-2.00	1.08	1.29	1.26	1.24	1.27	1.26	1.16
-4.00	1.06	1.27	1.25	1.22	1.25	1.24	1.15
-6.00	1.04	1.24	1.22	1.19	1.22	1.21	1.12
-8.00	1.01	1.21	1.18	1.16	1.19	1.18	1.09
-10.00	.96	1.15	1.13	1.11	1.13	1.12	1.04
-12.00	.92	1.09	1.07	1.05	1.07	1.06	.98
-14.00	.86	1.02	1.00	.98	1.00	.98	.91
-16.00	.79	.95	.92	.90	.91	.90	.82
-18.00	.73	.87	.84	.81	.81	.80	.73
-20.00	.67	.79	.75	.72	.71	.68	.61
-22.00	.65	.75	.70	.65	.61	.54	.45
-24.00	.70	.82	.76	.67	.57	.44	.29
-25.40	.76	1.00	1.01	.89	.69	.47	.27

Table 4.19. Inner Annulus Relative Power Distribution
Time = 27.058 Days

Axial Height (cm)	Radius (cm)						
	7.14	8.00	9.00	10.00	11.00	12.00	12.60
25.40	.49	.78	.97	1.04	1.03	.90	.75
24.00	.51	.78	.88	.88	.87	.81	.71
22.00	.44	.70	.79	.79	.77	.73	.64
20.00	.45	.73	.82	.81	.79	.74	.65
18.00	.49	.78	.88	.87	.86	.80	.70
16.00	.52	.84	.95	.94	.93	.87	.76
14.00	.56	.90	1.02	1.01	.99	.93	.81
12.00	.59	.95	1.08	1.08	1.06	.99	.86
10.00	.62	1.00	1.13	1.13	1.11	1.04	.91
8.00	.65	1.04	1.18	1.18	1.16	1.08	.95
6.00	.66	1.07	1.21	1.21	1.19	1.11	.97
4.00	.68	1.09	1.24	1.23	1.21	1.14	.99
2.00	.69	1.10	1.25	1.25	1.23	1.15	1.00
.00	.69	1.11	1.26	1.25	1.23	1.15	1.01
-2.00	.68	1.10	1.25	1.25	1.23	1.15	1.00
-4.00	.68	1.09	1.24	1.23	1.21	1.13	.99
-6.00	.66	1.07	1.21	1.21	1.18	1.11	.97
-8.00	.65	1.04	1.18	1.18	1.15	1.08	.94
-10.00	.62	1.00	1.13	1.13	1.10	1.03	.90
-12.00	.59	.95	1.08	1.07	1.05	.99	.86
-14.00	.56	.90	1.01	1.01	.99	.93	.81
-16.00	.52	.84	.95	.94	.92	.86	.75
-18.00	.49	.78	.88	.87	.85	.80	.70
-20.00	.45	.72	.81	.80	.78	.73	.64
-22.00	.44	.70	.79	.78	.76	.72	.63
-24.00	.51	.77	.87	.87	.85	.79	.70
-25.40	.48	.78	.96	1.03	1.01	.89	.74

Table 4.20. Outer Annulus Relative Power Distribution
Time = 27.058 Days

Axial Height (cm)	Radius (cm)						
	15.15	16.00	17.00	18.00	19.00	20.00	21.00
25.40	.77	1.05	1.10	1.01	.84	.64	.45
24.00	.71	.86	.83	.77	.70	.62	.51
22.00	.65	.78	.75	.71	.70	.66	.57
20.00	.66	.80	.78	.76	.76	.74	.66
18.00	.72	.88	.86	.84	.85	.83	.75
16.00	.78	.95	.94	.92	.93	.92	.83
14.00	.83	1.02	1.01	.99	1.01	.99	.89
12.00	.89	1.09	1.08	1.06	1.08	1.06	.96
10.00	.93	1.14	1.13	1.11	1.13	1.11	1.00
8.00	.97	1.19	1.18	1.16	1.18	1.16	1.05
6.00	1.00	1.22	1.21	1.19	1.22	1.19	1.08
4.00	1.02	1.25	1.24	1.22	1.24	1.22	1.10
2.00	1.03	1.27	1.25	1.23	1.26	1.24	1.12
.00	1.03	1.27	1.26	1.24	1.26	1.24	1.12
-2.00	1.03	1.27	1.25	1.23	1.26	1.24	1.12
-4.00	1.02	1.25	1.24	1.22	1.24	1.22	1.10
-6.00	.99	1.22	1.21	1.19	1.21	1.19	1.08
-8.00	.97	1.19	1.18	1.16	1.18	1.16	1.05
-10.00	.93	1.14	1.13	1.11	1.13	1.11	1.00
-12.00	.88	1.08	1.07	1.05	1.08	1.06	.96
-14.00	.83	1.02	1.01	.99	1.01	.99	.89
-16.00	.77	.95	.93	.91	.93	.91	.83
-18.00	.71	.87	.86	.83	.85	.83	.75
-20.00	.66	.80	.78	.75	.76	.74	.66
-22.00	.64	.77	.74	.70	.68	.64	.56
-24.00	.70	.84	.80	.74	.67	.58	.48
-25.40	.75	1.01	1.05	.95	.78	.57	.38

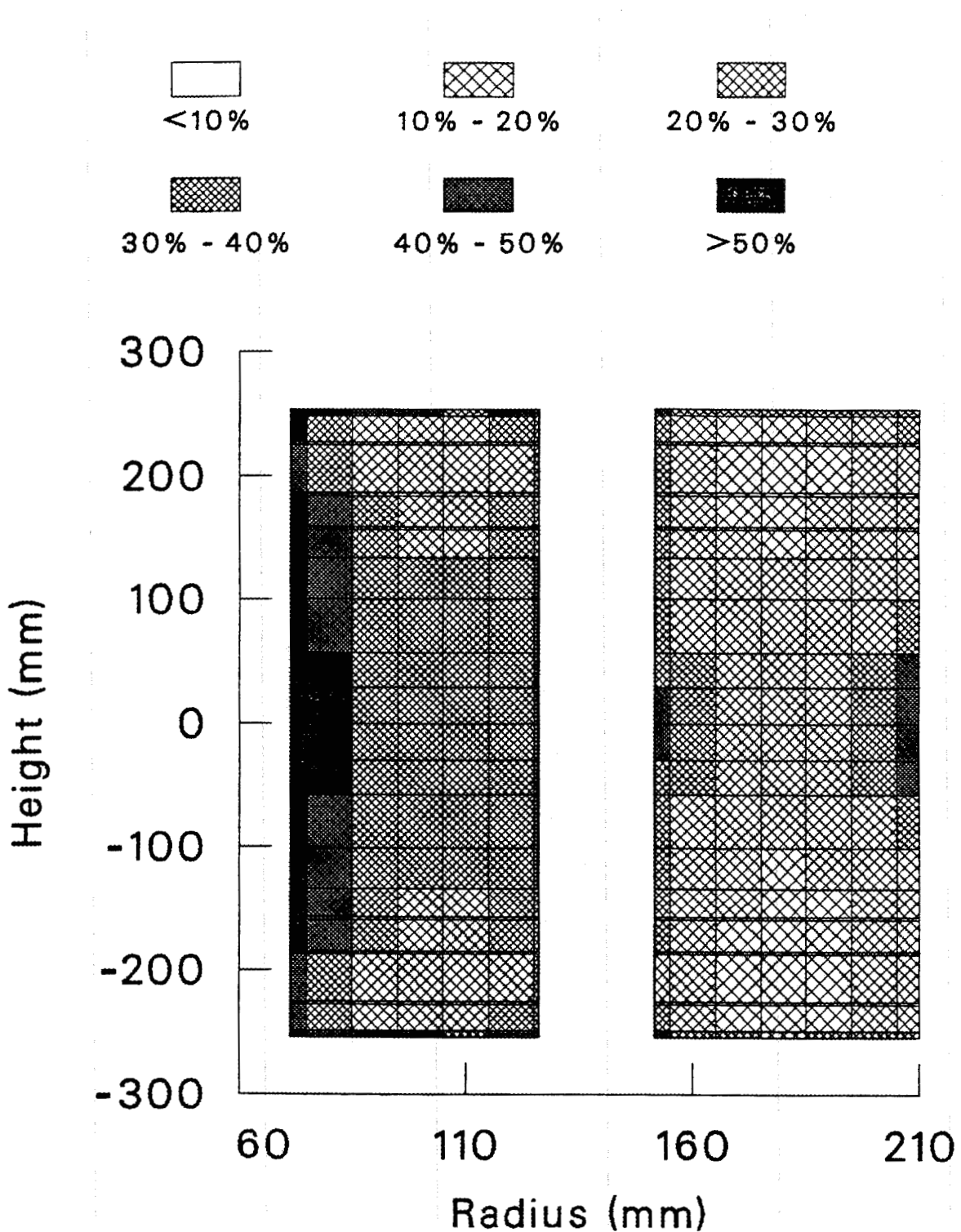


Fig. 4.25. Fuel depletion in HFIR at end-of-cycle.
(% of original U-235 destroyed)

The region with lowest burnup is along the upper portion of the outside edge of the outer element. This region is shielded by the control blade until the final few days of the cycle yielding poor fuel utilization.

The reduction in local power generation as one approaches the axial edge of the fuel element is apparent. This effect is the well-known cosine-like axial flux distribution for cylindrical reactors.

Experimental measurements of the spatially dependent U-235 depletion are reported in Ref. 10. "The fuel elements examined in this core evaluation program were identified as fuel elements 21-0 and 49-I (an I or 0 suffix designates an inner or outer annulus fuel element, respectively). Elements 21-0 and 49-I were selected primarily because (1) their in-reactor behavior appeared to be typical of that of the standard, nonpretreated HFIR fuel elements, and (2) they became available for examination during convenient periods for hot cell scheduling."⁵

"Fuel element 21-0 was used during cycle 16 of the HFIR, which was brought to power on December 10, 1967, and operated at 100 MW until January 2, 1968, when loss of reactivity caused a shutdown after 2309 MWd. Fuel element 49-I was used during cycle 35 of the HFIR, which was brought to power on May 19, 1969, and operated at 100 MWd until June 11, 1969, when loss of reactivity caused a shutdown after 2319 MWd."⁵

Single fuel plates were extracted from each of these two elements. "The plates selected for analytical burnup determinations were initially sectioned with a water-cooled abrasive cutoff wheel. Five samples were cut from each plate. The analytical burnup samples were selected to provide samples from two minimum burnup locations, two intermediate burnup locations, and a maximum burnup region. To determine the burnup at specific locations within the fuel plates, the five large burnup samples from each fuel plate were cut to provide samples from the inner edge, outer edge, and central region of each large section."⁵

"The individual burnup samples were then submitted for uranium mass-spectrographic analysis, and the atom percent of total uranium fissioned was calculated for each sample from changes in the isotopic composition. The burnup of some of the samples was also determined radiochemically (i.e., from uranium and ¹³⁷Cs analyses) as a secondary check; generally, excellent agreement was found."⁵

Table 4.21 provides a comparison of calculated and measured depletion percentages. The time-averaged calculated power density is underpredicted along the axial midplane at the element and overpredicted at the axial edges. The presence of control blades along the outside edge of the outer element probably explains the poor c/e ratios at the outermost radius. It should be noted that while measured values are reported for a specific location, they actually are volume-weighted values over approximately 1 square cm of surface area. Calculated values are similarly weighted, but approximation was necessary due to mesh point spacing.

Table 4.21. Comparison of Calculated and Measured HFIR Fuel Depletion

Radius ^(a) (mm)	Height ^(b) (mm)	Burnup (% of Uranium Destroyed)		
		Calculated	Measured	c/e Ratio
75.5	-247.65	41.80	37.41	1.117
100.0	-247.65	28.78	18.82	1.529
123.0	-247.65	33.00	24.86	1.327
154.5	-234.96	24.00	21.07	1.139
175.0	-234.96	14.06	10.31	1.364
205.0	-234.96	19.93	13.86	1.438
75.5	-133.35	42.32	49.91	.848
100.0	-133.35	23.63	25.77	.917
123.0	-133.35	29.38	31.73	.926
154.5	-120.65	26.69	27.72	.963
175.0	-120.65	15.59	15.43	1.011
205.0	-120.65	19.91	31.16	.639
75.5	19.05	47.41	54.65	.868
100.0	19.05	27.32	32.96	.829
123.0	19.05	33.73	38.72	.871
154.5	6.35	30.38	34.22	.888
175.0	6.35	19.16	20.88	.918
205.0	6.35	34.01	39.65	.858
75.5	95.25	45.12	51.70	.873
100.0	95.25	25.63	26.38	.972
123.0	95.25	31.73	32.24	.984
154.5	107.95	27.80	26.36	1.054
175.0	107.95	16.64	15.03	1.107
205.0	107.95	23.07	29.69	.777
75.5	209.55	36.22	36.14	1.002
100.0	209.55	19.48	16.93	1.151
123.0	209.55	25.25	21.59	1.169
154.5	222.25	23.24	18.24	1.274
175.0	222.25	13.72	7.76	1.768
205.0	222.25	22.02	10.33	2.132

^(a)Radii 75.5 - 123.0 are inside inner element, 154.5 - 205.0 are in outer element.

^(b)0.0 is at axial centerline, top of element is at 254.0 mm and bottom is at -254.0 mm.

The boron-10 and U-235 inventories at various times during the fuel cycle are shown in Table 4.22. By the middle of the cycle, 80% of the boron-10 is consumed. Indeed the reason for the long time step from 1.176 to 14.117 days is because reactivity control during this time is largely due to boron-10 depletion. The loss in reactivity due to U-235 consumption is almost exactly balanced by the gain in reactivity due to boron-10 depletion.

Table 4.22. Whole Core Quantities of Fuel and Burnable Poison

Time (d)	Boron-10 (g)	U-235 (kg)
0.0	2.800	9.469
0.588	2.624	9.406
1.176	2.463	9.344
14.117	0.609	7.976
18.823	0.394	7.561
21.176	0.319	7.366
23.529	0.260	7.177
27.058	0.192	6.902

Based on the HFIR 100 MW burnup limit of 2300 megawatt-days, the expected cycle length for an 85 MW cycle is 27.058 days. Data for that level of burnup for the fuel region are reported in Table 4.22. Note that data are provided for both VENTURE-BURNER calculations and for ORIGEN-S (Ref. 5) calculations. ORIGEN-S is a commonly used program for calculating time dependent behavior of nuclear systems. ORIGEN-S results are reported here as an aid to validating the VENTURE-BURNER methodology.

The individual zone atom densities which, when summed, yield the values given in Table 4.23 were supplied to other members of the Engineering Physics and Mathematics Division for use in transport, discrete ordinates calculations. That information is too voluminous to be presented here, but can be easily replicated using the datasets in Appendix A.

The BURNER module is that part of the VENTURE system which performs depletion calculations. By dividing the system to be investigated into a set of zones, multidimensional depletion calculations can be performed. In contrast, the ORIGEN program can only calculate zero-dimensional problems. This requires the entire reactor to be homogenized into a single point. The VENTURE-BURNER calculations would be expected to be more accurate because of the multidimensional treatment and because the BURNER neutronic data are more recent than the ORIGEN data (ENDF/B-V vs. ENDF/B-IV).

The level of agreement between calculations indicates that the input to BURNER was prepared correctly. Order-of-magnitude errors would result if depletion chains were entered improperly or fission yields were misordered. Note that the weights for the lumped fission products are based on a fictitious atomic weight of 117.5. The Xe and I concentrations as calculated by ORIGEN are much higher than that calculated with BURNER. This may indicate a cross-section processing problem in the data prepared for either or both programs. These nuclides can have a significant impact on the dose received during an accident scenario.

Table 4.23. End-of-Life Constituents of Both HFIR Fuel Elements

Element/Nuclide	Inventory (g)		
	VENTURE-BURNER	ORIGEN	% Difference
B-10	0.181	0.255	40.884
B-11	12.381	9.452	-23.657
C	4.210	4.24	0.713
Ce-141	54.324	67.6	24.439
Cs-133	56.871	57.1	0.403
Cs-134	1.902	1.10	-42.166
Cs-135	3.109	2.45	-21.197
I-135	0.923	1.53	65.764
Mod.abs.fiss.prod.	4.817		
Mo-97	51.692	58.7	13.557
Nd-143	33.795	29.1	-13.893
Nd-145	49.463	57.4	16.046
Nd-147	12.068	18.7	54.955
Np-237	16.063	9.89	-38.430
Np-238	0.325	0.160	-50.769
Np-239	2.658	1.01	-62.002
Pm-147	12.547	14.4	14.768
Pm-148	0.227	0.242	6.608
Pm-148M	0.202	0.0696	-65.545
Pm-149	1.698	2.42	42.521
Pr-143	38.353	48.1	25.414
Pu-238	0.944	.275	-70.869
Pu-239	13.430	3.49	-74.013
Pu-240	1.342	0.504	-62.444
Pu-241	0.594	0.133	-77.609
Pu-242	0.039	0.0068	-82.564
Rh-103	5.566	5.66	1.689
Rh-105	0.345	0.560	62.319
Ru-101	45.598	52.6	15.356
Ru-103	21.905	27.9	27.368
Sm-149	0.486	0.352	-27.572
Sm-150	12.094	15.0	24.028
Sm-151	1.308	1.18	-9.786
Sm-152	6.570	8.42	28.158
Sm-153	0.532	0.684	28.571
Tc-99	52.514	51.9	-1.169
U-234	87.617	86.5	-1.275
U-235	6896.485	6541.	-5.155
U-236	500.695	562.	12.244
U-238	532.609	542.	1.763
Weak.abs.fiss.prod.	4.084		
Xe-131	30.292	20.4	-32.655
Xe-133	18.842	28.1	49.135
Xe-135	0.055	0.0484	-12.000
Zr-93	53.168	61.3	15.295

Table 4.24 provides data on the quantities of actinides present in the campaign 65 target rods at beginning-of-life and after one cycle of irradiation. Regarding Cf-252 production, C.W. Alexander, Chemical Technology Division, states that targets are normally left in the reactor for one calendar year at which time 400 milligrams of Cf-252 are recovered. However, estimates are available as to the production rate after one irradiation cycle in the reactor. Alexander reports two numbers, one estimate - designated midplane - is based on the assumption that the flux over the entire rod is the same as the flux at the axial midplane of the target. The other - designated average - is based on the best estimate of the axial variation of the flux over the target.

Measured quantities of actinides from campaign 65 were not available but for campaign 64, the quantity of Cf-252 per target rod for the midplane case was 7.90 milligrams. The average value was 5.58 milligrams. Campaign 64 rods had an initial curium loading of 3.83 gr. Cm-244 and 3.6 gr. Cm-246. For campaign 62, the midplane value was 6.76 milligrams and the average value was 4.75 milligrams. The value from the VENTURE calculation for campaign 65 was 8.17 milligrams per rod. Thus it appears that the BURNER module and its associated input data can be used to predict actinide concentrations with reasonable accuracy.

Table 4.24. End-of-Life Constituents of HFIR Target Rods

Nuclide	Inventory (Kg)	
	Beginning-of-Cycle	End-of-Cycle
Am241	6.888488E-04	3.146947E-05
Am242	0.0	2.444230E-06
Am242m	0.0	2.821454E-07
Am243	2.195609E-03	1.210949E-03
Bk249	0.0	7.268685E-05
Cf249	0.0	4.928582E-07
Cf250	0.0	5.551047E-05
Cf251	0.0	1.563785E-05
Cf252	2.251142E-07	1.225701E-04
Cf253	0.0	1.220490E-06
Cm242	0.0	3.052012E-04
Cm243	0.0	8.183217E-06
Cm244	6.862979E-02	5.849830E-06
Cm245	9.844985E-04	1.073200E-03
Cm246	4.730847E-02	4.720799E-02
Cm247	1.334170E-03	1.421256E-03
Cm248	8.264707E-03	8.198053E-03
Es253	0.0	2.699753E-07
Pu238	1.665839E-05	1.471283E-05
Pu239	9.004579E-06	4.209478E-08
Pu240	3.199617E-03	1.614822E-04
Pu241	3.001523E-07	1.396997E-04
Pu242	8.554346E-06	6.600654E-04
Pu243	0.0	2.642709E-06

5. CONCLUSIONS

HFIR specific, few group neutron and coupled neutron-gamma libraries have been prepared. These are based on data from ENDF/B-V and beginning-of-life (BOL) conditions. The neutron library includes actinide data for curium target rods. In previous calculations reported in 1971, only simulated Pu-242 target data were utilized.

The six critical experiments, collectively designated HFIR critical experiment 4, were analyzed. Calculated k-effective was 2% high at BOL-typical conditions but was 1.0 at end-of-life-typical conditions. Since the experiments were performed to examine the ability to accurately calculate the core at various control blade positions, these results indicated that if exposure related parameters can be estimated accurately, an accurate estimate of cycle length should be attainable.

Through studies of the critical experiments, it was determined that a special blackness treatment was required in order to obtain correct diffusion coefficients for the europium regions of the control blades. Nevertheless, the variance in k-effective as a function of control blade position indicated that reviews of the exact positions of the control blades and the exact boron concentrations in the coolant were needed.

The local power density distributions were calculated for each of the critical experiments. The axially averaged values at a given radius were frequently within experimental error. However at individual points, the calculated local power densities were significantly different from the experimentally derived values (several times greater than experimental uncertainty). A reassessment of the foil activation data seems desirable.

One potential use of diffusion calculations is in the certification of reactor experiments. It is required that a given experiment configuration will not increase the peak local power density at the limiting point by more than 5%. The critical experiment calculations indicate that only certain experiments could be certified using diffusion theory.

If the reactivity worth of the experiment is small (control blade movement less than a centimeter), then unperturbed and perturbed distributions could be compared to determine percentage difference. However, if the pre- and post-experiment-insertion control blade positions are significantly different, then the differences in the power distributions among the critical experiments indicates that an effect due to the experiment would not be quantifiable. This is due to differences in calculation/experiment agreement for a given physical position among the critical experiments usually exceeding 5%. Again, a reassessment of foil activation data could modify this conclusion.

Using the results of the critical experiments study, a model of the current HFIR configuration was prepared. As with the critical experiments, BOL k-effective was high (3%). However, end-of-life k-effective was also high (2%). The end-of-life concentrations of fission products were compared to those generated using the ORIGEN code. Agreement was generally good through differences in the inventories of some important nuclides, Xe and I, need to be understood. End-of-cycle curium target isotopes based on measured, discharged target rods were compared to calculated values and agreement was good.

Axial flux plots at various irradiation positions were generated. Time-dependent power distributions based on two-dimensional calculations were provided. The former provide information to experiment planners and the latter serve as input to thermal-hydraulic analyses for safety studies.

6. REFERENCES

1. R. D. Cheverton and T. M. Sims, "HFIR Core Nuclear Design," ORNL-4621 (July 1971).
2. W. E. Ford, III, et al., "ANSL-V: ENDF/B-V Based Multigroup Cross-section Libraries for Advanced Neutron Source (ANS) Reactor Studies," ORNL-6618 (September 1990).
3. R. Kinsey, ed., "ENDF/B Summary Documentation," BNL-NCS-17541 (ENDF-201), 3rd ed., Brookhaven National Laboratory (1979).
4. N. M. Greene, et. al., "AMPX: A Modular Code System for Generating Coupled Multigroup Neutron-Gamma Libraries from ENDF/B," ORNL-TM-3706 (March 1976).
5. "SCALE: A Modular Code System for Performing Standardized Computer Analyses for Licensing Evaluation, Vols. 1-3," NUREG/CR-0200, U.S. Nuclear Regulatory Commission (originally issued July 1980, reissued January 1982, Rev. 1 issued July 1982, Rev. 2 issued June 1983, Rev. 3 issued December 1984).
6. R. T. Primm, III, "Accuracy of Calculated Power Distribution Using Few Group Cross-Section Sets," Trans. Am. Nucl. Soc., Vol. 61 (June 1990).
7. D. R. Vondy, T. B. Fowler, and G. W. Cunningham, III, "The Bold Venture Computation System for Nuclear Reactor Core Analysis, Version III," ORNL-5711 (June 1981).
8. D. R. Vondy and G. W. Cunningham, "Exposure Calculation Code Module for Reactor Core Analysis: BURNER," ORNL-5180 (February 1979).
9. R. T. Primm, III and N. M. Greene, "Generation of Lumped Fission Product Cross Sections for High-Burnup, Highly Enriched Uranium Fuel," Trans. Am. Nucl. Soc., Vol 56, pp. 592-594 (June 1988).
10. A. E. Rich, R. W. Knight, and G. W. Adamson, Jr., "Postirradiation Examination and Evaluation of the Performance of HFIR Fuel Elements," ORNL-4714 (December 1971).
11. A. F. Henry, Nuclear Reactor Analysis, The MIT Press, pp. 433-454 (1975).

APPENDIX A

The best, though admittedly most cumbersome, method of insuring that future investigators will understand the work which has been performed is to record the datasets which were input to the analysis codes. The following code input corresponds to the cross-section production work described in Section 2.

```

#AJAX
0$$ 92 91
1$$ 1 T
2$$ 91 85 T
3$$
1801 8016 14000 26000 29000 25055 12000 24000 22000 13027
952411 942381 942391 942401 942411 962441 942421
952431 962451 962461 962471 962481 982521
962421 972491 982491 982501 982511 982531 992531 962431 952421 942431
952420 47107 47109
420971 441011 441031 451031 451051 531351 541311 541331 541351 551331
551341 551351 601431 601451 601471 611481 611482 611491 621501 621511
621521 631551 631531 631541 611471 591431 621491 621531 430991 400931
581411 130112 230112
130271 5010 5011 6012 922341 922351 922361 922381 932371 932381 932391
631511 73181 73182 72000 4009
T
END
#BONAMI
0$$ 92 A4 93
1$$ 2 4 87 0 0 1005 T
3$$
36R1 46R2 4R3 4
4$$
1801 8016 14000 26000 29000 25055 12000 24000 22000 13027
952411 942381 942391 942401 942411 962441 942421
952431 962451 962461 962471 962481 982521
962421 972491 982491 982501 982511 982531 992531 962431 952421 942431
952420 47107 47109
420971 441011 441031 451031 451051 531351 541311 541331 541351 551331
551341 551351 601431 601451 601471 611481 611482 611491 621501 621511
621521 631551 631531 631541 611471 591431 621491 621531 430991 400931
581411 130112 230112
1801 8016 130271 5010 5011 6012 922341 922351 922361 922381
932371 932381 932391
631511 73181 73182 72000 4009
5**
3.97136E-02 1.98568E-02 6.00220E-05 5.28249E-05 2.65284E-05 1.15069E-05
1.38719E-04 2.83686E-05 1.31976E-05 1.50965E-02
9.14522E-07 2.23946E-08 1.20546E-08 4.26554E-06 3.98485E-10
8.99933E-05 1.13099E-08 2.89092E-06 1.28569E-06 6.15306E-05
1.72823E-06 1.06626E-05 2.85818E-10 13R1.0E-20
33R1.0E-20
3.26876E-02 1.69373E-02 1.53352E-05 6.21076E-05 2.4843E-4
7.76345E-05 2.21973E-06 2.07451E-04 8.89966E-07 1.20114E-05
3R1.0E-20
3.18E-3
1.46E-2 1.0E-20
1.0E-20
1.208E-1
6$$

```

```

1 2 3 4
7**
7.14 21.0 24.127 54.0
8** F343.0
10$$
1801 8016 14000 26000 29000 25055 12000 24000 22000 13027
952411 942381 942391 942401 942411 962441 942421
952431 962451 962461 962471 962481 982521
962421 972491 982491 982501 982511 982531 992531 962431 952421 942431
952420 47107 47109
420971 441011 441031 451031 451051 531351 541311 541331 541351 551331
551341 551351 601431 601451 601471 611481 611482 611491 621501 621511
621521 631551 631531 631541 611471 591431 621491 621531 430991 400931
581411 130112 230112
991801 998016 130271 5010 5011 6012 922341 922351 922361 922381
932371 932381 932391
631511 73181 73182 72000 4009
11$$
2 0 1 2
12**
10R343.0 26R430.0 33R430.0 6R343.0 7R430.0 5R343.0
T
END
#NITAWL
0$$ 93 A4 94 E
1$$ A2 85 A8 4 E T
2$$
1801 8016 14000 26000 29000 25055 12000 24000 22000 13027
952411 942381 942391 942401 942411 962441 942421
952431 962451 962461 962471 962481 982521
962421 972491 982491 982501 982511 982531 992531 962431 952421 942431
952420 47107 47109
420971 441011 441031 451031 451051 531351 541311 541331 541351 551331
551341 551351 601431 601451 601471 611481 611482 611491 621501 621511
621521 631551 631531 631541 611471 591431 621491 621531 430991 400931
581411 130112 230112
130271 5010 5011 6012 922341 922351 922361 922381
932371 932381 932391
631511 73181 73182 72000 4009
3**
922341 430.0 2 21.0 1.774E-3 7.14 7.1624E-6 1 1 9.58E4 1 15.9994
9.43E3 1 1.0
922351 430.0 2 21.0 1.774E-3 7.14 6.6939E-4 1 1 1.03E3 1 15.9994
1.01E2 1 1.0
922361 430.0 2 21.0 1.774E-3 7.14 2.87168E-6 1 1 2.39E5 1 15.9994
2.35E4 1 1.0
922381 430.0 2 21.0 1.774E-3 7.14 3.87577E-5 1 1 1.77E4 1 15.9994
1.74E3 1 1.0
4**
10R343.0 26R430.0 33R430.0 4R343.0 7R430.0 5R343.0
T
END
#XSDRNPM
HFIR, PREPARED 1/17/90, Modified 7/30/91
0$$ A3 94 A5 2 E
1$$ 2 32 119 1 0 28 394 8 3 1 10 10 E
2$$ -2 0 0 A9 41 E
3$$ 1 A4 40 100 A6 0 E
4$$ 1 7 20 -2 85 E
5** A3 0.144E+18 0 0 A7 50.8 E T
13$$
10R1 36R2 10R3 10R4
33R5 17R5 17R6 17R7 17R8 17R9 17R10 17R11 17R12

```

10R13 14R14 14R15 14R16 14R17 14R18 14R19 14R20 14R21 14R22
 3R22
 2R23 4R24 5R25 5R26 4R27
 14\$
 1801 8016 14000 26000 29000 25055 12000 24000 22000 13027
 952411 942381 942391 942401 942411 962441 942421
 952431 962451 962461 962471 962481 982521
 962421 972491 982491 982501 982511 982531 992531 962431 952421 942431
 952420 47107 47109
 1801 8016 14000 26000 29000 25055 12000 24000 22000 13027
 1801 8016 14000 26000 29000 25055 12000 24000 22000 13027
 1801 8016 14000 26000 29000 25055 12000 24000 22000 13027
 420971 441011 441031 451031 451051 531351 541311 541331 541351 551331
 551341 551351 601431 601451 601471 611481 611482 611491 621501 621511
 621521 631551 631531 631541 611471 591431 621491 621531 430991 400931
 581411 130112 230112
 14000 26000 29000 25055 12000 24000 22000 130271
 1801 8016 5010 5011 6012 922341 922351 922361 922381
 7Q17
 1801 8016 14000 26000 29000 25055 12000 24000 22000 13027
 14000 26000 29000 25055 12000 24000 22000 130271
 1801 8016 922341 922351 922361 922381
 8Q14
 932371 932381 932391
 1801 8016
 631511 631531 8016 13027
 73181 73182 13027 1801 8016
 72000 1801 8016 13027 4009
 1801 8016 13027 4009
 15**
 3.97136E-02 1.98568E-02 6.00220E-05 5.28249E-05 2.65284E-05 1.15069E-05
 1.38719E-04 2.83686E-05 1.31976E-05 1.50965E-02
 9.14522E-07 2.23946E-08 1.20546E-08 4.26554E-06 3.98485E-10
 8.99933E-05 1.13099E-08 2.89092E-06 1.28569E-06 6.15306E-05
 1.72823E-06 1.06626E-05 2.85818E-10 13R1.0E-20
 3.97136E-02 1.98568E-02 6.14583E-05 5.40890E-05 2.71632E-05 1.17823E-05
 1.42038E-04 2.90474E-05 1.35134E-05 1.54577E-02
 3.97136E-02 1.98568E-02 9.09042E-05 8.00041E-05 4.01777E-05 1.74274E-05
 2.10091E-04 4.29647E-05 1.99880E-05 2.28639E-02
 1.074E-2 5.37E-3 1.90843E-4 1.67959E-4 8.43483E-5 3.65867E-5
 4.41062E-4 9.01992E-5 4.19625E-5 4.8E-2
 33R1.0E-20
 1.04562E-04 9.20241E-05 4.62141E-05 2.00457E-05 2.41656E-04 4.94198E-05
 2.29911E-05 2.62990E-02 3.26876E-02 1.69373E-02 1.53352E-05 6.21076E-05
 2.55517E-05 2.21973E-06 2.07451E-04 8.89966E-07 1.20114E-05
 1.06416E-04 9.36558E-05 4.70335E-05 2.04011E-05 2.45941E-04 5.02960E-05
 2.33987E-05 2.67653E-02 3.26876E-02 1.70847E-02 1.30670E-05 5.29214E-05
 2.17724E-05 2.77094E-06 2.58966E-04 1.11096E-06 1.49941E-05
 1.08348E-04 9.53561E-05 4.78874E-05 2.07715E-05 2.50406E-04 5.12092E-05
 2.38235E-05 2.72512E-02 3.26876E-02 1.72383E-02 1.07034E-05 4.33486E-05
 1.78341E-05 3.34533E-06 3.12648E-04 1.34126E-06 1.81023E-05
 1.10839E-04 9.75486E-05 4.89885E-05 2.12491E-05 2.56163E-04 5.23866E-05
 2.43713E-05 2.78778E-02 3.26876E-02 1.74363E-02 7.65574E-06 3.10057E-05
 1.27561E-05 4.08595E-06 3.81864E-04 1.63820E-06 2.21099E-05
 1.13033E-04 9.94791E-05 4.99580E-05 2.16697E-05 2.61233E-04 5.34233E-05
 2.48536E-05 2.84295E-02 3.26876E-02 1.76107E-02 4.97174E-06 2.01356E-05
 8.28397E-06 4.73819E-06 4.42822E-04 1.89971E-06 2.56394E-05
 1.13434E-04 9.98325E-05 5.01355E-05 2.17466E-05 2.62161E-04 5.36131E-05
 2.49419E-05 2.85305E-02 3.26876E-02 1.76426E-02 4.48069E-06 1.81468E-05
 7.46577E-06 4.85753E-06 4.53974E-04 1.94755E-06 2.62851E-05
 1.12356E-04 9.88834E-05 4.96588E-05 2.15399E-05 2.59669E-04 5.31034E-05
 2.47048E-05 2.82593E-02 3.26876E-02 1.75569E-02 5.80024E-06 2.34910E-05
 9.66441E-06 4.53686E-06 4.24005E-04 1.81898E-06 2.45499E-05

1.10411E-04 9.71721E-05 4.87994E-05 2.11671E-05 2.55175E-04 5.21844E-05
 2.42772E-05 2.77702E-02 3.26876E-02 1.74023E-02 8.17885E-06 3.31243E-05
 1.36277E-05 3.95882E-06 3.69984E-04 1.58723E-06 2.14220E-05
 2.75E-2 1.375E-2 1.40508E-4 1.23660E-4 6.21015E-5 2.69370E-5
 3.24732E-4 6.64092E-5 3.08949E-5 3.534E-2
 1.07284E-04 9.44196E-05 4.74171E-05 2.05675E-05 2.47947E-04 5.07062E-05
 2.35895E-05 2.69836E-02 3.26876E-02 1.75490E-02 4.50716E-06 4.21230E-04
 1.80708E-06 2.43892E-05
 1.09748E-04 9.65884E-05 4.85063E-05 2.10400E-05 2.53642E-04 5.18709E-05
 2.41314E-05 2.76034E-02 3.26876E-02 1.78405E-02 5.59742E-06 5.23124E-04
 2.24420E-06 3.02889E-05
 1.11844E-04 9.84329E-05 4.94326E-05 2.14418E-05 2.58486E-04 5.28615E-05
 2.45922E-05 2.81305E-02 3.26876E-02 1.80884E-02 6.52459E-06 6.09775E-04
 2.61593E-06 3.53060E-05
 1.13286E-04 9.97020E-05 5.00699E-05 2.17182E-05 2.61818E-04 5.35431E-05
 2.49093E-05 2.84932E-02 3.26876E-02 1.82590E-02 7.16248E-06 6.69390E-04
 2.87168E-06 3.87577E-05
 1.12786E-04 9.92618E-05 4.98489E-05 2.16223E-05 2.60662E-04 5.33067E-05
 2.47993E-05 2.83674E-02 3.26876E-02 1.81998E-02 6.94119E-06 6.48710E-04
 2.78296E-06 3.75603E-05
 1.10081E-04 9.68811E-05 4.86533E-05 2.11037E-05 2.54411E-04 5.20281E-05
 2.42045E-05 2.76870E-02 3.26876E-02 1.78798E-02 5.74454E-06 5.36873E-04
 2.30319E-06 3.10850E-05
 1.07293E-04 9.44273E-05 4.74210E-05 2.05692E-05 2.47967E-04 5.07104E-05
 2.35915E-05 2.69858E-02 3.26876E-02 1.75500E-02 4.51105E-06 4.21593E-04
 1.80863E-06 2.44102E-05
 1.05383E-04 9.27465E-05 4.65769E-05 2.02031E-05 2.43553E-04 4.98077E-05
 2.31715E-05 2.65055E-02 3.26876E-02 1.73241E-02 3.66617E-06 3.42632E-04
 1.46989E-06 1.98384E-05
 1.03658E-04 9.12283E-05 4.58145E-05 1.98724E-05 2.39566E-04 4.89924E-05
 2.27922E-05 2.60716E-02 3.26876E-02 1.71200E-02 2.90300E-06 2.71308E-04
 1.16391E-06 1.57087E-05
 3R1.0E-20
 6.53753E-02 3.26876E-02
 2.93E-3 3.18E-3 9.16E-3 3.50E-2
 1.46E-2 1.0E-20 4.17E-2 2.72E-3 1.38E-3
 1.0E-20 3.2797E-3 1.6399E-3 5.52E-4 1.167E-1
 0.99407E-3 0.49704E-3 5.6E-4 1.208E-1
 16\$
 1801 8016 14000 26000 29000 25055 12000 24000 22000 13027
 952411 942381 942391 942401 942411 962441 942421
 952431 962451 962461 962471 962481 982521
 962421 972491 982491 982501 982511 982531 992531 962431 952421 942431
 952420
 420971 441011 441031 451031 451051 531351 541311 541331 541351 551331
 551341 551351 601431 601451 601471 611481 611482 611491 621501 621511
 621521 631551 631531 631541 611471 591431 621491 621531 430991 400931
 581411 130112 230112
 130271 5010 5011 6012 922341 922351 922361 922381
 631511 73181 73182 72000 4009
 932371 932381 932391 47107 47109
 18U
 ((10(1X,A4,A2)))
 H O SI FE CU MN55 MG CR TI AL1
 AM241 PU238 PU239 PU240 PU241 CM244 PU242 AM243 CM245 CM246
 CM247 CM248 CF252 CM242 BK249 CF249 CF250 CF251 CF253 ES253
 CM243 AM242M PU243 AM242 M097 RU101 RU103 RH103 RH105 I135
 XE131 XE133 XE135 CS133 CS134 CS135 ND143 ND145 ND147 PM148
 PM148M PM149 SM150 SM151 SM152 EU155 EU153 EU154 EU154 PR143
 SM149 SM153 TC99 ZR93 CE141 MAFP WAFP AL2 B10 B11
 C U234 U235 U236 U238 EU151 TA181 TA182 HF BE
 NP237 NP238 NP239 AG107 AG109

T

```

35** 3I0.0 5I0.887 5I3.547 1I6.4
1I7.14 1I7.5 1I8.0 1I8.5 1I9.5 1I10.5 1I11.5 1I12.0
4I12.6
1I15.15 1I15.5 1I16.0 1I16.5 1I17.5 1I18.5 1I19.5 1I20.0 1I20.5 2I21.0
3I21.7678 3I22.024 3I22.659 3I22.987 3I23.622 3I23.967 15I24.127
1I133.0 6I54.0 75.0
36$$
4R1 6R2 6R3 2R4
2R5 2R6 2R7 2R8 2R9 2R10 2R11 2R12
5R13
2R14 2R15 2R16 2R17 2R18 2R19 2R20 2R21 2R22
3R23 4R24 4R25 4R26 4R27 4R28 4R29 16R30 12R31 7R32
39$$
1 2 3 4 5 6 7 8 9 10 11 12 13 14 15 16 17 18 19 20 21 22
4 23 24 23 25 23 4 26 27 23
51$$ 7R1 4R2 8R3 3R4 3R5 3R6 11R7
T
END

```

The following XSDRNPM dataset is for generating a coupled neutron-gamma library which was used in HFIR gamma heating calculations. The geometry and nuclide concentrations are essentially the same as those specified in the previous XSDRNPM dataset. However, since the neutron-gamma library does not include all the nuclides that are contained in the neutron library, various fission products and actinides had to be omitted.

```

#XSDRNPM
HFIR, n-gamma model PREPARED from 1/17/90 model
0$$ 20 A3 94 A5 2 E
1$$ 2 32 119 1 0 27 389 8 3 1 10 50 E
2$$ -2 0 0 A9 41 E
3$$ 1 A4 40 100 A6 0 E
4$$ 1 57 30 -2 3 28 84 E
5** A3 0.144E+18 0 0 A7 50.8 E T
13$$
10R1 34R2 10R3 10R4
33R5 17R5 17R6 17R7 17R8 17R9 17R10 17R11 17R12
10R13 14R14 14R15 14R16 14R17 14R18 14R19 14R20 14R21 14R22
2R23 4R24 5R25 5R26 4R27
14$$
1801 8016 14000 26000 8016 25055 12000 24000 22000 13027
8016 8016 942391 942401 942411 8016 942421
17r8016
1801 8016 14000 26000 29000 25055 12000 24000 22000 13027
1801 8016 14000 26000 29000 25055 12000 24000 22000 13027
1801 8016 14000 26000 29000 25055 12000 24000 22000 13027
33r8016
14000 26000 29000 25055 12000 24000 22000 130271
1801 8016 5010 5011 6012 92234 922352 92236 922382
7Q17
1801 8016 14000 26000 29000 25055 12000 24000 22000 13027
14000 26000 29000 25055 12000 24000 22000 130271
1801 8016 92234 922352 92236 922382
8Q14
1801 8016
631511 631531 8016 13027
73181 8016 13027 1801 8016
72000 1801 8016 13027 4009
1801 8016 13027 4009
15**

```

3.97136E-02 1.98568E-02 6.00220E-05 5.28249E-05 2.65284E-05 1.15069E-05
 1.38719E-04 2.83686E-05 1.31976E-05 1.50965E-02
 9.14522E-07 2.23946E-08 1.20546E-08 4.26554E-06 3.98485E-10
 8.99933E-05 1.13099E-08 2.89092E-06 1.28569E-06 6.15306E-05
 1.72823E-06 1.06626E-05 2.85818E-10 11R1.0E-20
 3.97136E-02 1.98568E-02 6.14583E-05 5.40890E-05 2.71632E-05 1.17823E-05
 1.42038E-04 2.90474E-05 1.35134E-05 1.54577E-02
 3.97136E-02 1.98568E-02 9.09042E-05 8.00041E-05 4.01777E-05 1.74274E-05
 2.10091E-04 4.29647E-05 1.99880E-05 2.28639E-02
 1.074E-2 5.37E-3 1.90843E-4 1.67959E-4 8.43483E-5 3.65867E-5
 4.41062E-4 9.01992E-5 4.19625E-5 4.8E-2
 33R1.0E-20
 1.04562E-04 9.20241E-05 4.62141E-05 2.00457E-05 2.41656E-04 4.94198E-05
 2.29911E-05 2.62990E-02 3.26876E-02 1.69373E-02 1.53352E-05 6.21076E-05
 2.55517E-05 2.21973E-06 2.07451E-04 8.89966E-07 1.20114E-05
 1.06416E-04 9.36558E-05 4.70335E-05 2.04011E-05 2.45941E-04 5.02960E-05
 2.33987E-05 2.67653E-02 3.26876E-02 1.70847E-02 1.30670E-05 5.29214E-05
 2.17724E-05 2.77094E-06 2.58966E-04 1.11096E-06 1.49941E-05
 1.08348E-04 9.53561E-05 4.78874E-05 2.07715E-05 2.50406E-04 5.12092E-05
 2.38235E-05 2.72512E-02 3.26876E-02 1.72383E-02 1.07034E-05 4.33486E-05
 1.78341E-05 3.34533E-06 3.12648E-04 1.34126E-06 1.81023E-05
 1.10839E-04 9.75486E-05 4.89885E-05 2.12491E-05 2.56163E-04 5.23866E-05
 2.43713E-05 2.78778E-02 3.26876E-02 1.74363E-02 7.65574E-06 3.10057E-05
 1.27561E-05 4.08595E-06 3.81864E-04 1.63820E-06 2.21099E-05
 1.13033E-04 9.94791E-05 4.99580E-05 2.16697E-05 2.61233E-04 5.34233E-05
 2.48536E-05 2.84295E-02 3.26876E-02 1.76107E-02 4.97174E-06 2.01356E-05
 8.28397E-06 4.73819E-06 4.42822E-04 1.89971E-06 2.56394E-05
 1.13434E-04 9.98325E-05 5.01355E-05 2.17466E-05 2.62161E-04 5.36131E-05
 2.49419E-05 2.85305E-02 3.26876E-02 1.76426E-02 4.48069E-06 1.81468E-05
 7.46577E-06 4.85753E-06 4.53974E-04 1.94755E-06 2.62851E-05
 1.12356E-04 9.88834E-05 4.96588E-05 2.15399E-05 2.59669E-04 5.31034E-05
 2.47048E-05 2.82593E-02 3.26876E-02 1.75569E-02 5.80024E-06 2.34910E-05
 9.66441E-06 4.53686E-06 4.24005E-04 1.81898E-06 2.45499E-05
 1.10411E-04 9.71721E-05 4.87994E-05 2.11671E-05 2.55175E-04 5.21844E-05
 2.42772E-05 2.77702E-02 3.26876E-02 1.74023E-02 8.17885E-06 3.31243E-05
 1.36277E-05 3.95882E-06 3.69984E-04 1.58723E-06 2.14220E-05
 2.75E-2 1.375E-2 1.40508E-4 1.23660E-4 6.21015E-5 2.69370E-5
 3.24732E-4 6.64092E-5 3.08949E-5 3.534E-2
 1.07284E-04 9.44196E-05 4.74171E-05 2.05675E-05 2.47947E-04 5.07062E-05
 2.35895E-05 2.69836E-02 3.26876E-02 1.75490E-02 4.50716E-06 4.21230E-04
 1.80708E-06 2.43892E-05
 1.09748E-04 9.65584E-05 4.85063E-05 2.10400E-05 2.53642E-04 5.18709E-05
 2.41314E-05 2.76034E-02 3.26876E-02 1.78405E-02 5.59742E-06 5.23124E-04
 2.24420E-06 3.02889E-05
 1.11844E-04 9.84329E-05 4.94326E-05 2.14418E-05 2.58486E-04 5.28615E-05
 2.45922E-05 2.81305E-02 3.26876E-02 1.80884E-02 6.52459E-06 6.09775E-04
 2.61593E-06 3.53060E-05
 1.13286E-04 9.97020E-05 5.00699E-05 2.17182E-05 2.61818E-04 5.35431E-05
 2.49093E-05 2.84932E-02 3.26876E-02 1.82590E-02 7.16248E-06 6.69390E-04
 2.87168E-06 3.87577E-05
 1.12786E-04 9.92618E-05 4.98489E-05 2.16223E-05 2.60662E-04 5.33067E-05
 2.47993E-05 2.83674E-02 3.26876E-02 1.81998E-02 6.94119E-06 6.48710E-04
 2.78296E-06 3.75603E-05
 1.10081E-04 9.68811E-05 4.86533E-05 2.11037E-05 2.54411E-04 5.20281E-05
 2.42045E-05 2.76870E-02 3.26876E-02 1.78798E-02 5.74454E-06 5.36873E-04
 2.30319E-06 3.10850E-05
 1.07293E-04 9.44273E-05 4.74210E-05 2.05692E-05 2.47967E-04 5.07104E-05
 2.35915E-05 2.69858E-02 3.26876E-02 1.75500E-02 4.51105E-06 4.21593E-04
 1.80863E-06 2.44102E-05
 1.05383E-04 9.27465E-05 4.65769E-05 2.02031E-05 2.43553E-04 4.98077E-05
 2.31715E-05 2.65055E-02 3.26876E-02 1.73241E-02 3.66617E-06 3.42632E-04
 1.46989E-06 1.98384E-05
 1.03658E-04 9.12283E-05 4.58145E-05 1.98724E-05 2.39566E-04 4.89924E-05

```

2.27922E-05 2.60716E-02 3.26876E-02 1.71200E-02 2.90300E-06 2.71308E-04
1.16391E-06 1.57087E-05
6.53753E-02 3.26876E-02
2.93E-3 3.18E-3 9.16E-3 3.50E-2
1.46E-2 1.0E-20 4.17E-2 2.72E-3 1.38E-3
1.0E-20 3.2797E-3 1.6399E-3 5.52E-4 1.167E-1
0.99407E-3 0.49704E-3 5.6E-4 1.208E-1
T
35** 3I0.0 5I0.887 5I3.547 1I6.4
1I7.14 1I7.5 1I8.0 1I8.5 1I9.5 1I10.5 1I11.5 1I12.0
4I12.6
1I15.15 1I15.5 1I16.0 1I16.5 1I17.5 1I18.5 1I19.5 1I20.0 1I20.5 2I21.0
3I21.7678 3I22.024 3I22.659 3I22.987 3I23.622 3I23.967 15I24.127
1I133.0 6I54.0 75.0
36$$
4R1 6R2 6R3 2R4
2R5 2R6 2R7 2R8 2R9 2R10 2R11 2R12
5R13
2R14 2R15 2R16 2R17 2R18 2R19 2R20 2R21 2R22
3R23 4R24 4R25 4R26 4R27 4R28 4R29 16R30 12R31 7R32
39$$
1 2 3 4 5 6 7 8 9 10 11 12 13 14 15 16 17 18 19 20 21 22
4 23 24 23 25 23 4 26 27 23
51$$ 37I1 39 4r40 3r41 3r42 2r43 2r44 45 3r46 2r47 4r48
2r49 50 2r51 4r52 53 54 2r55 3r56 4r57
T
END

```

The following input to VENTURE is for the calculations discussed in Section 4. The critical experiment models used for the calculations in Section 3 were essentially simplifications of the following model and thus have not been included here.

```

=CONTROL1
HFIR WITH CONTROL ROD MOVEMENT AT 85 MW   8/91 Version    7 Gps
400000
2   6   2   7   9   1   2   13  99   7   9   -5   7   13   7   9   0
1
ISOTXS
END
DCRSRP
1   1   1   1   2
85           1
H   H           1.0
O   O           16.0
SI  SI           28.0
FE  FE           56.0
CU  CU           63.5
MN55 MN55         55.0
MG  MG           24.3
CR  CR           52.0
TI  TI           47.9
AL1 AL           27.0
AM241 AM241        241.0  3.236E-11
PU238 PU238        238.0  3.236E-11
PU239 PU239        239.0  3.236E-11
PU240 PU240        240.0  3.236E-11
PU241 PU241        241.0  3.236E-11
CM244 CM244        244.0  3.236E-11
PU242 PU242        242.0  3.236E-11
AM243 AM243        243.0  3.236E-11
CM245 CM245        245.0  3.236E-11

```

CM246	CM246	246.0	3.236E-11	1
CM247	CM247	247.0	3.236E-11	1
CM248	CM248	248.0	3.236E-11	1
CF252	CF252	252.0	3.236E-11	1
CM242	CM242	242.0	3.236E-11	1
BK249	BK249	249.0	3.236E-11	1
CF249	CF249	249.0	3.236E-11	1
CF250	CF250	250.0	3.236E-11	1
CF251	CF251	251.0	3.236E-11	1
CF253	CF253	253.0	3.236E-11	1
ES253	ES253	253.0	3.236E-11	1
CM243	CM243	243.0	3.236E-11	1
AM242	MAM242M	242.0	3.236E-11	1
PU243	PU243	243.0	3.236E-11	1
AM242	AM242	241.0	3.236E-11	1
MO97	MO97	97.0		
RU101	RU101	101.0		
RU103	RU103	103.0		
RH103	RH103	103.0		
RH105	RH105	105.0		
I135	I135	135.0		
XE131	XE131	131.0		
XE133	XE133	133.0		
XE135	XE135	135.0		
CS133	CS133	133.0		
CS134	CS134	134.0		
CS135	CS135	135.0		
ND143	ND143	143.0		
ND145	ND145	145.0		
ND147	ND147	147.0		
PM148	PM148	148.0		
PM148	MPM148M	148.0		
PM149	PM149	149.0		
SM150	SM150	150.0		
SM151	SM151	151.0		
SM152	SM152	152.0		
EU155	EU155	155.0		
EU153	EU153	153.0		
EU154	EU154	154.0		
PM147	PM147	147.0		
PR143	PR143	143.0		
SM149	SM149	149.0		
SM153	SM153	153.0		
TC99	TC99	99.0		
ZR93	ZR93	93.0		
CE141	CE141	141.0		
MAFP	MAFP	117.5		
WAFF	WAFF	117.5		
AL2	AL	27.0		
B10	B10	10.0		
B11	B11	11.0		
C	C	12.0		
U234	U234	234.0		2
U235	U235	235.0	3.236E-11	1
U236	U236	236.0		2
U238	U238	238.0	3.236E-11	2
NP237	NP237	237.0		2
NP238	NP238	238.0		2
NP239	NP239	239.0		2
EU151	EU151	151.0		
AG107	AG107	107.0		
AG109	AG109	109.0		
TA181	TA181	181.0		

63	63	1	63	1.0
64	64	1	64	1.0
65	65	1	65	1.0
66	66	1	66	1.0
67	67	1	67	1.0
68	68	1	68	1.0
70	70	1	70	1.0
71	71	1	71	1.0
72	72	1	72	1.0
73	73	1	73	1.0
74	74	1	74	1.0
75	75	1	75	1.0
76	76	1	76	1.0
77	77	1	77	1.0
78	78	1	78	1.0
79	79	1	79	1.0
80	80	1	80	1.0
81	81	1	81	1.0
82	82	1	82	1.0
83	83	1	83	1.0
84	84	1	84	1.0
85	85	1	85	1.0
86	86	1	86	1.0
87	87	1	87	1.0
88	88	1	88	1.0
90	90	1	90	1.0
91	91	1	91	1.0
92	92	1	92	1.0
93	93	1	93	1.0
94	94	1	94	1.0
95	95	1	95	1.0
96	96	1	96	1.0
97	97	1	97	1.0
98	98	1	98	1.0
99	99	1	99	1.0
100100	1100			1.0
101101	1101			1.0
102102	1102			1.0
103103	1103			1.0
104104	1104			1.0
105105	1105			1.0
106106	1106			1.0
107107	1107			1.0
108108	1108			1.0
46	46	1	46	1.0
19	19	1	19	1.0
20	20	1	20	1.0
21	21	1	21	1.0
22	22	1	22	1.0
23	30	1	23	1.0
33	45	1	23	1.0
1	14	1	1	1.0
15	18	1	2	1.0

013

85

85

H	O	SI	FE	CU	MN55	MG	CR	TI	AL1	AM241	PU238
PU239	PU240	PU241	CM244	PU242	AM243	CM245	CM246	CM247	CM248	CF252	CM242
BK249	CF249	CF250	CF251	CF253	ES253	CM243	AM242	MPU243	AM242	MO97	RU101
RU103	RH103	RH105	I135	XE131	XE133	XE135	CS133	CS134	CS135	ND143	ND145
ND147	PM148	PM148	MPM149	SM150	SM151	SM152	EU155	EU153	EU154	PM147	PR143
SM149	SM153	TC99	ZR93	CE141	MAFP	WAFP	AL2	B10	B11	C	U234

SI	4.96169E-05FE	4.36674E-05CU	2.19306E-05MN55	9.51213E-06
MG	1.14671E-04CR	2.34507E-05TI	1.09098E-05AL2	1.24794E-02
H	3.26876E-02O	1.75578E-02U234	4.54026E-06U235	4.24323E-04
U236	1.82035E-06U238	2.45683E-05		
102102				
SI	5.01902E-05FE	4.41720E-05CU	2.21840E-05MN55	9.62205E-06
MG	1.15996E-04CR	2.37217E-05TI	1.10358E-05AL2	1.26236E-02
H	3.26876E-02O	1.79686E-02U234	6.07667E-06U235	5.67913E-04
U236	2.43635E-06U238	3.28822E-05		
103103				
SI	5.05954E-05FE	4.45286E-05CU	2.23631E-05MN55	9.69973E-06
MG	1.16933E-04CR	2.39132E-05TI	1.11249E-05AL2	1.27256E-02
H	3.26876E-02O	1.82590E-02U234	7.16248E-06U235	6.69390E-04
U236	2.87168E-06U238	3.87577E-05		
104104				
SI	5.05129E-05FE	4.44560E-05CU	2.23266E-05MN55	9.68390E-06
MG	1.16742E-04CR	2.38742E-05TI	1.11068E-05AL2	1.27048E-02
H	3.26876E-02O	1.81998E-02U234	6.94119E-06U235	6.48709E-04
U236	2.78296E-06U238	3.75603E-05		
105105				
SI	5.00663E-05FE	4.40630E-05CU	2.21293E-05MN55	9.59829E-06
MG	1.15710E-04CR	2.36632E-05TI	1.10086E-05AL2	1.25925E-02
H	3.26876E-02O	1.78798E-02U234	5.74454E-06U235	5.36873E-04
U236	2.30319E-06U238	3.10850E-05		
106106				
SI	4.94439E-05FE	4.35152E-05CU	2.18542E-05MN55	9.47897E-06
MG	1.14271E-04CR	2.33690E-05TI	1.08717E-05AL2	1.24359E-02
H	3.26876E-02O	1.74339E-02U234	4.07674E-06U235	3.81004E-04
U236	1.63451E-06U238	2.20601E-05		
107107				
SI	4.90309E-05FE	4.31517E-05CU	2.16716E-05MN55	9.39979E-06
MG	1.13317E-04CR	2.31738E-05TI	1.07809E-05AL2	1.23321E-02
H	3.26876E-02O	1.71379E-02U234	2.97001E-06U235	2.77571E-04
U236	1.19078E-06U238	1.60713E-05		
108108				
SI	4.89084E-05FE	4.30439E-05CU	2.16175E-05MN55	9.37631E-06
MG	1.13034E-04CR	2.31159E-05TI	1.07540E-05AL2	1.23013E-02
H	3.26876E-02O	1.70502E-02U234	2.64177E-06U235	2.46894E-04
U236	1.05918E-06U238	1.42952E-05		
71 71				
SI	1.03766E-04FE	9.13234E-05CU	4.58644E-05MN55	1.98931E-05
MG	2.39816E-04CR	4.90435E-05TI	2.28160E-05AL2	2.60988E-02
H	3.26876E-02O	1.68740E-02B10	2.15244E-05B11	8.71738E-05
C	2.71745E-05U234	1.98304E-06U235	1.85331E-04U236	7.95070E-07
U238	1.07307E-05			
72 72				
SI	1.04600E-04FE	9.20572E-05CU	4.62329E-05MN55	2.00529E-05
MG	2.41743E-04CR	4.94375E-05TI	2.29993E-05AL2	2.63085E-02
H	3.26876E-02O	1.69403E-02B10	2.01781E-05B11	8.17215E-05
C	2.54749E-05U234	2.23093E-06U235	2.08498E-04U236	8.94457E-07
U238	1.20720E-05			
73 73				
SI	1.07402E-04FE	9.45241E-05CU	4.74718E-05MN55	2.05903E-05
MG	2.48221E-04CR	5.07623E-05TI	2.36156E-05AL2	2.70134E-02
H	3.26876E-02O	1.71631E-02B10	1.56525E-05B11	6.33926E-05
C	1.97613E-05U234	3.06425E-06U235	2.86378E-04U236	1.22856E-06
U238	1.65813E-05			
74 74				
SI	1.10839E-04FE	9.75487E-05CU	4.89908E-05MN55	2.12491E-05
MG	2.56163E-04CR	5.23866E-05TI	2.43713E-05AL2	2.78778E-02
H	3.26876E-02O	1.74363E-02B10	1.01038E-05B11	4.09204E-05
C	1.27561E-05U234	4.08595E-06U235	3.81864E-04U236	1.63820E-06
U238	2.21099E-05			

75	75				
SI	1.13033E-04FE	9.94792E-05CU	4.99603E-05MN55	2.16697E-05	
MG	2.61233E-04CR	5.34233E-05TI	2.48536E-05AL2	2.84295E-02	
H	3.26876E-02O	1.76107E-02B10	6.56156E-06B11	2.65743E-05	
C	8.28397E-06U234	4.73819E-06U235	4.42822E-04U236	1.89971E-06	
U238	2.56394E-05				
76	76				
SI	1.13434E-04FE	9.98326E-05CU	5.01378E-05MN55	2.17466E-05	
MG	2.62161E-04CR	5.36131E-05TI	2.49419E-05AL2	2.85305E-02	
H	3.26876E-02O	1.76426E-02B10	5.91348E-06B11	2.39496E-05	
C	7.46577E-06U234	4.85752E-06U235	4.53974E-04U236	1.94755E-06	
U238	2.62851E-05				
77	77				
SI	1.11488E-04FE	9.81199E-05CU	4.92777E-05MN55	2.13736E-05	
MG	2.57663E-04CR	5.26934E-05TI	2.45140E-05AL2	2.80411E-02	
H	3.26876E-02O	1.74880E-02B10	9.05531E-06B11	3.66740E-05	
C	1.14323E-05U234	4.27901E-06U235	3.99907E-04U236	1.71560E-06	
U238	2.31546E-05				
78	78				
SI	1.09419E-04FE	9.62989E-05CU	4.83631E-05MN55	2.09769E-05	
MG	2.52881E-04CR	5.17154E-05TI	2.40590E-05AL2	2.75206E-02	
H	3.26876E-02O	1.73235E-02B10	1.23965E-05B11	5.02056E-05	
C	1.56505E-05U234	3.66379E-06U235	3.42411E-04U236	1.46894E-06	
U238	1.98256E-05				
79	79				
SI	1.09124E-04FE	9.60390E-05CU	4.82326E-05MN55	2.09203E-05	
MG	2.52199E-04CR	5.15759E-05TI	2.39941E-05AL2	2.74464E-02	
H	3.26876E-02O	1.73000E-02B10	1.28733E-05B11	5.21369E-05	
C	1.62526E-05U234	3.57599E-06U235	3.34205E-04U236	1.43374E-06	
U238	1.93504E-05				
80	80				
SI	4.94161E-05FE	4.34907E-05CU	2.18419E-05MN55	9.47364E-06	
MG	1.14207E-04CR	2.33558E-05TI	1.08656E-05AL2	1.24289E-02	
H	3.26876E-02O	1.74139E-02U234	4.00218E-06U235	3.74035E-04	
U236	1.60461E-06U238	2.16566E-05			
81	81				
SI	4.96169E-05FE	4.36674E-05CU	2.19306E-05MN55	9.51213E-06	
MG	1.14671E-04CR	2.34507E-05TI	1.09098E-05AL2	1.24794E-02	
H	3.26876E-02O	1.75578E-02U234	4.54026E-06U235	4.24323E-04	
U236	1.82035E-06U238	2.45683E-05			
82	82				
SI	5.01902E-05FE	4.41720E-05CU	2.21840E-05MN55	9.62205E-06	
MG	1.15996E-04CR	2.37217E-05TI	1.10358E-05AL2	1.26236E-02	
H	3.26876E-02O	1.79686E-02U234	6.07667E-06U235	5.67913E-04	
U236	2.43635E-06U238	3.28822E-05			
83	83				
SI	5.05954E-05FE	4.45286E-05CU	2.23631E-05MN55	9.69973E-06	
MG	1.16933E-04CR	2.39132E-05TI	1.11249E-05AL2	1.27256E-02	
H	3.26876E-02O	1.82590E-02U234	7.16248E-06U235	6.69390E-04	
U236	2.87168E-06U238	3.87577E-05			
84	84				
SI	5.05129E-05FE	4.44560E-05CU	2.23266E-05MN55	9.68390E-06	
MG	1.16742E-04CR	2.38742E-05TI	1.11068E-05AL2	1.27048E-02	
H	3.26876E-02O	1.81998E-02U234	6.94119E-06U235	6.48709E-04	
U236	2.78296E-06U238	3.75603E-05			
85	85				
SI	5.00663E-05FE	4.40630E-05CU	2.21293E-05MN55	9.59829E-06	
MG	1.15710E-04CR	2.36632E-05TI	1.10086E-05AL2	1.25925E-02	
H	3.26876E-02O	1.78798E-02U234	5.74454E-06U235	5.36873E-04	
U236	2.30319E-06U238	3.10850E-05			
86	86				
SI	4.94439E-05FE	4.35152E-05CU	2.18542E-05MN55	9.47897E-06	
MG	1.14271E-04CR	2.33690E-05TI	1.08717E-05AL2	1.24359E-02	

H	3.26876E-020	1.74339E-02U234	4.07674E-06U235	3.81004E-04
U236	1.63451E-06U238	2.20601E-05		
87 87				
SI	4.90309E-05FE	4.31517E-05CU	2.16716E-05MN55	9.39979E-06
MG	1.13317E-04CR	2.31738E-05TI	1.07809E-05AL2	1.23321E-02
H	3.26876E-020	1.71379E-02U234	2.97001E-06U235	2.77571E-04
U236	1.19078E-06U238	1.60713E-05		
88 88				
SI	4.89084E-05FE	4.30439E-05CU	2.16175E-05MN55	9.37631E-06
MG	1.13034E-04CR	2.31159E-05TI	1.07540E-05AL2	1.23013E-02
H	3.26876E-020	1.70502E-02U234	2.64177E-06U235	2.46894E-04
U236	1.05918E-06U238	1.42952E-05		
51 51				
SI	1.03766E-04FE	9.13234E-05CU	4.58644E-05MN55	1.98931E-05
MG	2.39816E-04CR	4.90435E-05TI	2.28160E-05AL2	2.60988E-02
H	3.26876E-020	1.68740E-02B10	2.15244E-05B11	8.71738E-05
C	2.71745E-05U234	1.98304E-06U235	1.85331E-04U236	7.95070E-07
U238	1.07307E-05			
52 52				
SI	1.04600E-04FE	9.20572E-05CU	4.62329E-05MN55	2.00529E-05
MG	2.41743E-04CR	4.94375E-05TI	2.29993E-05AL2	2.63085E-02
H	3.26876E-020	1.69403E-02B10	2.01781E-05B11	8.17215E-05
C	2.54749E-05U234	2.23093E-06U235	2.08498E-04U236	8.94457E-07
U238	1.20720E-05			
53 53				
SI	1.07402E-04FE	9.45241E-05CU	4.74718E-05MN55	2.05903E-05
MG	2.48221E-04CR	5.07623E-05TI	2.36156E-05AL2	2.70134E-02
H	3.26876E-020	1.71631E-02B10	1.56525E-05B11	6.33926E-05
C	1.97613E-05U234	3.06425E-06U235	2.86378E-04U236	1.22856E-06
U238	1.65813E-05			
54 54				
SI	1.10839E-04FE	9.75487E-05CU	4.89908E-05MN55	2.12491E-05
MG	2.56163E-04CR	5.23866E-05TI	2.43713E-05AL2	2.78778E-02
H	3.26876E-020	1.74363E-02B10	1.01038E-05B11	4.09204E-05
C	1.27561E-05U234	4.08595E-06U235	3.81864E-04U236	1.63820E-06
U238	2.21099E-05			
55 55				
SI	1.13033E-04FE	9.94792E-05CU	4.99603E-05MN55	2.16697E-05
MG	2.61233E-04CR	5.34233E-05TI	2.48536E-05AL2	2.84295E-02
H	3.26876E-020	1.76107E-02B10	6.56156E-06B11	2.65743E-05
C	8.28397E-06U234	4.73819E-06U235	4.42822E-04U236	1.89971E-06
U238	2.56394E-05			
56 56				
SI	1.13434E-04FE	9.98326E-05CU	5.01378E-05MN55	2.17466E-05
MG	2.62161E-04CR	5.36131E-05TI	2.49419E-05AL2	2.85305E-02
H	3.26876E-020	1.76426E-02B10	5.91348E-06B11	2.39496E-05
C	7.46577E-06U234	4.85752E-06U235	4.53974E-04U236	1.94755E-06
U238	2.62851E-05			
57 57				
SI	1.11488E-04FE	9.81199E-05CU	4.92777E-05MN55	2.13736E-05
MG	2.57663E-04CR	5.26934E-05TI	2.45140E-05AL2	2.80411E-02
H	3.26876E-020	1.74880E-02B10	9.05531E-06B11	3.66740E-05
C	1.14323E-05U234	4.27901E-06U235	3.99907E-04U236	1.71560E-06
U238	2.31546E-05			
58 58				
SI	1.09419E-04FE	9.62989E-05CU	4.83631E-05MN55	2.09769E-05
MG	2.52881E-04CR	5.17154E-05TI	2.40590E-05AL2	2.75206E-02
H	3.26876E-020	1.73235E-02B10	1.23965E-05B11	5.02056E-05
C	1.56505E-05U234	3.66379E-06U235	3.42411E-04U236	1.46894E-06
U238	1.98256E-05			
59 59				
SI	1.09124E-04FE	9.60390E-05CU	4.82326E-05MN55	2.09203E-05
MG	2.52199E-04CR	5.15759E-05TI	2.39941E-05AL2	2.74464E-02

H	3.26876E-02O	1.73000E-02B10	1.28733E-05B11	5.21369E-05
C	1.62526E-05U234	3.57599E-06U235	3.34205E-04U236	1.43374E-06
U238	1.93504E-05			
60 60				
SI	4.94161E-05FE	4.34907E-05CU	2.18419E-05MN55	9.47364E-06
MG	1.14207E-04CR	2.33558E-05TI	1.08656E-05AL2	1.24289E-02
H	3.26876E-02O	1.74139E-02U234	4.00218E-06U235	3.74035E-04
U236	1.60461E-06U238	2.16566E-05		
61 61				
SI	4.96169E-05FE	4.36674E-05CU	2.19306E-05MN55	9.51213E-06
MG	1.14671E-04CR	2.34507E-05TI	1.09098E-05AL2	1.24794E-02
H	3.26876E-02O	1.75578E-02U234	4.54026E-06U235	4.24323E-04
U236	1.82035E-06U238	2.45683E-05		
62 62				
SI	5.01902E-05FE	4.41720E-05CU	2.21840E-05MN55	9.62205E-06
MG	1.15996E-04CR	2.37217E-05TI	1.10358E-05AL2	1.26236E-02
H	3.26876E-02O	1.79686E-02U234	6.07667E-06U235	5.67913E-04
U236	2.43635E-06U238	3.28822E-05		
63 63				
SI	5.05954E-05FE	4.45286E-05CU	2.23631E-05MN55	9.69973E-06
MG	1.16933E-04CR	2.39132E-05TI	1.11249E-05AL2	1.27256E-02
H	3.26876E-02O	1.82590E-02U234	7.16248E-06U235	6.69390E-04
U236	2.87168E-06U238	3.87577E-05		
64 64				
SI	5.05129E-05FE	4.44560E-05CU	2.23266E-05MN55	9.68390E-06
MG	1.16742E-04CR	2.38742E-05TI	1.11068E-05AL2	1.27048E-02
H	3.26876E-02O	1.81998E-02U234	6.94119E-06U235	6.48709E-04
U236	2.78296E-06U238	3.75603E-05		
65 65				
SI	5.00663E-05FE	4.40630E-05CU	2.21293E-05MN55	9.59829E-06
MG	1.15710E-04CR	2.36632E-05TI	1.10086E-05AL2	1.25925E-02
H	3.26876E-02O	1.78798E-02U234	5.74454E-06U235	5.36873E-04
U236	2.30319E-06U238	3.10850E-05		
66 66				
SI	4.94439E-05FE	4.35152E-05CU	2.18542E-05MN55	9.47897E-06
MG	1.14271E-04CR	2.33690E-05TI	1.08717E-05AL2	1.24359E-02
H	3.26876E-02O	1.74339E-02U234	4.07674E-06U235	3.81004E-04
U236	1.63451E-06U238	2.20601E-05		
67 67				
SI	4.90309E-05FE	4.31517E-05CU	2.16716E-05MN55	9.39979E-06
MG	1.13317E-04CR	2.31738E-05TI	1.07809E-05AL2	1.23321E-02
H	3.26876E-02O	1.71379E-02U234	2.97001E-06U235	2.77571E-04
U236	1.19078E-06U238	1.60713E-05		
68 68				
SI	4.89084E-05FE	4.30439E-05CU	2.16175E-05MN55	9.37631E-06
MG	1.13034E-04CR	2.31159E-05TI	1.07540E-05AL2	1.23013E-02
H	3.26876E-02O	1.70502E-02U234	2.64177E-06U235	2.46894E-04
U236	1.05918E-06U238	1.42952E-05		
46 46				
H	6.53753E-20	3.26876E-2		
45 45				
H	6.53753E-20	3.26876E-2		
19 19				
AL1	.301125E-01H	.326876E-01O	.163438E-01	
20 20				
SI	1.90843E-04FE	1.67959E-04CU	8.43483E-05MN55	3.65867E-05
MG	4.41062E-04CR	9.01992E-05TI	4.19625E-05AL1	4.80000E-02
H	1.07400E-20	5.37000E-3		
41 41				
SI	1.40508E-04FE	1.23660E-04CU	6.21015E-05MN55	2.693706-05
MG	3.24732E-04CR	6.64092E-05TI	3.08949E-05AL1	3.53400E-02
H	2.75000E-20	1.37500E-2		
21 21				

SI 9.09042E-05FE 8.00041E-05CU 4.01777E-05MN55 1.74274E-05
 MG 2.10091E-04CR 4.29647E-05TI 1.99880E-05AL1 2.28639E-02
 H 3.97136E-20 1.98568E-3
 24 24
 H 3.835E-20 1.9200E-2AL1 2.36E-02
 22 22
 O 1.92E-3
 23 23
 BE 1.17E-1H 3.28E-30 1.64E-3AL1 5.52E-4
 44 44
 BE 1.208E-1H 9.94E-40 4.97E-4AL1 5.60E-4
 42 42
 SI 6.14583E-05FE 5.40890E-05CU 2.71632E-05MN55 1.17823E-05
 MG 1.42038E-04CR 2.90474E-05TI 1.35134E-05AL1 1.54577E-02
 AM241 9.14522E-07PU238 2.23946E-08PU239 1.20546E-08PU240 4.26554E-06
 PU241 3.98485E-10CM244 8.99933E-05PU242 1.13099E-08AM243 2.89092E-06
 CM245 1.28569E-06CM246 6.15306E-05CM247 1.72823E-06CM248 1.06626E-05
 CF252 2.85818E-10H 3.97136E-20 1.98568E-3
 43 43
 SI 6.00220E-05FE 5.28249E-05CU 2.65284E-05MN55 1.15069E-05
 MG 1.38719E-04CR 2.83686E-05TI 1.31976E-05AL1 1.50965E-02
 H 3.97136E-20 1.98568E-3
 30 30
 H 3.1407E-30 1.5703E-2AL1 5.7401E-2
 15 18
 H 2.770E-30 1.385E-3AL1 4.17246E-2TA181 1.4555E-2
 1 14
 EU151 2.9299E-3EU153 3.17604E-3AL1 3.49722E-20 9.1589E-3
 END
 INPUT PROCESSOR
 OVEXPOSE 1 1
 1D 1 75 0 1 0 8 33 29 0 0 0 0 0 471 0 0 0 0 0 0
 2D
 67HENDF/B-V DEPLETION DATA FOR THERMAL REACTORS, PRIMM & WRIGHT, 11/89
 60HZR93 MO97 TC99 RU101 RU103 RH103 RH105 I135 XE131 XE133
 60HXE135 CS133 CS134 CS135 CE141 PR143 ND143 ND145 ND147 PM147
 60HPM148 PM148MPM149 SM149 SM150 SM151 SM152 SM153 EU153 EU154
 60HEU155 MAFP WAEP TH232 U233 U234 U235 U236 U238 NP237
 60HNP238 NP239 PU238 PU239 PU240 PU241 PU242 PU243 AM241 AM242
 60HAM242MAM243 CM242 CM243 CM244 CM245 CM246 CM247 CM248 BK249
 60HCF249 CF250 CF251 CF252 CF253 ES253 B10 HE LI CD
 25HTA181 TA182 EU151 D T
 3D 0.
 34 35 37 38 39 44 45 46
 1 2 3 4 5 6 7 8 9 10 11 12 13 14 15 16 17 18 19 20 21 22 23 24
 25 26 27 28 29 30 31 32 33
 1 3 5 7 8 10 11 13 14 15 16 19 20 21 22 23 26 28 30 31 32 33 41 42
 48 50 53 60 65
 4D
 1.46000E-14 1.03000E-13 2.04400E-07 5.44000E-06 2.92400E-05 1.52800E-06
 2.12000E-05 1.06400E-08 7.32000E-15 2.47000E-07 5.91000E-07 7.30000E-07
 8.37250E-09 1.49000E-06 1.94000E-07 3.63000E-06 2.44000E-10 4.12000E-06
 2.58000E-09 4.64000E-09 7.21615E-5 3.97431E-5 3.78000E-6 3.40660E-6
 3.885E-5 1.20248E-5 4.92785E-8 2.507E-8 4.507E-7
 SD / TH232, U233(TH), U235(TH), U236, U238, PU239(TH), PU240, PU241(TH)
 6.73051E-02 7.01394E-02 6.38333E-02 5.69292E-02 4.97480E-02 3.89554E-02
 3.77779E-02 3.08988E-02
 4.45385E-02 5.45848E-02 5.94127E-02 5.07680E-02 5.52536E-02 5.39642E-02
 5.14687E-02 4.85607E-02
 2.87561E-02 4.87389E-02 6.11911E-02 5.91164E-02 6.24788E-02 6.15613E-02
 5.99595E-02 6.27019E-02
 7.30503E-03 3.23116E-02 5.07374E-02 5.29346E-02 6.08435E-02 5.89887E-02
 6.05317E-02 6.00612E-02

1.52769E-03 1.66930E-02 3.04185E-02 4.20658E-02 6.22897E-02 6.94980E-02
 6.71258E-02 6.15095E-02
 0.00000E+00 4.20826E-11 4.31904E-12 7.06993E-13 2.15252E-14 1.09035E-10
 1.97020E-11 1.37039E-12
 4.61732E-04 4.82949E-03 9.67387E-03 2.47029E-02 3.97489E-02 5.36227E-02
 5.54896E-02 6.14640E-02
 5.35142E-02 4.91300E-02 6.29661E-02 5.63072E-02 6.83489E-02 6.44939E-02
 6.74761E-02 7.06975E-02
 1.62119E-02 3.60597E-02 2.88306E-02 3.03390E-02 3.23266E-02 3.84640E-02
 3.54415E-02 2.84278E-02
 3.96380E-02 6.02226E-02 6.70172E-02 7.02632E-02 6.61965E-02 6.97540E-02
 7.00540E-02 6.76991E-02
 8.03094E-05 4.44640E-03 7.05883E-04 4.12076E-04 1.16036E-04 4.20583E-03
 1.85025E-03 6.71049E-04
 2.97072E-11 3.72846E-07 8.34814E-09 2.24998E-09 2.54298E-11 2.65086E-07
 4.25042E-08 2.52071E-09
 4.22102E-09 1.32045E-05 1.26972E-07 1.70998E-07 3.14368E-09 9.89320E-06
 1.82018E-06 1.85052E-07
 2.30056E-07 1.85553E-04 2.08254E-05 4.28996E-06 1.80211E-07 1.58831E-04
 4.41244E-05 6.71189E-06
 7.30330E-02 6.53143E-02 5.79611E-02 5.54088E-02 5.45594E-02 5.25717E-02
 4.76464E-02 4.96383E-02
 6.51899E-02 5.89179E-02 5.93726E-02 6.08466E-02 4.55850E-02 4.42815E-02
 4.72014E-02 4.70421E-02
 0.00000E+00 1.33945E-10 2.05954E-12 1.21999E-13 0.00000E+00 3.65118E-11
 3.74037E-12 1.75049E-13
 5.28346E-02 3.39175E-02 3.91741E-02 3.66786E-02 3.75491E-02 2.99151E-02
 3.27715E-02 3.34353E-02
 3.01132E-02 1.74996E-02 2.25336E-02 2.34063E-02 2.53057E-02 2.04283E-02
 2.23321E-02 2.36772E-02
 2.89070E-12 2.01917E-08 9.45789E-10 9.90990E-11 1.09128E-12 1.45047E-08
 7.89078E-11 1.56044E-10
 4.49109E-11 3.53854E-09 4.05910E-11 1.24999E-09 2.45287E-11 1.12036E-07
 1.48015E-08 2.22062E-09
 1.08026E-10 9.80595E-09 7.44834E-11 2.99997E-09 5.88690E-11 2.36076E-07
 3.55035E-08 4.68132E-09
 8.83247E-03 7.77062E-03 1.06662E-02 1.36911E-02 1.61003E-02 1.23930E-02
 1.36947E-02 1.52403E-02
 1.68041E-13 3.01875E-09 1.10975E-10 1.13999E-11 1.39163E-13 2.68087E-09
 2.64026E-10 2.16061E-11
 3.70090E-08 2.80184E-05 3.03932E-07 1.24999E-06 8.00938E-08 1.15838E-05
 1.14011E-05 2.78078E-06
 3.14161E-03 3.15328E-03 4.18395E-03 4.22682E-03 8.01067E-03 7.72062E-03
 8.43189E-03 9.36900E-03
 7.59054E-04 2.13551E-03 2.67834E-03 3.87746E-03 5.20746E-03 5.85171E-03
 6.57575E-03 7.46591E-03
 3.32460E-04 1.04778E-03 1.61350E-03 2.55329E-03 4.10947E-03 3.63685E-03
 5.79669E-03 5.48158E-03
 2.96072E-12 4.16828E-08 2.34948E-09 6.57993E-10 1.78209E-11 8.24268E-08
 1.64016E-08 2.04057E-09
 2.11051E-11 2.27906E-07 2.68940E-08 8.72991E-09 3.44404E-10 9.22300E-07
 1.74017E-07 3.62102E-08
 3.82793E-05 2.17930E-04 3.20479E-04 9.23191E-04 1.32803E-03 1.65477E-03
 2.47628E-03 2.41746E-03
 1.02693 0.976661 0.931698 0.923419 0.889572 0.891592
 0.890217 0.895461
 0.479453 0.455982 0.434990 0.431124 0.415322 0.416265
 0.415623 0.418071
 8D
 34 +2 35 +2 36 +2 37 +2 38 +2 40 +2 41 +1 43 0 / TH232, U235 TO PU238
 39 +5 -40 +2 -41 +1 -43 0 / U238 TO PU238
 39 +2 42 +1 44 +2 45 +2 46 +2 47 +2 48 +1 52 +2 55 +2 56
 +2 57 +2 58 +2 59 +2 60 +2 62 +2 63 +2 64 +2 65 +1 66 0 /

```

/ U238, PU239, CF250 TO ES253
39 +2 42 +1 44 +2 45 +2 46 +2 47 +2 48 +1 52 +2 55 +2 56
+2 57 +2 58 +2 59 +2 60 +1 61 +2 -62 +2 -63 +2 -64 +2 -65 +1 -66 0 /
/ U238, PU239, CF249 TO ES253
39 +2 42 +1 44 +2 45 +2 46 +1 49 +899662 50 +2 -52 +2 -55 +2 -56
+2 -57 +2 -58 +2 -59 +2 -60 +2 -62 +2 -63 +2 -64 +2 -65 +1 -66 0 /
/ PU239, PU241, AM242, AM243, CF250 TO ES253
39 +2 42 +1 44 +2 45 +2 46 +1 49 +100342 51 +2 -52 +2 -55 +2 -56
+2 -57 +2 -58 +2 -59 +2 -60 +2 -62 +2 -63 +2 -64 +2 -65 +1 -66 0 /
/ PU239, PU241, AM241, AM242M, AM243, CF250 TO ES253
39 +2 42 +1 44 +2 45 +2 46 +1 49 +899662 50 +2 -52 +2 -55 +2 -56
+2 -57 +2 -58 +2 -59 +2 -60 +1 -61 +2 -62 +2 -63 +2 -64 +2 -65 +1 -66 0
/ PU239, PU241, AM242, AM243, CF249 TO ES253
39 +2 42 +1 44 +2 45 +2 46 +1 49 +100342 51 +2 -52 +2 -55 +2 -56
+2 -57 +2 -58 +2 -59 +2 -60 +1 -61 +2 -62 +2 -63 +2 -64 +2 -65 +1 -66 0
/ PU239, PU241, AM241, AM242M, AM243, CF249 TO ES253
39 +2 42 +1 44 +2 45 +2 46 +1 49 +899662 50 +173001 -47 0
/ PU239, PU241, AM242 TO PU242
39 +2 42 +1 44 +2 45 +2 46 +1 49 +899662 50 +827001 53 +2 54 +2 -55 +2
-56 +2 -57 +2 -58 +2 -59 +2 -60 +2 -62 +2 -63 +2 -64 +2 -65 +1 -66 0 /
/ PU239, PU241, AM242, CM239 +2 42 +1 44, CF250 TO ES253
39 +2 42 +1 44 +2 45 +2 46 +1 49 +899662
50 +827001 53 +2 54 +2 -55 +2 -56
+2 -57 +2 -58 +2 -59 +2 -60 +1 -61 +2 -62 +2 -63 +2 -64 +2 -65 +1 -66 0
/ PU239, PU241, AM242, CM239 +2 42 +1 44, CF249 TO ES253
39 +2 42 +1 44 +2 45 +2 46 +1 49 +899662
50 +827001 53 +1 -43 0 /PU239,CM242->PU238
19 +1 20 +470002 22 +2 23 +1 24 +2 25 +2 26 +2 27 +2 28 +1 29
+2 30 +2 31 0 / ND147, PM148M TO EU155
19 +1 20 +530002 21 +2 -23 +1 -24 +2 -25 +2 -26 +2 -27 +2 -28
+1 -29 +2 -30 +2 -31 0 / ND147, PM148 TO EU155
8 +1 11 +1 14 0 / I135 TO CS135
10 +1 12 +2 13 0 / XE133 TO CS134
5 +1 6 0 / RU103 TO RH103
16 +1 17 0 / PR143 TO ND143
1 0 2 0 3 0 4 0 7 0 9 0 15 0 18 0 / SINGLE FISSION PRODUCTS
32 0 33 0 / LUMPED FISSION PRODUCTS
71 +2 72 0 / TA181 TO TA182
67 0 / B10
73 0 / EU151
0
STOP
END
DUTLIN
EXPINS      0  1  0 30  1
0.588
0  0  0  0  1  3
2  0  2       1
END
DENMAN
018
1
020
13 14      18
18 18      30
END
DUTLIN
EXPINS      0  1  0 30  1
0.588
0  0  0  0  1  3
2  0  2       1
DTNINS      0 30  0 72  1
85.+6    1.00   1.0

```

1.0
 0.0 0.01937 0.001665 .0645
 0.0
 2 1 1 130
 2 1 0 0 0 1 0 6
 2 2 0 2 0 0
 END
 DENMAN
 018
 1
 020
 10 12 13
 17 17 30
 END
 DUTLIN
 EXPINS 0 1 0 30 1
 12.941
 0 0 0 0 1 3
 2 0 2 1
 DTNINS 0 30 0 72 1
 85.+6 1.00 1.0
 1.0
 0.0 0.01937 0.001665 .0645
 0.0
 2 1 1 130
 2 1 0 0 0 1 0 4
 2 2 0 2 0 0
 END
 DENMAN
 018
 1
 020
 7 9 13
 16 16 30
 END
 DUTLIN
 EXPINS 0 1 0 30 1
 4.706
 0 0 0 0 1 3
 2 0 2 1
 DTNINS 0 30 0 72 1
 85.+6 1.00 1.0
 1.0
 0.0 0.01937 0.001665 .0645
 0.0
 2 1 1 130
 2 1 0 0 0 1 0 3
 2 2 0 2 0 0
 END
 DENMAN
 018
 1
 020
 6 6 13
 14 15 30
 END
 DUTLIN
 EXPINS 0 1 0 30 1
 2.353
 0 0 0 0 1 3
 2 0 2 1
 DTNINS 0 30 0 72 1
 85.+6 1.00 1.0

1.0
 0.0 0.01937 0.001665 .0645
 0.0
 2 1 1 130 2.12 -05
 2 0 0 1 0 0 0 1 0 2
 2 2 0 2 0
 END
 DENMAN
 018
 1
 020
 4 5 13
 12 13 30
 END
 DUTLIN
 EXPINS 0 1 0 30 1
 2.353
 0 0 0 0 1 3
 2 0 2 1
 DTNINS 0 30 0 72 1
 85.+6 1.00 1.0
 1.0
 0.0 0.01937 0.001665 .0645
 0.0
 2 1 1 130 2.12 -05
 2 0 0 1 0 0 0 1 0 1
 2 2 0 2 0
 END
 DENMAN
 018
 1
 020
 3 3 6
 11 11 30
 END
 DUTLIN
 EXPINS 0 1 0 30 1
 3.529
 0 0 0 0 1 3
 2 0 2 1
 DTNINS 0 30 0 72 1
 85.+6 1.00 1.0
 1.0
 0.0 0.01937 0.001665 .0645
 0.0
 2 1 1 130 2.12 -05
 2 0 0 1 0 0 0 1 0 1
 2 2 2 2 0
 END
 DENMAN
 018
 1
 020
 2 2 6
 9 10 30
 END
 END

APPENDIX B

Equivalent Diffusion Theory Coefficients Derived From Transport Theory Calculations

Initial calculations of the six critical experiments showed that those in which the control blades were fully or nearly fully withdrawn yielded k-effectives close to 1.0. However, those in which the control blades were inserted yielded k-effectives which were low (0.9). After verifying the model input regarding control blade position and boron content in the coolant, it was suspected that the diffusion coefficients as generated by the computational procedure described in Section 2 were in error. A procedure by A. F. Henry (Ref. 11) for dealing with bladed control rods was employed to derive new diffusion coefficients.

Henry states, "for the one dimensional case, we use the fact that parameters which preserve all the integrated reaction rates within all subregions V_i must necessarily preserve the net leakage rate out of each V_i In slab geometry (or in this case, annular geometry in which the height \gg thickness of the annulus) this extra restriction implies that, if we know from more accurate calculations (in this case discrete ordinates calculations from XSDRNPM) the column vector $J(r_i)$ of group currents at the point r_i separating a zone of thickness Δ_{i-1} from its neighbor of thickness Δ_i , we want the equivalent diffusion-theory parameters for these zones to be such that solution of the group diffusion equations containing the effective constants will reproduce the $J(r_i)$. If we also require that the column vector of group fluxes $\Phi(r_i)$ at all the interfaces match those values known from more accurate calculations (again, discrete ordinates calculations using XSDRNPM), a systematic procedure for finding the equivalent parameters emerges."

"We consider first the one-group case with the material inside Δ_i homogeneous but not of a nature such that diffusion theory should be valid." In this case, a control blade with no annular or axial (height \gg thickness) variation. If equivalent constants $v \sum_f, \sum_a$, and \bar{D} can be found for this case, they will be such that within Δ_i the one-group P_1 equations are

$$\frac{d}{dr} J(r) + \overline{\sum_a} \Phi(r) = v \overline{\sum_f} \Phi(r),$$

$$\frac{d}{dr} \Phi(r) + \frac{1}{\bar{D}} J(r) = 0.$$

Note that for this problem $v \sum_f = 0$. Also note, that the above equations are applicable to the multigroup solution if we assume that there is no scattering between groups. Given the seven-group energy structure shown in Section 2 and the fact that the control blades are composed of europium oxide dispersed in an aluminum matrix (atomic weight of Eu=150.92) this is a good assumption.

In matrix form these become:

$$\frac{d}{dr} \begin{bmatrix} \Phi \\ J \end{bmatrix} = - \begin{bmatrix} 0 & \frac{1}{\bar{D}} \\ \sum_a & 0 \end{bmatrix} \begin{bmatrix} \Phi \\ J \end{bmatrix}, \quad (1)$$

and, with the definitions:

$$[u(r)] \equiv \begin{bmatrix} \Phi(r) \\ J(r) \end{bmatrix}, \quad [N] \equiv \begin{bmatrix} 0 & \frac{1}{\bar{D}} \\ \sum_a & 0 \end{bmatrix}$$

(1) becomes

$$\frac{d}{dr} [u(r)] + [N] [u(r)] = 0. \quad (2)$$

The solution to this equation is given in Ref. 11 and is shown to be

$$\begin{bmatrix} \Phi(r_{i+1}) \\ J(r_{i+1}) \end{bmatrix} = \begin{bmatrix} \cosh \kappa \Delta & -(\bar{D}\kappa)^{-1} \sinh \kappa \Delta \\ -\bar{D} \sinh \kappa \Delta & \cosh \kappa \Delta \end{bmatrix} \begin{bmatrix} \Phi(r_i) \\ J(r_i) \end{bmatrix}.$$

where the subscripts $i, i+1$ represent intervals in the problem and $\kappa^2 = \frac{\sum_a - v \sum_f}{\bar{D}} = \frac{\sum_a}{\bar{D}}$.

Defining blackness coefficients α and β by

$$\alpha \equiv \frac{J(r_i) - J(r_{i+1})}{\Phi(r_i) + \Phi(r_{i+1})}, \quad \beta \equiv \frac{J(r_i) + J(r_{i+1})}{\Phi(r_i) - \Phi(r_{i+1})},$$

it can be shown that

$$\sinh \kappa \Delta = \sqrt{(\cosh^2 \kappa \Delta - 1)} = \frac{2\sqrt{(2\beta)}}{\beta - 2}$$

and

$$\bar{D} = \frac{1}{\kappa} \sqrt{(\alpha\beta)}$$

For the calculations described in this document, multigroup flux and current values for mesh points on the front and rear faces of the control blade were used to define α and β . The group diffusion coefficients were then determined directly.

Henry notes in Ref. 10 that, in those instances where the within group scattering cross-section approaches zero, it is necessary to modify the absorption cross section of the control blade material. The value of the effective absorption cross-section was computed according to the procedure specified by Henry using the values of α and β . It was determined that no correction was needed.

The VENTURE neutronics module has an input option whereby two constants, a and b , can be entered and the value of the diffusion coefficients, for a given zone, as calculated from the cross-section data library are modified according to the formula

$$\text{new diffusion coefficient} = a (\text{old diffusion coefficient}) + b$$

The diffusion coefficients for the europium region of the control rod were compared to the "old" values derived from the data library and could be linearly correlated with a correlation coefficient R^2 , equal to 0.998. The value of a was determined to be 0.01937 and the value of b was determined to be 0.001665.

INTERNAL DISTRIBUTION

- | | |
|------------------------|---|
| 1. D. H. Cook | 22. L. R. Williams |
| 2. W. W. Engle | 23-27. B. A. Worley |
| 3. G. F. Flanagan | 28. EPMD Reports Office |
| 4. H. A. Glovier | 29. RRD/CARTS |
| 5. R. W. Hobbs | 30. RRD/DCC |
| 6. D. T. Ingersoll | 31-32. Laboratory Records
Department |
| 7. R. D. Lawson | 33. Laboratory Records,
ORNL-RC |
| 8. J. V. Pace | 34. Document Reference
Section |
| 9-13. R. T. Primm, III | 35. Central Research Library |
| 14. J. B. Richard | 36. ORNL Patent Section |
| 15-19. R. B. Rothrock | |
| 20. K. R. Thoms | |
| 21. R. C. Ward | |

EXTERNAL DISTRIBUTION

- 37-46. Office of Scientific and Technical Information, P.O. Box 62, Oak Ridge
TN 37831
47. Office of Assistant Manager for Energy Research and Development,
Department of Energy-Oak Ridge Field Office, P.O. Box 2008,
Oak Ridge, TN 37831